NATIONAL BUREAU OF STANDARDS REPORT

9028

PRELIMINARY REPORT

ON THE THERMODYNAMIC PROPERTIES OF

SELECTED LIGHT-ELEMENT AND

SOME RELATED COMPOUNDS

(Supplement to NBS Reports 6297, 6484, 6645, 6928, 7093,
7192, 7437, 7587, 7796, 8033, 8186, 8504, 8628, and 8919)

1 January 1966

◆ **NBS** ◆

U.S. DEPARTMENT OF COMMERCE

NATIONAL BUREAU OF STANDARDS

NATIONAL BUREAU OF STANDARDS REPORT

NBS PROJECT

221-0405
221-0426A
221-0426B
221-0426C
221-0426D
221-0441
222-0423
223-0513
223-0442
313-0430

1 January 1966

NBS REPORT

9028

PRELIMINARY REPORT

ON THE THERMODYNAMIC PROPERTIES OF

SELECTED LIGHT-ELEMENT AND

SOME RELATED COMPOUNDS

(Supplement to NBS Reports 6297, 6484, 6645, 6928, 7093, 7192, 7437, 7587, 7796, 8033, 8186, 8504, 8628, and 8919)

Fifteenth Technical Summary Report
on the Thermodynamic Properties
of Light-Element Compounds

Reference: U. S. Air Force Order No. OAR ISSA 65-8

<NBS>

U. S. DEPARTMENT OF COMMERCE
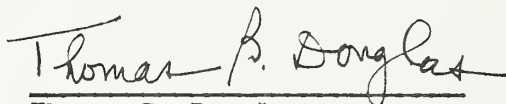## NATIONAL BUREAU OF STANDARDS

ABSTRACT

This is the fifteenth semiannual report on the current program of research, at the National Bureau of Standards, on the thermodynamic properties of selected light-element and some related compounds of primary interest in high-temperature research and application. The bulk of the report describes in detail new apparatus design and testing, data, and data analysis and interpretation originating in this program. Most of the results reported are thermodynamic properties of various oxides of aluminum and beryllium in the solid, liquid, and gaseous states as determined by a variety of techniques. Included also are an improved method for accurate fluorine-compound flame calorimetry, and new molecular-structure information on the boron trihalides.
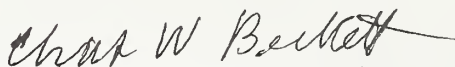
Oxides of Al and Be: Accurate measurements of the heat capacity of two solid oxides are reported -- $BeO \cdot Al_2O_3$ from 273 to 1173°K, and $BeO \cdot 3Al_2O_3$ from 15 to 1173°K -- with agreement by the two methods used of 0.0 to 0.5% in the range of overlap. These and earlier data from the program were smoothed and carefully extrapolated to give tables of the thermodynamic functions from 0 to 2150°K (approximately the melting points). With detailed description of new apparatus designed for accurate measurements up to 2500°K, 21 measurements of the enthalpy (relative to room temperature) of solid and liquid Al_2O_3 from 1171 to 2388°K are reported which yield for the heat of fusion tentative values of 29.2 to 29.7 kcal/mole which are subject to some revision following a planned redetermination of the heat capacity of tungsten. Mass-spectrometric data on the gaseous Al-Be-O system reported a year ago (NBS Report 8628) have been carefully reanalyzed; the identification and thermodynamic properties of the new species $AlOBe(g)$ prove to be soundly based, but the heat of formation of $Al_2O(g)$, while in agreement with the existing literature values, still shows some discrepancy. The mixing process between exploding aluminum wires and a confined air environment was investigated, using photographic and photoelectric techniques for time resolution of the explosion spectrum. Results, which showed $AlO(g)$ bands against a strong background continuum, suggested a method for estimating the average temperature of the exploding vapor. Differential thermal analysis and X-ray diffraction of "amorphous" vapor-deposited Al_2O_3 and BeO (from arc-image melts) followed their

crystallization processes, suggesting a release of strain energy from the Al_2O_3 at 600°K and that the BeO film is probably composed of very small crystallites. The rate of vaporization of liquid Al_2O_3 was repeated using an automatic pyrometer.

Halides: In fluorine flame calorimetry, presently concentrated on $OF_2(g)$, a new burner designed for increased accuracy (including independence from the uncertainties in the thermochemistry of $HF(g)$) is described in detail. After verifying a method for determining Coriolis zeta constants from infrared data, it was applied to the molecules BF_3, BCl_3, BBr_3, and BI_3; the general force fields determined indicated that the stretch-bend interaction constant is large and negative, and decreases from BF_3 to BI_3. The isotopic shifts of the infrared spectra of the matrix-isolated several isotopic varieties of BCl_3 show excellent agreement with those predicted by the newly derived force field.

Thomas B. Douglas
Project Leader

Charles W. Beckett
Assistant Division Chief for Thermodynamics
Heat Division, Institute for Basic Standards

TABLE OF CONTENTS

TABLE OF CONTENTS (Continued)

TABLE OF CONTENTS (Continued)

TABLE OF CONTENTS (Continued)

Chapter 1

PHOTOGRAPHIC AND SPECTROSCOPIC STUDIES
OF EXPLODING WIRES IN A SEALED VESSEL

by

E. C. Cassidy and K. K. Neumann*
National Bureau of Standards,
Washington, D. C., U.S.A.

1. ABSTRACT. Investigations of the mixing process between exploding wires and a confined air environment are described. Various combinations of high-speed framing camera, drum camera, photoelectric, spectroscopic, periodic still, and ultraviolet photographic techniques were employed for time resolution. Results suggested a method for estimating the average temperature of the exploding vapor column. Phenomena apparently due to reflecting shock waves were observed in later stages of the explosion.

2. INTRODUCTION. In recent years, exploding wires have been studied extensively [1], and high-speed photography has provided detailed information about the discharge-explosion process. However, it is clear that there is no "ideal" wire explosion. The gross features of the explosion depend upon such parameters as wire material and dimensions, environment, electrical energy input, discharge circuit, and so on. Change in a single parameter may so effect the discharge that one process, rather than another, becomes important.

The present work, where our principal purpose was to develop a sealed system for high-temperature (above 2,000°K) optical studies, was somewhat unusual: (1) The stored energy was high (1500 to 12,000 joules) for the mass of the sample wires (about 2.5 mg); (2) a sealed vessel was employed to contain chemical reactions and products and (3) the discharge-explosion behavior was observed over the entire duration of light emission and for up to one hour after the explosion.

3. EXPERIMENTAL APPARATUS AND PROCEDURE. The experimental apparatus is shown schematically in Fig. 1. The sample wires were 99.999% pure aluminum (Diam. = 0.14 mm, length = 6.2 cm). The wire was enclosed in a sealed, acrylic resin cylinder (O.D. = 8.3 cm, I. D. = 7.1 cm, length = 6.2 cm) containing air under normal laboratory conditions. Quartz windows were used at times for transmission of ultraviolet radiation. Two overruling practical considerations were found important in choice of a vessel: (1) the vessel should be larger than the scarred area left by the arc on the electrodes

---

*Present address: Technische Hochschule, 33 Braunschweig, Institut fur Chemische Technologie, Hans-Sommer Str. 10, West Germany.

1

which clamp the wire, and (2) the diameter of the vessel should be large enough to ensure complete oxidation of all the metal before the vapor reaches the walls. These precautions preclude vessel failure (explosion) and blackening of the walls, and inhibit introduction of impurities from the electrodes and walls.

The instrumentation included a 35 mm framing camera, a 35 mm drum camera, a 70 mm drum camera for time-resolved spectral photography, a photomultiplier tube with special filters for recording the intensity of selected bands of wavelengths as a function of time, and a plane-grating spectrograph (dispersion 20 Å/mm in the first order). The latter was equipped with four photomultiplier tubes for time-resolved intensity observations at selected wavelengths. Sequential framing camera observations of the entire explosion were obtained by mounting the drum camera on the framing camera so that the drum recorded only one frame per revolution of the framing camera.

4. RESULTS. Experiments with 15 μF at 10 to 14 kV showed light emission for about 3.5 msec (though the electrical current ceased at $t \approx 90$ μsec), with maximum radiation intensity at $t \approx 750$ μsec (see record from photomultiplier in Fig. 2). There was little mixing between the metal vapor and surrounding air until after about 600 μsec. Photographic results indicated that rapid expansion of the vapor ceased at about 150 μsec, and that a series of periodic pulsations in diameter ($f \approx 8800$ Hz) occurred in later stages of the explosion. Intensity pulsations of approximately the same frequency were observed in the photomultiplier (Fig. 2) and spectroscopic drum camera results. The duration of the radiation and the timing of the maximum intensity are quite different from those reported by Muller [2] and Funfer et al, [3], probably because the latter performed their experiments in the open atmosphere, rather than in a sealed vessel. Experiments with an open vessel supported this viewpoint: the pulsations were aperiodic; radiation was less intense; and radiation persisted only about 1.5 msec.

Fig. 3 shows the more interesting earlier stages of an explosion, as recorded (without backlighting) by the framing camera. Because of the slow turbine speed and long (about 15 μsec) exposure time per frame, the first frame shows the initial, very rapid expansion of the wire (during the "first pulse", "dark pause", and early "restrike" portions of the discharge) in composite form. The line of intense radiation along the central axis is the wire at a very early stage. The superimposed larger column of radiation shows the vapor's expansion after about 15 μsec.

In the higher energy (60 μF at 10 to 14 kV) explosions, the radiation was much more intense and the entire event was much faster. Fig. 4 (ultraviolet photographs obtained by use of Kodak Wratten 18A filter) shows the

most interesting portion of a higher energy explosion, without masking by visible light from surrounding cooler gases. The familiar "striations" show up clearly in the first frame. Between 10 and 15 μsec the arc is sharply defined, apparently quite uniform, and there is little mixing between the metal vapor and the surrounding air. At t ≈ 16 μsec, ejected particles and reaction products begin to envelop the column, thus disturbing the spectroscopic measurements. However, the more uniform period between 10 and 15 μsec was quite reproducible. At lower energies, where the explosion was less rapid, this phase lasted from t ≈ 50 to 200 μsec.

Immediately after radiation ceased, the interior of the vessel was clear and transparent. Within a minute, continuously moving solid particles (Al_2O_3), which gradually grew in size and number, began to appear. After about an hour, the particles settled into parabaloidal webs as shown in Fig. 5.

The spectroscopic results showed lines from neutral Al atoms (3082, 3093, 3944, and 3962Å) and bands from AlO molecules (the blue-green system with the transition $A^2\Sigma \rightarrow X^2\Sigma$, and part of the ultraviolet system – 3113Å and below). There were no features from heated air. The most informative part of the spectrum (3900 to 5000 Å) is shown in Fig. 6

The photomultiplier records for selected wavelengths (traces B thru E in Fig. 7 showed "first pulses", "dark pauses", and "restrikes" in intensity which coincided with their respective counterparts in the discharge current (trace A). The difference between traces B and C (Al-line and nearby continuum, respectively) and between traces D and E (AlO band and nearby continuum) indicates that line and band radiation was emitted, probably by ejected particles which reacted with the surrounding air, from the very beginning of the discharge. The similarity between the continuum traces (C and E) suggests that the high-pressure vapor may be treated as a grey-body source for about 100 μsec. Drum camera photographs (of the spectra), which showed intense continuum during the first 100 μsec, supported this assumption.

5. CONCLUSIONS. The photographic studies showed no period (during the light-emitting stages of the explosion) of ideal mixing between the metal vapor and the air in the vessel. The wire expanded symmetrically for a time, and then underwent a series of pulsations apparently caused by reflecting shock or pressure waves. Perhaps because of this phenomena, radiation was more intense and enduring when the explosion was contained in a sealed vessel. Intervals occurred during the explosion when there was a sharp boundary and little mixing between the high-pressure metal vapor and the surrounding cooler air. The timing and duration of these intervals were found to depend upon the energy input, being from t ≈ 50 to

200 μsec with about 1500 joules energy storage, and from t $\approx$ 10 to 15 μsec with 3000 joules. Correlation of results suggested that during these intervals intensity measurements in the continuum might be useful in calculating the average temperature of the vapor column. This method has the advantages that it does not assume chemical equilibrium or require knowledge of the concentrations of various components in the mixture.

6. ACKNOWLEDGEMENTS. The authors are grateful to Mr. W. A. Bagley for assistance in setting up the drum camera system.

7. REFERENCES.

1. W. G. Chace and H. K. Moore ed., Exploding Wires, Vols. 1-3, Plenum Press, N. Y. (1960, 1962, 1964).

2. W. Muller, Z. Physik 149, 397 (1957) and Exploding Wires 1, 186 (1959).

3. V. E. Funfer, M. Keilhacker, and G. Lehner, Z. Angew, Phys. 10, 11 (1958).
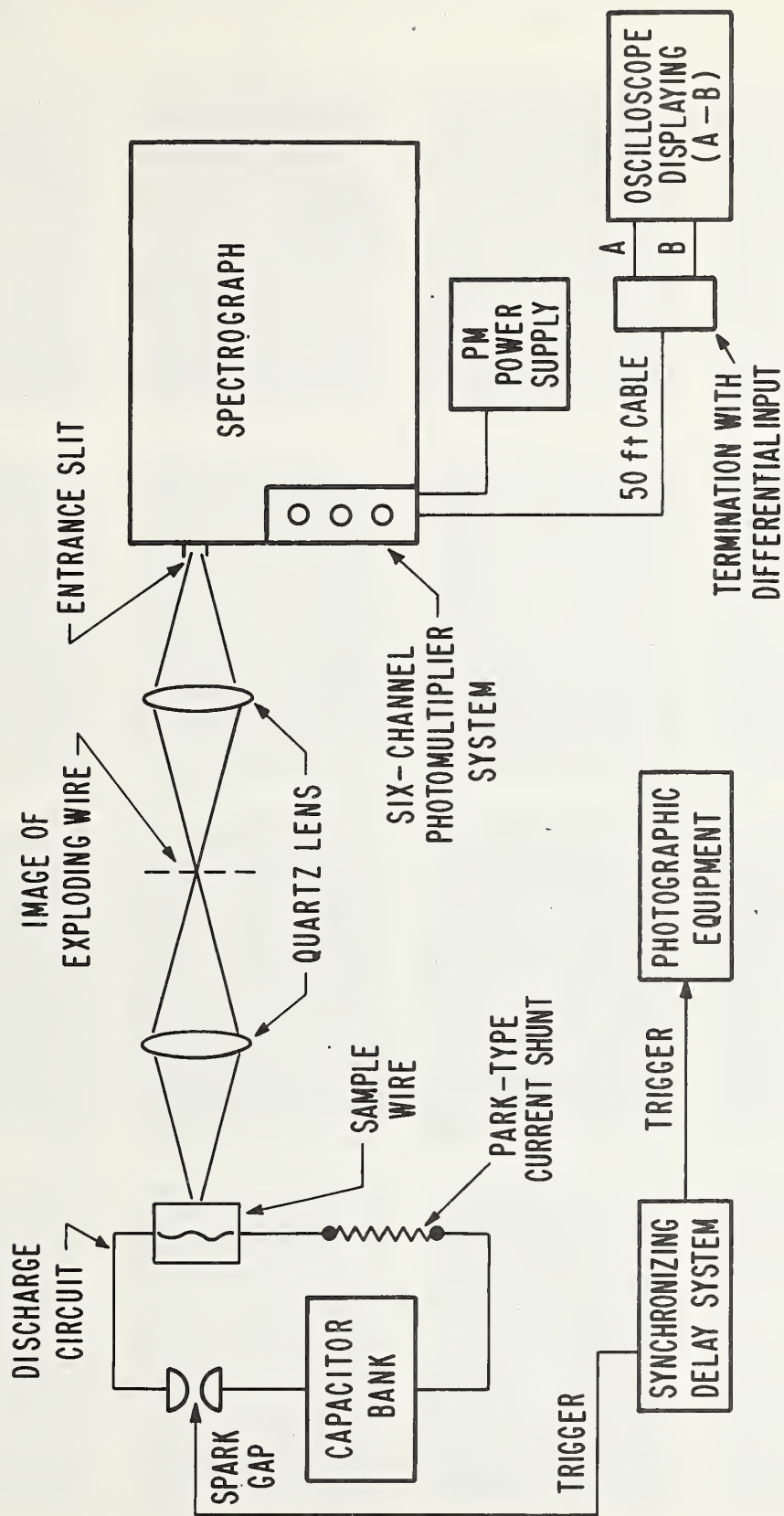
Fig. 1. Schematic diagram of the experimental setup.

5
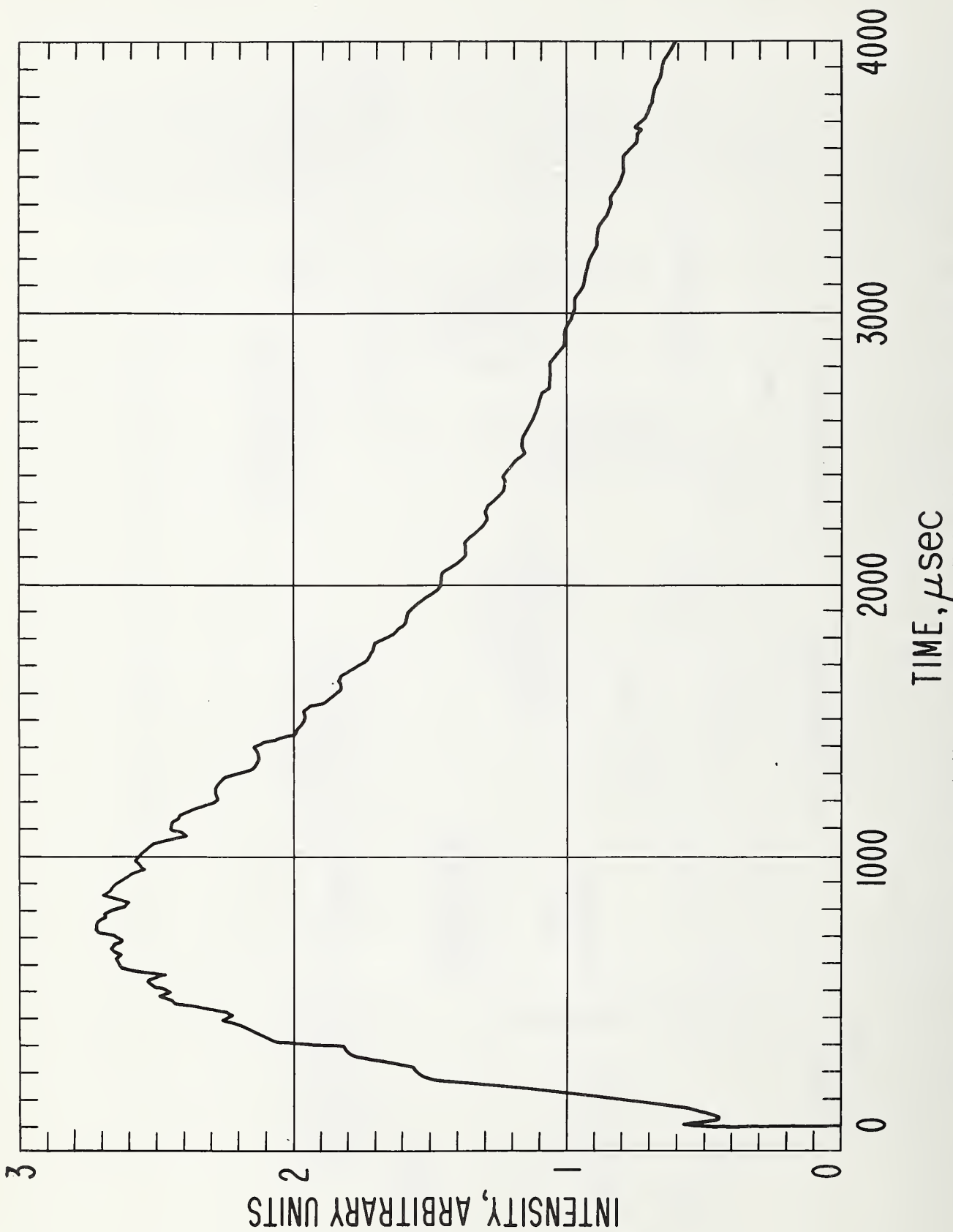
Fig. 2. Radiation Intensity in the Region 560 to 590 mμ (continuum) during Entire Course of an Explosion. Energy Stored: 15 μF at 14 kV.

6
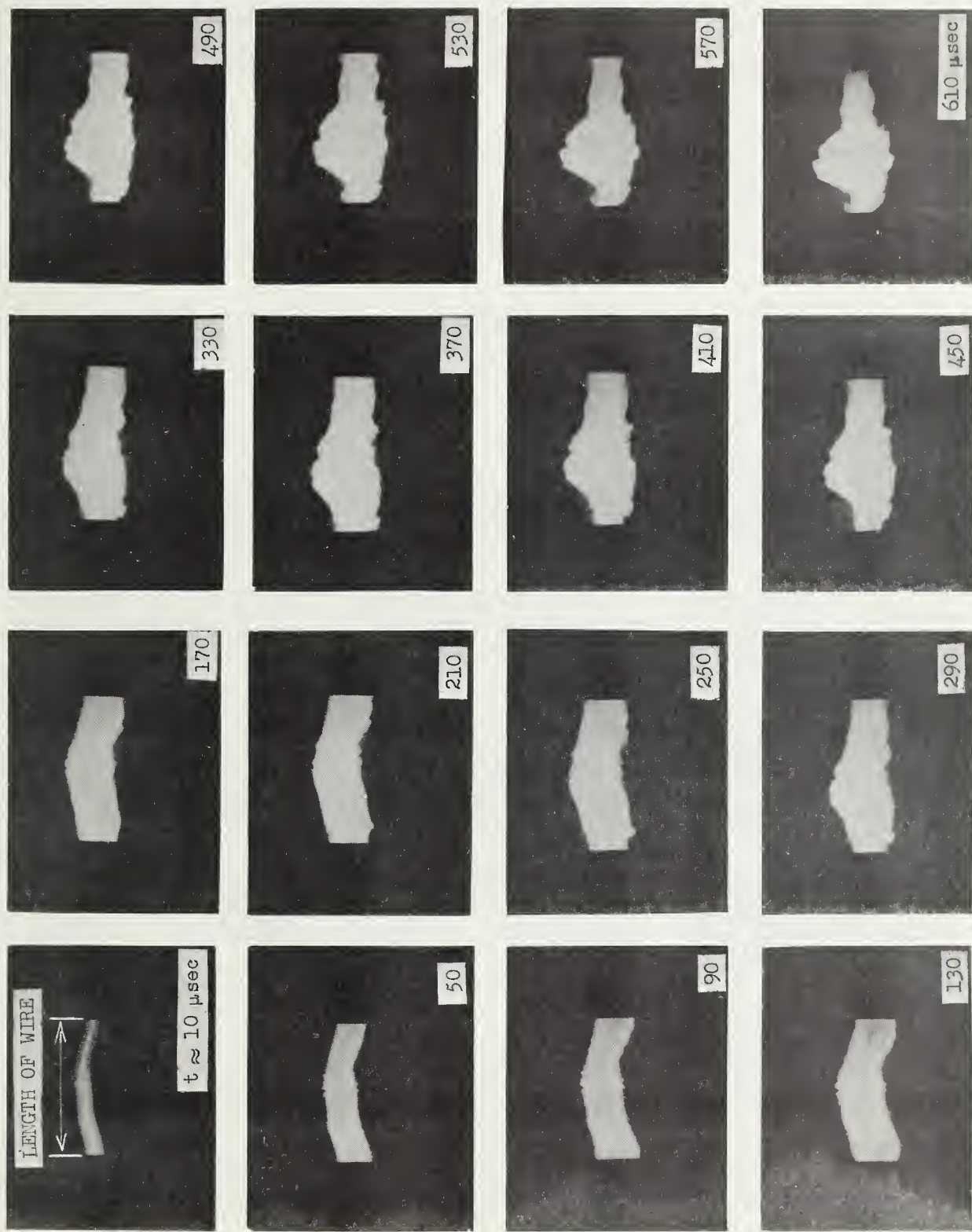
Fig. 3. Framing camera record of the Early Stages (610 μsec) of an Explosion. Energy Stored: 15 μF at 14 kV. Exposure time: about 15 μsec, Filter: Neutral density (20% transmittance), Film: Plus-X.

7
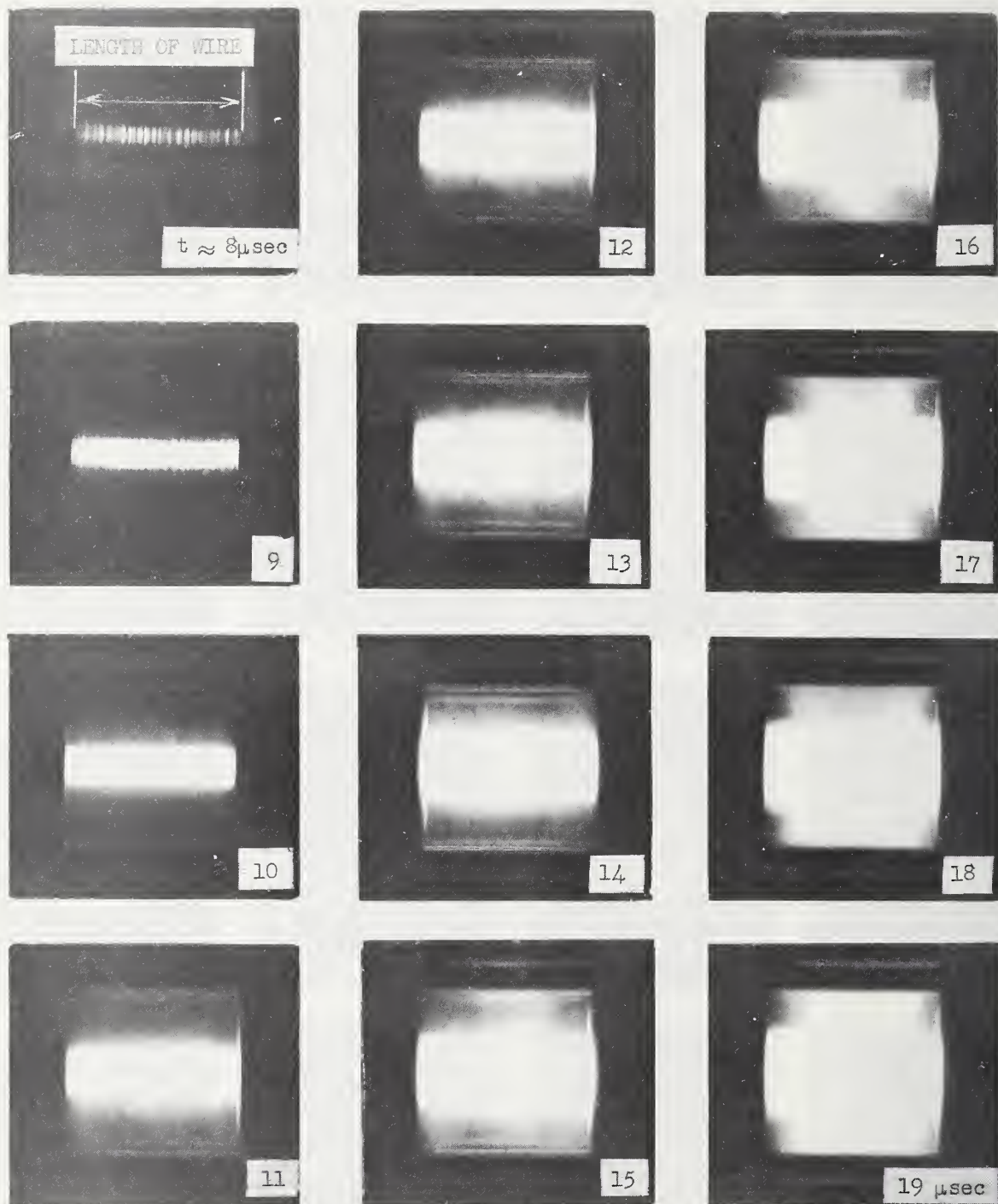
Fig. 4. Framing Camera Record (with near-ultraviolet light) of Time between 8 and 19 μsec after Current Starts. Stored Energy: 60 μF at 10 kV. Exposure Time: about 0.4 μsec, Filter: Kodak Wratten filter 18A (transmittance between 300 and 400 mμ), Film: Plus-X.

8
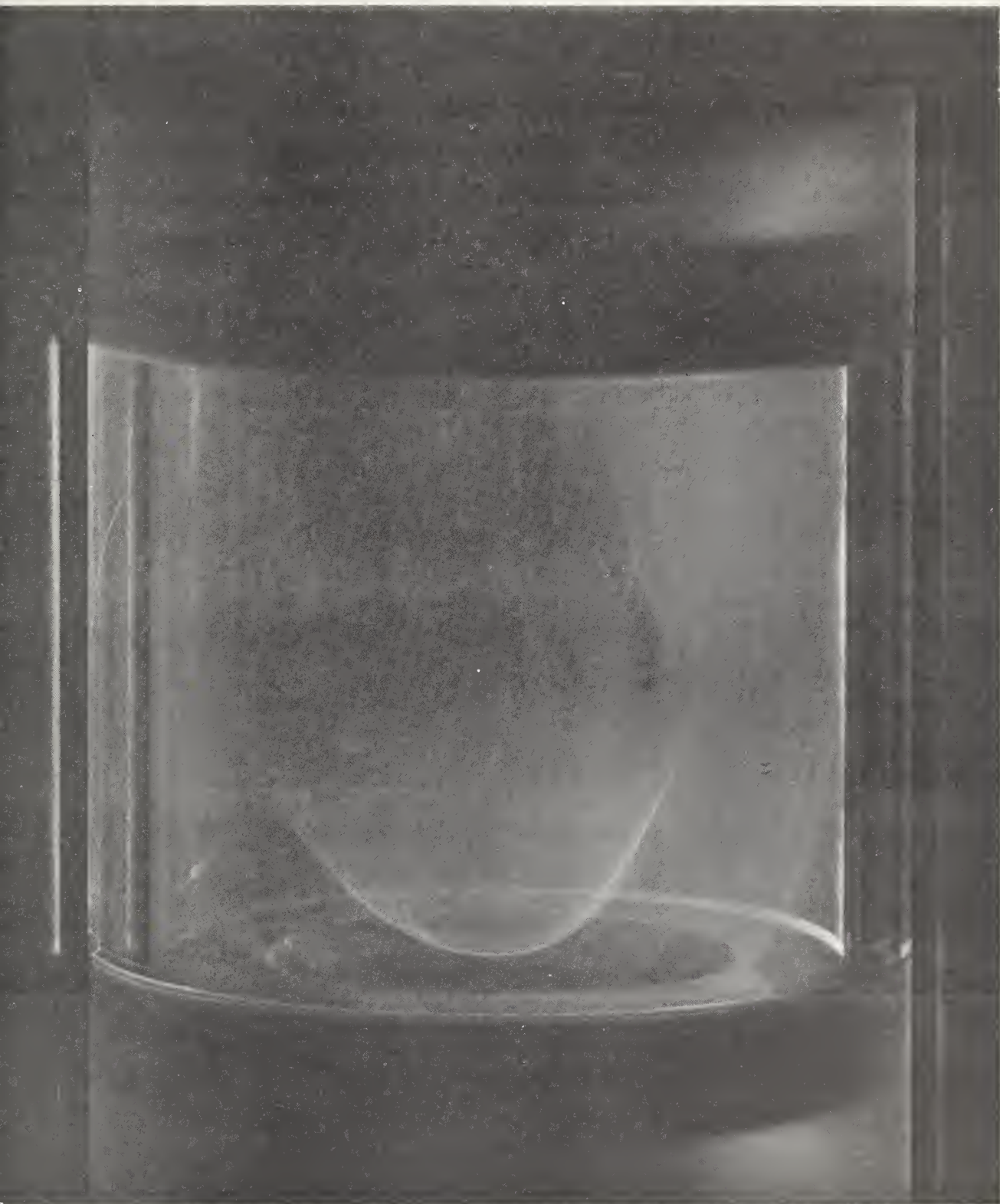
Fig. 5. Interior of Exploding Wire Vessel about an hour after Explosion
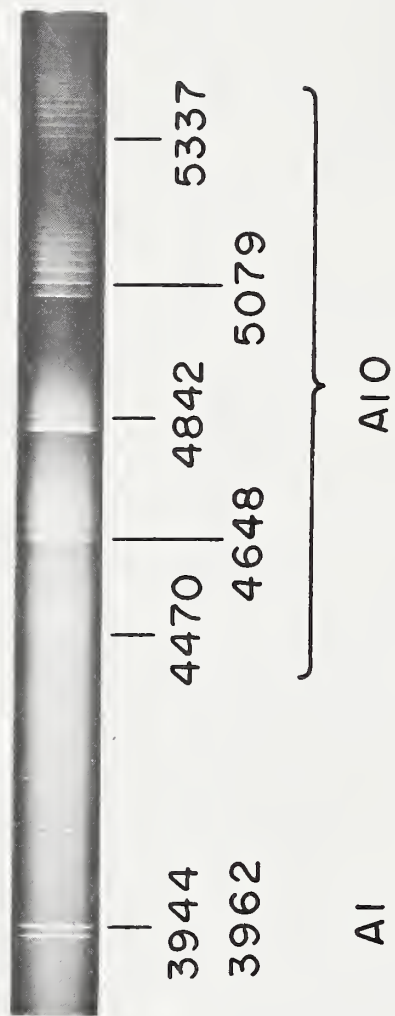
Fig. 6. Integrated Spectrum (3900–5500Å) from an Exploding Wire Experiment. Energy Stored: 15 μF at 14 kV.
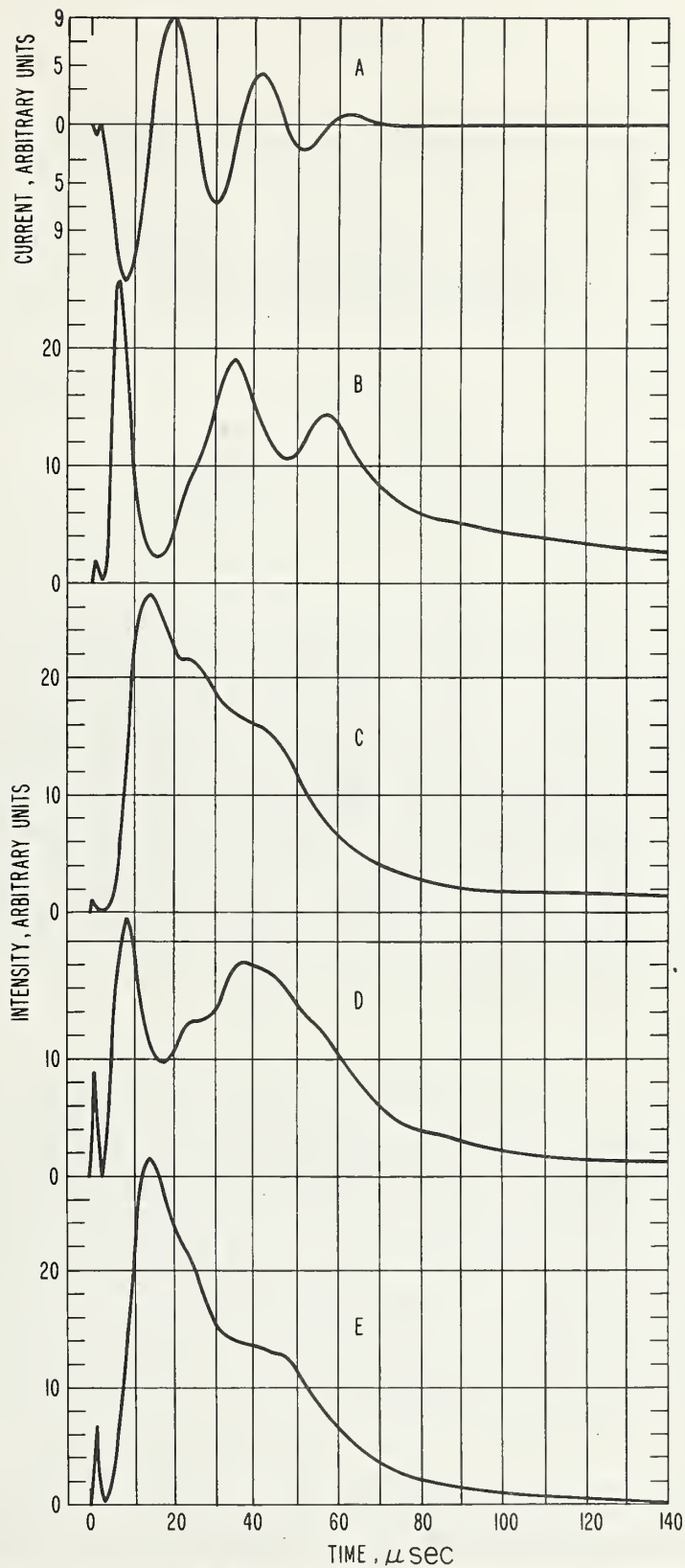
Fig. 7. Discharge Current and Radiation Intensity Measurements. Stored Energy: 60 μF at 12 kV. A = discharge current; B, C, D, E = radiation intensities at 3962 Å (Al-line), 3922 Å (continuum), 5079 Å (AlO band head), and 5119 Å (continuum), respectively.

11

Chapter 2

FORCE FIELDS FOR THE BORON TRIHALIDES

Ira W. Levin
National Institute of Arthritis and Metabolic Diseases
National Institutes of Health
Bethesda, Maryland 20014

and

Stanley Abramowitz
National Bureau of Standards
Washington, D. C. 20234

ABSTRACT

     The method of Edgell and Moynihan for determining Coriolis zeta
constants from the infrared band contours of degenerate vibrational
modes was verified for selected molecules and was then applied to-
ward computing the zeta values for the E symmetry vibrations of the
boron trihalide molecules. Since it is not feasible to define
unique potential functions for BX_3 species from only frequency
data, general force fields were determined for the series by
combining both the Coriolis zeta constants and the observed isotopic
frequency data in a least-squares refinement scheme. The final
force fields indicate that the sensitive stretch-bend interaction
constant is a significantly large negative quantity that decreases
as the series progresses from BF_3 to BI_3.

INTRODUCTION

     The unique specification of general harmonic force fields for
polyatomic molecules usually depends upon supplementing the vibra-
tional secular equation with additional molecular information other
than isotopic frequency data. Rotation-vibration interaction
constants provide a convenient source of additional data for
molecules in which favorable values of the moments of inertia
permit the resolution of the rotational features of their infrared
gas phase bands. These interaction constants, particularly, the
Coriolis zeta constants, are important for determining unique
potential fields, since the coupling data represent moderately
sensitive functions of the force constants.[1,2] As most molecules
display relatively smooth band contours, rather than a resolvable
fine structure, it is necessary to consider alternative methods
to a complete rotational analysis for obtaining the rotation-vibra-
tion interaction information that is implicit in the shapes of the

band envelopes. Edgell and Moynihan examined this problem for spherical and symmetrical top molecules and derived expressions for determining the zeta values of degenerate vibrations from their characteristic band shapes.[3,4]

In this study the method of Edgell and Moynihan was applied toward computing values of the Coriolis zeta constants for the boron trihalide molecules. These data were then used to augment the vibrational frequency data in the determination of the force fields for the BX_3 series.

The vibrational representation for the planar BX_3 configuration of D_{3h} symmetry is $\Gamma_v = A_1 + A_2 + 2E$. The doubly degenerate E species is of principal concern since the measured zeta constants specifically reflect the interaction of the rotational and vibrational angular momenta of these degenerate pairs of vibrations. For the E species, the factored secular determinant requires three symmetrized force constants for a complete specification of the F matrix. Since both boron-10 and boron-11 isotopic frequency data are experimentally available, it appears that a unique force field evaluation is feasible with frequency data alone. However, it will be noted later in the discussion that the additional frequency data is still insufficient for either reliably specifying or limiting the sensitive cross terms in the potential energy expressions. The wide range of values for these cross terms exhibited by the numerous force field calculations for the BX_3 series[5-13] reflects the serious limitations of attempting to characterize a general force field with only frequency data.

EXPERIMENTAL

The four boron trihalides were obtained commercially in sufficient purities for observing their infrared spectra.

Several infrared spectrophotometers were used in obtaining the spectra of the BX_3 molecules. A Perkin-Elmer 112 G spectrophotometer[a], with spectral slit widths of about 0.7 cm^{-1}, was used for the ν_3 vibrations of $BC\ell_3$, BBr_3 and BI_3. A Perkin-Elmer 521 spectrophotometer, with comparable spectral slit widths, was used in observing ν_3 and ν_4 of BF_3, and the ν_3 vibrations of $BC\ell_3$, BBr_3, and BI_3. The ν_4 vibration of $BC\ell_3$ was obtained on a Beckman IR-7 spectrophotometer equipped with a CsI interchange, and the ν_4 fundamental of BBr_3 was determined separately on a Beckman IR-11 and a Perkin-Elmer 301 spectrophotometer.

_____

[a] Certain commercial instruments are identified in this paper in order to specify adequately the experimental procedure. In no case does such identification imply recommendation or endorsement by NBS or NIH.

Unfortunately, the vapor pressure of BI_3 was too low to observe the ν_4 transition at 100 cm^{-1} in a conventional cell, and no spectral information was obtained for this vibration. All spectral results observed on more than one instrument were consistent with one another. The spectra of the boron trihalides were observed with conventional 5 and 10 cm pathlength gas cells. The far infrared spectrum of BBr_3, however, was observed with a multiple pass cell. The high pressure spectra that are discussed in the next section were obtained in a cell that has been previously described.[14]

GAS PHASE BAND CONTOURS

For molecules in which a complete rotational analysis is inapplicable, Edgell and Moynihan establish relationship between the experimentally observed gas phase P and R branch maxima and the Coriolis coupling data of the degenerate vibrational modes. A convenient result for the zeta constants of spherical top molecules is obtained by first expressing an average absorption coefficient $\langle \alpha(\nu) \rangle$ in terms of the rotational energy levels of the P and R branches.[3] The maximum positions for both branches are established by then differentiating this average absorption coefficient with respect to a reduced frequency parameter. Setting this result equal to zero, the final expression related the P-R separation to the zeta constant by

$$\Delta\nu_{P-R} = 4 \; \left(\frac{BkT}{hc}\right)^{1/2} (1 - \zeta_i) \; . \tag{1}$$

$\Delta\nu_{P-R}$ represents the experimental P-R separation, B is the rotational constant, ζ_i is the Coriolis zeta constant for the ith vibration, T is the absolute temperature, and k, h, and c designate the fundamental constants. The validity of this equation depends upon the conditions for which the computed average absorption coefficient corresponds to the actual absorption coefficient. Normally, these conditions are nearly satisfied for heavy molecules at room temperature.

Edgell and Moynihan extended their band structure considerations to the perpendicular bands of symmetric top molecules.[4] Again, a mean absorption coefficient was determined for the P, Q and R branches by considering the contributions from the various transitions to the absorption coefficient at a particular frequency. The expressions were simplified by removing the line shape functions in the definition of the mean absorption coefficient. Approximating the various sums by integrals, the band envelope curves were computed as a function of

a moment of inertia parameter β and the coupling constant ζ. β is defined in terms of the moments of inertia as $(\frac{I_{xx}}{I_{zz}} - 1)$. Since the P-R separation of a band can be measured easily and reliably, while other band contour features tend to be quite sensitive to instrumental conditions and higher order molecular features not necessarily taken into account in this treatment, plots of the P-R separations were presented as a function of zeta for a range of values of the moment of inertia parameter β. Figure 1 displays several computed curves as a function of zeta for the value of β corresponding to that for the BX_3 molecules. The ordinate of the plots is $\overline{\alpha(x)}/\Delta$, where $\overline{\alpha(x)}$ is a mean absorption coefficient in terms of a reduced frequency x, and Δ is a function of the transition moments, the rotational constant, and the band center. The abscissa x is related to the frequency by $\nu = 2(BkT/hc)^{1/2}x$, where ν is in cm^{-1}, and B, k, T, h and c have their usual meanings. The reduced frequency factor x is then a dimensionless quantity.

The validity of the zeta constants that are determined from band contour measurements can be established in several ways. Zeta constants obtained from band shape considerations may be compared directly with the zeta constants from a complete fine structure analysis, or they may be examined from the standpoint of the agreement with the theoretical zeta sum rules.

The only existing comparison between the approximate and exact methods for a zeta value is that for CF_4. Originally, Edgell and Moynihan obtained a value from the band shape for $\zeta_4 = -0.35$; while a subsequent high resolution study of the band structure indicated that $\zeta_4 = -0.344$.[15] The two methods are in excellent agreement.

We have attempted to confirm the validity of the contour method through an application to several hydride molecules; namely, GeH_4, GeD_4, and NH_3. Since the small moments of inertia for the hydrides cause a relatively widely spaced rotational structure, the absorption coefficient rapidly fluctuates as the band is scanned across the narrow lines. The addition of an inert infrared gas to the samples increases the line widths as a function of the total pressure. At a sufficiently high pressure, which is experimentally determined, the rotational structure is smoothed and the absorption coefficient is approximately constant over the slit function. Under these conditions, of an approximately continuous set of rotational energy levels, the experimental integrated absorption coefficient corresponds to the true total

15

band intensity. Thus, as long as pressure induced absorptions which distort the band shape are avoided, the P and R branch maxima obtained from this broadened spectrum correspond to the most probable J values necessary for obtaining a valid P-R separation for subsequent use in the treatments of Edgell and Moynihan.

The rotational structures of the hydrides were completely broadened at pressures of 1000 to 1100 psi of added nitrogen. The adequacy of these broadening pressures was demonstrated by a linear Beer's law plot for the integrated absorption coefficient; that is, plots of $\Gamma p l$ against $p l$ were linear and passed through the origin.[14,18] Γ represents the integrated absorption coefficient, p the sample pressure, and l the cell path length. Table 1 presents the values of $\Delta \nu_{P-R}$ for the broadened spectra and the zeta values calculated by equation (1) and from the curves of reference (4). These computed values compare remarkably well with the zeta values obtained from complete rotational analyses. The value of ζ_4 for the ν_4 vibrations of ammonia was not expected to agree as well with the measured zeta constant since it was necessary to interpolate between the results of the computed curves in reference (4) for $\beta = -0.3$ and $\beta = -0.4$. However, the reasonable agreement with the measured zeta constant lends confidence to the method.

For the ν_4 vibrations of GeH_4 and GeD_4, the Coriolis perturbations that result from the proximity of ν_2 lead to a merging of the Q and P branch structures. Since a P branch maximum cannot be easily established, the zeta constants in Table 1 for these bands were estimated by first doubling the R-Q distance and then by applying equation (1).

Although the zeta constants are functions of the molecular geometry, the atomic masses, and the potential function, it can be demonstrated that the sum of the zeta values is independent of the force field.[17] For example, the zeta sum for the F_2 symmetry species of spherical top molecules assumes the form $\zeta_3 + \zeta_4 = \frac{1}{2}$. Table 1 also gives the comparison for CF_4, GeH_4 and GeD_4 between the measured zeta values and the zeta sum rule. Since the dependence of the zeta constants upon vibrational anharmonicities is not well understood, it is difficult to assess the experimental lack of agreement with the sum rule. However, with the added approximation contained in the zetas from the ν_4 band contours, 5 to 10% discrepancies would not be unreasonable.

One can conclude from the data of molecules in which the coupling constants can be independently calculated that use of gas phase band contours for determining zeta constants appears to be quite reliable. Consequently, it is felt that the method may confidently be applied to molecules for which rotational analyses are impractical. In these cases, the validity of the approximation rests upon the consistency of the data with the zeta sum rule relations.

EXPERIMENTAL BX₃ BAND SHAPES

The gas phase band contours for the ν_3 and ν_4 vibrations of $B^{10}F_3$ and $B^{11}F_3$ are reproduced in Fig. 2. The ν_4 vibrations for the two isotopic species are essentially superimposed. Since the B^{11} isotope is roughly four times as abundant as the B^{10} isotope, the measured P-R separation for the 480 cm^{-1} band was attributed entirely to the B^{11} species. The ν_4 band shape did not exhibit any asymmetry which would reflect distortions due to the B^{10} vibration. These bands show the general correspondence to the calculated curves of Edgell and Moynihan which appear in Fig. 1. A comparison with the calculated curves shows that the ν_3 P-R spacing indicates a relatively large positive zeta constant, while the ν_4 contour reflects a correspondingly large negative coupling constant. The sum rule statement for these molecules is that $\zeta_3 + \zeta_4 = 0$ for the E vibrational modes. This requirement is well satisfied for the B^{11} species.

The ν_4 fundamentals for $BC\ell_3$ were treated analogously as those for BF_3. The ν_3 contours, reproduced in figure 3, however, are complicated by chlorine isotope effects. The isotopic splitting was better observed in a low temperature matrix spectrum in which the intensities and splittings were readily interpreted with the $BC\ell_3$ force field derived in the next section.[18] Zeta constants obtained from the gas phase spectra were both consistent and in reasonable agreement with the zeta sum rule.

No splitting was observed in the ν_3 bands of either BBr_3 or BI_3. A comparison with the computed curves of Fig. 1 show that a high positive zeta constant is predicted. P-R separations corresponding to a zeta constant as large as 0.94 could be resolved with the experimental spectral slit width that was used. Therefore, the zeta constant lay in the range between 0.94 and 1.0.

The contour of BBr_3 at 150 cm^{-1} was observed. Within the error of the measurement of the P-R separation, ζ_4 fell within the range between -0.92 and -1.0. A value of -0.95 ±0.05 was considered representative for this coupling parameter.

No contour was observed for the ν_4 band of BI_3 as a consequence of its low vapor pressure. However, since a large positive zeta value was predicted from the ν_3 vibrations, the value for $\zeta_3 = +0.95$ ±0.05 for the B^{10} and B^{11} species probably covers the range adequately for this interaction coupling constant.

A compilation of the observed frequencies, P-R separations and computed zeta constants for BF_3, $BC\ell_3$, BBr_3 and BI_3 are found in Table 2.

17

The errors in the zeta constants shown in Table 2 are calculated from the maximum and minimum differences in the P-R separations. The necessary rotational constants B for BCl_3, BBr_3, and BI_3 were calculated from the interatomic distances listed in Table 3, while B for BF_3 was obtained from a rotational analysis for the ν_2 vibration.[19] The calculation of $\Delta\nu_{P-R}$ in terms of the parameter x was determined at T equal 300°K. As stated earlier, it is difficult to assess completely the error associated with the zeta constants obtained from band contours. The uncertainties in the P-R separation can be limited to less than 0.5 cm^{-1} by averaging several scans, if necessary. The final judgment of the validity of the zeta constants lies in the sum rule statement. For the purposes of the normal coordinate calculation, the values for ζ_4 for BI_3 and BBr_3 were considered to have a ten percent uncertainty, while the other zeta constants were felt to reflect only a five percent error. Table 2 indicates good agreement for the coupling constants with the sum rules for BF_3 and BCl_3. In addition, the final coupling values are consistent within the entire BX_3 series.

NORMAL COORDINATE ANALYSIS

The difficulty of determining a unique force field for the BX_3 molecules arises in the solution of the vibrational secular determinant for the E symmetry species, since this factored block requires three symmetrized force constants for a complete specification of the force field. The observed frequencies, rather than the harmonic frequencies were used in the secular determinant. This is not unreasonable since the observed product rule values agree quite well with the calculated values, as shown in Table 4.[20]

The vibrational secular equation is customarily solved in the form

$$|GF - \lambda_K E| L = 0 \ , \tag{2}$$

where the G matrix, which is only a function of the atomic masses and the molecular geometry, represents terms related to the kinetic energy of the molecule, and the F matrix characterizes the force field. $\lambda_K = 4\pi^2 c^2 \tilde{\nu}^2_K/N$, where $\tilde{\nu}_K$ is the observed vibrational frequency, N is Avogodro's number, and c is the velocity of light. The E and L matrices in equation (2) represent the identity matrix and the eigenvector matrix, respectively. The vibrational problem is carried out in terms of the symmetry coordinates that are defined for the E species in Fig. 4.

If one considers only the B^{10} isotope, the three elements of the E block of the F matrix cannot be determined from the two observed vibrations, ν_3 and ν_4. The added data from the B^{11} isotope in the form of

two more observed frequencies should give the extra equations necessary for making the problem determinate. The equations that arise from expanding the secular determinant for each isotope form ellipses, whose intersections indicate the solutions in terms of the force constants. However, the lower portions of Figs. 5-8 demonstrate the difficulty that can arise in only using frequency information in solving the vibrational problem. Only the portions of the ellipses that are of interest appear in the figures. The diagonal force constants, F_{33} and F_{44}, the symmetrized stretching and bending force constants, respectively, are plotted as a function of the sensitive interaction force constant F_{34} for each isotope of the BX_3 series. In the figures, the B^{10} species is represented by a solid line, while the dotted line characterizes the B^{11} isotope. The figures show that the intersections of the ellipses are not obvious; that is, the solutions for both isotopes are nearly superimposable for each species. Therefore, in this series of molecules, the indistinguishability of unique solutions indicates the inadequacy of frequency data used alone for calculating a force field.

The top portions of Figs. 5-8 demonstrate the functional relationship between the force field and the Coriolis zeta constants. The solid and dotted lines represent the calculated zeta constants for the force fields given in the lower part of the figures for both the B^{10} and B^{11} species. These curves were calculated from the eigenvectors and a C matrix by the expression

$$\zeta^z = L^{-1} C^z (L')^{-1} \tag{3}$$

The L and L^{-1} matrices are the transformation matrices from symmetry coordinates to normal coordinates Q and vice-versa:

$$S = LQ \tag{4}$$

$$Q = L^{-1}S \tag{5}$$

The C^z matrix is easily derived and is a function of the geometry and masses of the molecule.[21] The elements of the C^z matrix are given by the relation

$$C^z_{ij} = e^z \cdot \sum_a \mu_a (s_{ia} \times s_{ja}) . \tag{6}$$

This equation is closely related to the expression for determining the G matrix elements; that is, s_{ia} and s_{ja} are the Wilson s-vectors for infinitesimal atomic displacements.[22] μ_a designates the reciprocal masses of the atoms and e^z is the unit vector in the Z direction. The summation is made for the atoms whose motion is involved in the symmetrized displacement. In order for the C^z matrix to factor correctly,

19

the symmetry coordinates must be oriented properly, as shown in Fig. 4. The diagonal elements of ζ^Z are $\zeta^Z_{3a,3b}$ and $\zeta^Z_{4a,4b}$, which we have abbreviated by ζ_3 and ζ_4. The ja, jb subscripts designate the degenerate pairs of symmetry coordinates, while the Z superscript indicates the angular momentum in the positive Z direction.

The curves for the zetas represent reasonably sensitive functions of the force constants. Consequently, by stipulating the zeta constants, denoted by solid circles on the zeta plots, it is possible to narrow the range of force constants that are consistent with the observed data.

The additional coupling data now offer the possibility of refining the force field over the entire set of observables; that is, determining the force field that best reproduces the observed frequencies and zeta constants. The mechanism of the force constant adjustment procedure first consists of solving the secular determinant with an approximate set of force constants. Since the resulting eigenvalues do not usually correspond to the observed frequencies, corrections to the elements of the force constant matrix are desired such that a final set of force constants are the best least-squares fit of the calculated frequencies to the observed frequencies. This calculation has been discussed in several places with the following result for the relation between the force constant corrections, ΔF, and the frequency deviations, Δ[23-25]:

$$L'\Delta F L = \Delta_\Lambda \tag{7}$$

This derivation assumes that the corrections are small and that the zero-order normal coordinates closely approximate the true eigenvectors. The Jacobian matrix J necessary for each least-squares cycle in the refinement is written as

$$J_\Lambda \Delta F = \Delta_\Lambda \tag{8}$$

The Jacobian of the zeta constants with respect to the force constants is now desired. For convenience, the following expression for relating the coupling data to the force field has been utilized:

$$L'FC(L')^{-1} = \Lambda\zeta \ , \tag{9}$$

where all terms have been previously defined. To the level of approximation of neglecting the higher order corrections to the L vectors as the F matrix is corrected, expressions analogous to equations 7 and 8 are obtained:

$$L'\Delta FC(L')^{-1} = \Delta(\Lambda\zeta), \tag{10}$$

and

$$J_{\Lambda\zeta}\Delta F = \Delta(\Lambda\zeta) \tag{11}$$

20

The complete J matrix for the least-squares refinement is then

$$J = \frac{J_\Lambda}{J_{\Lambda\zeta}}$$ (12)   while the error vector ΔD is

$$\Delta D = \frac{\Delta(\Lambda\zeta)}{(\Lambda\zeta)}$$ (13)

Following Overend and Scherer, the least-squares solutions of the normal equations for ΔF, as well as a statistical analysis for each refinement cycle, were obtained in the form[25,26]

$$\Delta F = (J'PJ)^{-1} J'P(\Delta D)$$ (14)

$$\sigma\{\overline{F}\} = \left\{ (J'PJ)_{ii}^{-1} \right\}^{1/2} \left\{ \Delta D'P\Delta D/N{-}M \right\}^{1/2}.$$ (15)

P is a weight matrix, N is the number of observed data, and M is the number of unknown parameters.

The weights for the frequencies were taken proportional to $(1/\lambda)$, while the weights for the $(\Lambda\zeta)$ terms reflected the 5-10% errors in the zeta constants, as well as the uncertainty in the frequency factor λ. For example, ζ_4 for BBr_3 and ζ_3 for BI_3 were weighted appropriately for a 10% error in these data. The final values of both the force constants and their dispersions for different weight possibilities did not suggest that varying the weight choice was critical.

DISCUSSION

During the refinement process, the tendency for the solutions to vary slowly over a relatively narrow range, rather than convergin to one set of values, was found. Aldous and Mills[2] attribute this behavior to the near singularity of the $(J'PJ)$ matrix. Although the values of $|J'PJ|$ were of the order of 10^{-3} or 10^{-4}, the matrix elements of $(J'PJ)^{-1}$ were not of a magnitude to cause either rounding errors in the inversion scheme or large uncertainties in the force constants. The slow variation of the force constants is indicative of a very high correlation between the F_{33} force constant and the inter-action force constant F_{34}. Thus, if a correlation matrix C is defined such that its elements are[26]

$$C_{ij} = A_{ij}^{-1}/(A_{ii}^{-1})^{1/2}(A_{jj}^{-1})^{1/2},$$ (16)

then the C_{ij} terms are measures of the degree of linear dependence between the i and j. terms. In this expression, matrix A is equal to (J'PJ). One finds for the BX_3 series that F_{33} and F_{34} are correlated by values of the order of -0.98 and -0.99. That is, values of -1.0 would indicate that the two force constants are completely linearly related. It is possible that large dispersions may be found for highly correlated force constants when they are adjusted independently in the refinement scheme.[23] In the present calculation, however, the added coupling data obviated any constraints upon either of the strongly dependent force constants.

The vertical dotted lines on figures 5-8 represent the preferred choices for the force field for the E species. For the calculations whose solutions varied, the preferred solution was that with the smallest dispersions in the force constants. In the case of BI_3 the two dotted lines on the plot indicate the limits for the probably values. Table 6 lists the preferred solutions for the series. The values of the force constants for BI_3 were obtained by setting $\zeta_3 = +0.95$ with an associated weight reflecting a 10% error. A comparison between the observed and calculated data, using the final set of force constants, appears in Table 7.

Table 6 also contains a summary of the force constants for the A_1 and A_2 species. Since only one vibration appears in each symmetry species, the symmetrized F elements are easily found from a first degree equation. Dispersions are listed only for the E species force constants.

A comparison of the force constants of the BX_3 series indicates that the stretch-bend interaction constant, F_{34}, is a significantly large negative quantity, decreasing as the series progresses from BF_3 to BI_3. The significance of the actual values of the dispersions of the force constants may be questioned since the difference between the number of equations and the number of unknowns is small. However, the relatively small dispersions do indicate that the interaction force constant can be specified within narrow limits through the use of rotation-vibration interaction data.

ACKNOWLEDGMENTS

REFERENCES

1. J. L. Duncan and I. M. Mills, Spectrochim. Acta 20, 523 (1964).

2. J. Aldous and I. M. Mills, Spectrochim. Acta 19, 1567 (1963).

3. W. F. Edgell and R. E. Moynihan, J. Chem. Phys. 27, 155 (1957).

4. R. E. Moynihan, Ph. D. Thesis, Studies in Molecular Spectroscopy:
    The Influence of Coriolis Coupling on Infrared Band Shapes,
    Purdue University, 1954.

5. L. Beckman, L. Gutjahr, and R. Mecke, Spectrochim. Acta 21,
    141 (1965).

6. J. L. Duncan, J. Mol. Spectroscopy 13, 338 (1964).

7. J. A. Ladd, W. J. Orville-Thomas, and B. C. Cox, Spectrochim.
    Acta 19, 1911 (1963).

8. S. J. Cyvin, Acta Chem. Scand. 13, 334 (1959).

9. C. W. F. T. Pistorius, J. Chem. Phys. 29, 1174 (1958).

10. T. Wentink and V. H. Tiensuu, J. Chem. Phys. 28, 826 (1958).

11. L. P. Lindeman and M. K. Wilson, J. Chem. Phys. 24, 242 (1956).

12. W. R. Heslop and J. W. Linnett, Trans. Faraday Soc. 49, 1262 (1953).

13. D. C. McKean, J. Chem. Phys. 24, 1002 (1956).

14. I. W. Levin, J. Chem. Phys. 42, 1244 (1965)

15. A. Maki, E. K. Plyler, R. Thibault, J. Chem. Phys. 37, 1899 (1962).

16. Unpublished data.

17. H. C. Allen, Jr. and P. C. Cross, Molecular Vib-Rotors, John Wiley
    and Sons, Inc., New York (1963).

18. J. J. Comeford, S. Abramowitz, and I. W. Levin (to be published).

19. A. H. Nielsen, J. Chem. Phys. 22, 659 (1954).

20. The anharmonicity factors may be estimated from the product rule expressions, if the anharmonicities for ν_4 and ν_4' are considered equal. (The primed quantity represents the B^{11} isotope.) Thus, the anharmonicity factors x_i can be calculated from the following relations:

$$\frac{\nu_3 \nu_4 \ (1 + x_3)}{\nu_3' \nu_4' \ (1 + x_3')} = \text{product rule values,}$$

and

$$x_i' = (\nu_i'/\nu_i) x_i \ .$$

The observed and calculated product rule values are found in Table 4. The anharmonicity factors are listed in Table 5. x_4 and x_4' were estimated from the product rule relations applied to the ν_2 vibration for each member of the series. Since the corrections seem large for the ν_3 vibrations of BF_3 and $BC\ell_3$, possibly from the inherent uncertainty associated with the general approximations, the anharmonic, or observed frequencies, were used for the entire BX_3 set in the normal coordinate analysis.

21. J. H. Meal and S. R. Polo, J. Chem. Phys. 24, 1126 (1956).

22. E. B. Wilson, J. C. Decius, and P. C. Cross, Molecular Vibrations, McGraw-Hill Book Co., Inc., New York (1955).

23. T. Shimanouchi and I. Suzuki, J. Chem. Phys. 42, 296 (1965).

24. J. H. Schachtschneider and R. G. Snyder, Spectrochim. Acta 19, 117 (1963).

25. J. Overend and J. R. Scherer, J. Chem. Phys. 32, 1289 (1960).

26. N. Arley and K. R. Buch, Introduction to the Theory of Probability and Statistics (John Wiley and Sons, Inc., New York, 1950).

Table 1. A comparison between the zeta values obtained from the method of Edgell and Moynihan and from complete rotational analyses. Values for the zeta sum rules are also given.

	$\Delta\nu_{P-R}$ cm^{-1}	ζ_1^{calc}	ζ_1^{meas}	$\Sigma\zeta_1$	Sum Rule
CF$_4$					
ν_3	4.9	+0.80[a]			
ν_4	34.4	-0.35[b]	-0.344[c]		
				0.45	0.50
GeH$_4$					
ν_3	98.0	-0.04	-0.042[d]		
ν_4	40.0	0.58[e]			
				0.54	0.50
GeD$_4$					
ν_3	69.0	-0.02	-0.025[d]		
ν_4	31.0	0.54[e]			
				0.52	0.50
NH$_3$					
ν_4	182.0	-0.20	-0.255[f]		

[a] S. Abramowitz and R. P. Bauman, Spectrochim. Acta 17, 25 (1964).

[b] Reference 3.

[c] Reference 15.

[d] L. P. Lindeman and M. K. Wilson, Z. Phys. Chem. (N. F.) 9, 29 (1956).

[e] These values were obtained by doubling the R-Q separation and then by applying equation (1).

[f] W. S. Benedict and E. K. Plyler, Can. J. Phys. 35, 1235 (1957).

Table 2. The observed data for the BX_3 series. $\Delta\nu_{P-R}$ represents the P-R separation in cm^{-1}. The frequencies are in cm^{-1}; the ζ_i are dimensionless.

	Observed frequency cm^{-1}	$\Delta\nu_{P-R}$	ζ_i
$B^{10}F_3$			
ν_3	1504.7	9.5	0.70 ± 0.04
ν_4	482.0		
$B^{11}F_3$			
ν_3	1453.6	11.0	0.64 ± 0.03
ν_4	480.4	35.5	-0.66 ± 0.03
$B^{10}Cl_3$			
ν_3	994.0	3.5	0.80 ± 0.04
ν_4	255.0		
$B^{11}Cl_3$			
ν_3	954.0	3.8	0.78 ± 0.04
ν_4	255.0	20.0	-0.73 ± 0.04
$B^{10}Br_3$			
ν_3	856		(≥ 0.94)
ν_4	151		
$B^{11}Br_3$			
ν_3	819		(≥ 0.94)
ν_4	151	13.2	-0.95 $(-0.92 \leq \zeta_4 \leq -1.0)$

Table 2 continued

	Observed frequency cm^{-1}	$\Delta\nu_{P-R}$	ζ_i
$B^{10}I_3$			
ν_3	737		(≥ 0.94)
ν_4	100		
$B^{11}I_3$			
ν_3	704		(≥ 0.94)
ν_4	100		-0.95[a]

[a]
The value for ζ_4 for BI_3 was estimated on the basis of the trend for the zeta constants in the BX_3 series. The other zeta values were obtained from P-R separation considerations.

Table 3. Structural data for the BX_3 series.

Molecule	Bond length Å
BF_3	1.295[a]
BCl_3	1.73[b]
BBr_3	1.87[b]
BI_3	2.10[c]

All valence angles are equal to $120°$.

[a] Reference 19.

[b] H. A. Levy and L. O. Brockway, J. Am. Chem. Soc. _59_, 2085 (1937).

[c] Reference 10.

Table 4. Product rule relations for the E species for the BX_3 series.

	Observed	Calculated[a]
BF_3	1.0352	1.0409
BCl_3	1.0419	1.0443
BBr_3	1.0452	1.0467
BI_3	1.0426	1.0475

a
The product rule values were calculated from the ratios of the appropriate
G matrix determinants.

Table 5. Estimated anharmonicity factors for the BX_3 series. Refer to footnote 20 for a discussion of these values.

Vibration	$B^{10}F_3$	$B^{11}F_3$
ν_2	0.058	0.056
ν_3	0.068	0.066
ν_4	0.06	0.06
	$B^{10}Cl_3$	$B^{11}Cl_3$
ν_2	0.019	0.018
ν_3	0.061	0.059
ν_4	0.02	0.02
	$B^{10}Br_3$	$B^{11}Br_3$
ν_2	0	0
ν_3	0.035	0.033
ν_4	0	0
	$B^{10}I_3$	$B^{11}I_3$
ν_2	0	0
ν_3	0.012	0.012
ν_4	0	0

Table 6. Force constants for the BX$_3$ series. Dispersions, $\sigma\{\overline{F}\}$, are given for the E species. All force constants were fit to the observed vibrational frequencies and Coriolis zeta constants. The units are expressed in millidynes/Å.

Species	Force Constant	BF$_3$ $\overline{F}$	$\sigma\{\overline{F}\}$	BCl$_3$ $\overline{F}$	$\sigma\{\overline{F}\}$	BBr$_3$ $\overline{F}$	$\sigma\{\overline{F}\}$	BI$_3$ $\overline{F}$	$\sigma\{\overline{F}\}$
A$_1$	$F_{11} = fr + 2frr$	8.82		4.63		3.64		2.70	
A$_2$	$F_{22} = f_\tau$[a]	0.86		0.41		0.29		0.24	
E	$F_{33} = fr - frr$	7.82	0.06	4.19	0.05	2.80	0.02	2.25	0.01
	$F_{34} = fr\alpha - fr\alpha'$	-0.81	0.03	-0.51	0.02	-0.20	0.006	-0.17	0.004
	$F_{44} = f\alpha - f\alpha\alpha$	0.50	0.002	0.25	0.002	0.19	0.001	0.13	0.001

a
The coordinate τ represents the out-of-plane displacement of the atoms.

Table 7. The observed and calculated frequencies and zeta constants for the BX_3 molecules. The frequencies are in cm^{-1}. The zeta constants are dimensionless.

	OBSERVED VALUES		CALCULATED VALUES	
Molecule	Frequency	ζ_1	Frequency	ζ_1
$B^{10}F_3$				
ν_3	1504.7		1504.0	
ν_4	482.0		482.5	
ζ_3		0.70		0.70
$B^{11}F_3$				
ν_3	1453.6			
ν_4	480.4			
ζ_3		0.64		0.67
ζ_4		-0.66		-0.67
$B^{10}Cl_3$				
ν_3	994.0			
ν_4	255.0			
ζ_3		0.80		0.79
$B^{11}Cl_3$				
ν_3	954.0		955.2	
ν_4	255.0		254.4	
ζ_3		0.78		0.77
ζ_4		-0.73		-0.77
$B^{10}Br_3$				
ν_3	856.0		856.0	
ν_4	151.0		151.1	
$B^{11}Br_3$				
ν_3	819.0		819.0	
ν_4	151.0		150.9	
ζ_4		-0.95		-0.94
$B^{10}I_3$				
ν_3	737.0		736.8	
ν_4	100.0		100.1	0.95
ζ_3		0.95		$\downarrow$
$B^{11}I_3$				
ν_3	704.0		704.2	
ν_4	100.0		99.9	
ζ_3		0.95		0.95

BAND ENVELOPES FOR SYMMETRIC TOP MOLECULES (BX₃)

Calculated by W. Edgell and R.E. Moynihan
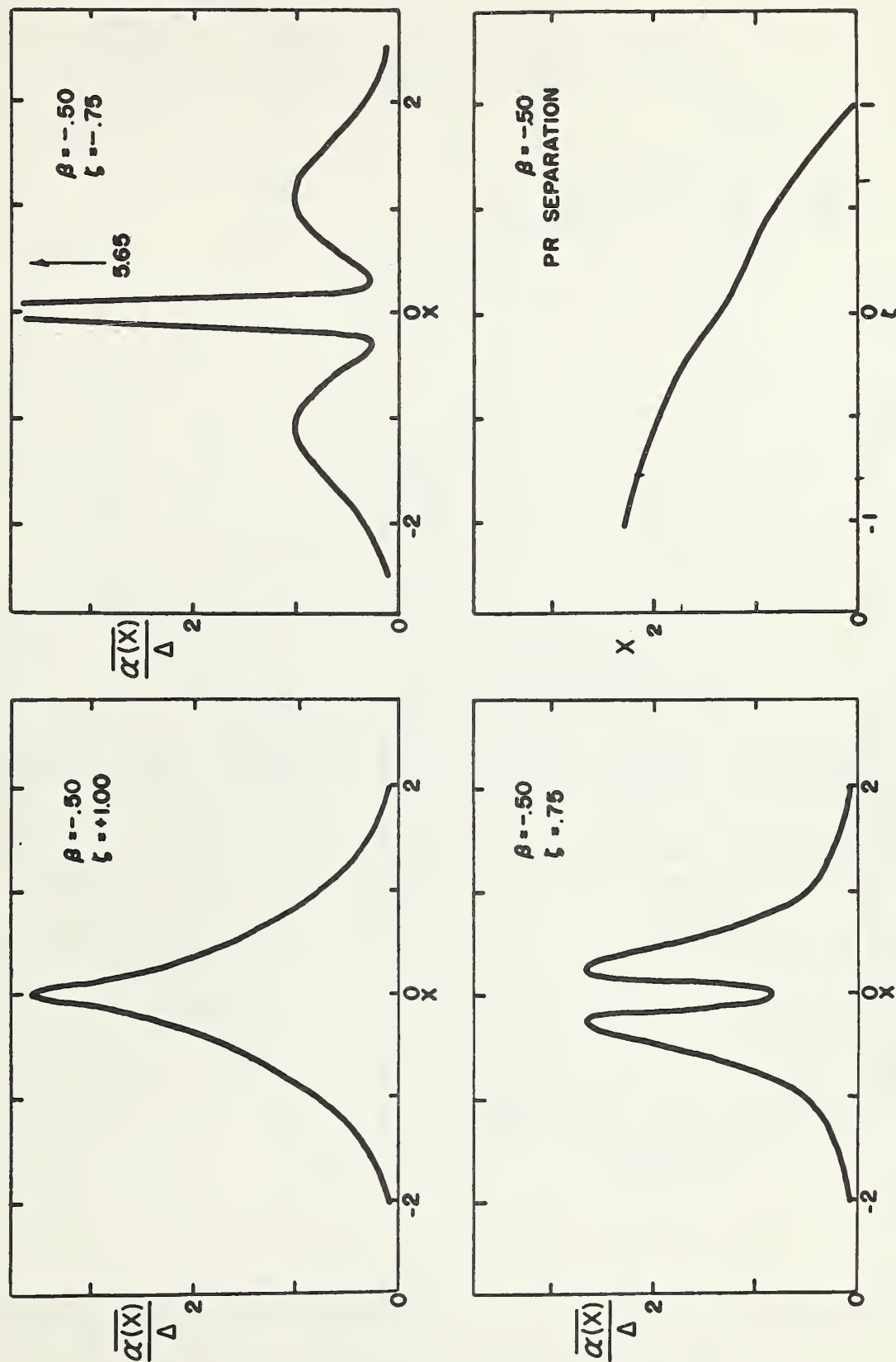
Fig. 1. Computed band envelopes for the BX₃ molecules for $\beta = -0.50$ and for selected values of the zeta constant. A more complete set of curves are found in reference (1).
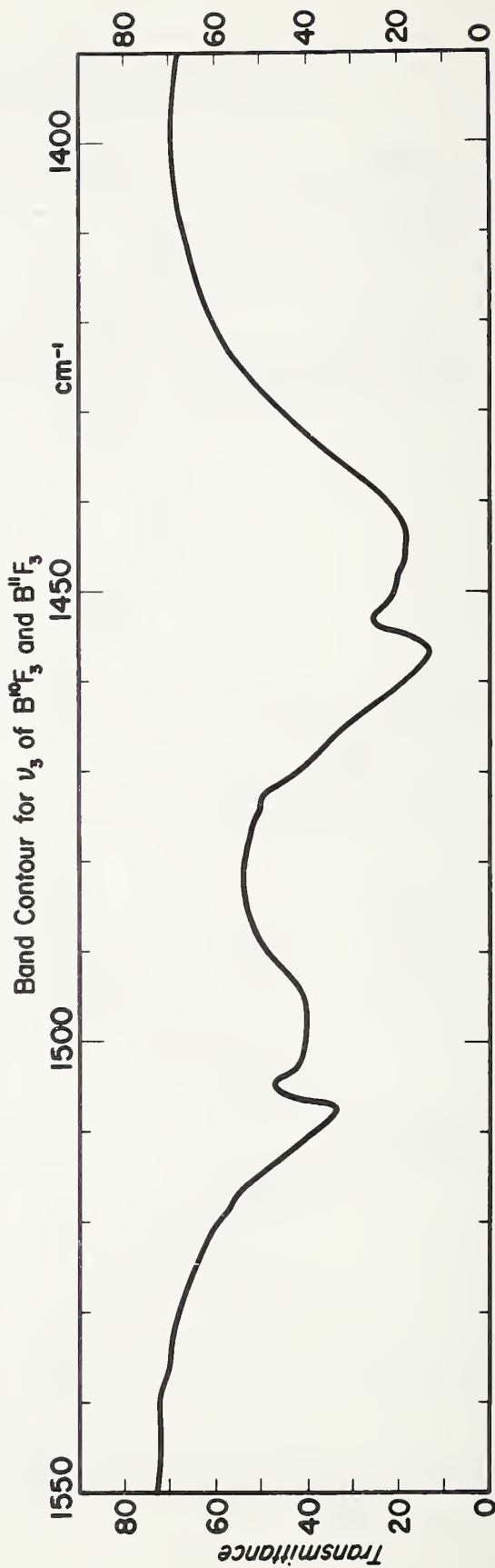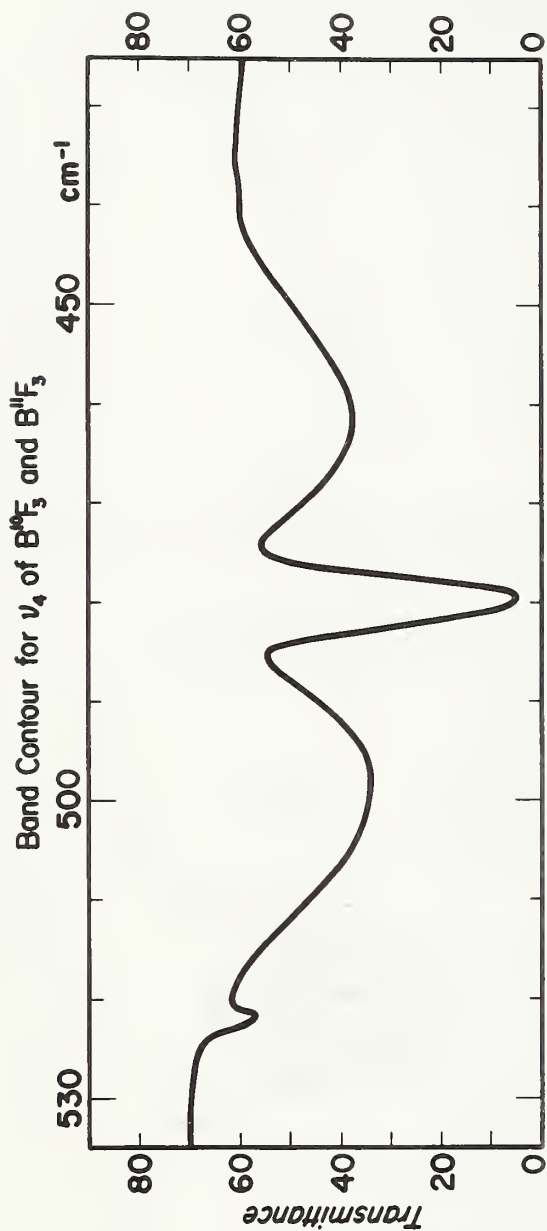
Fig. 2. Observed infrared gas phase contours for the degenerate modes of BF_3.
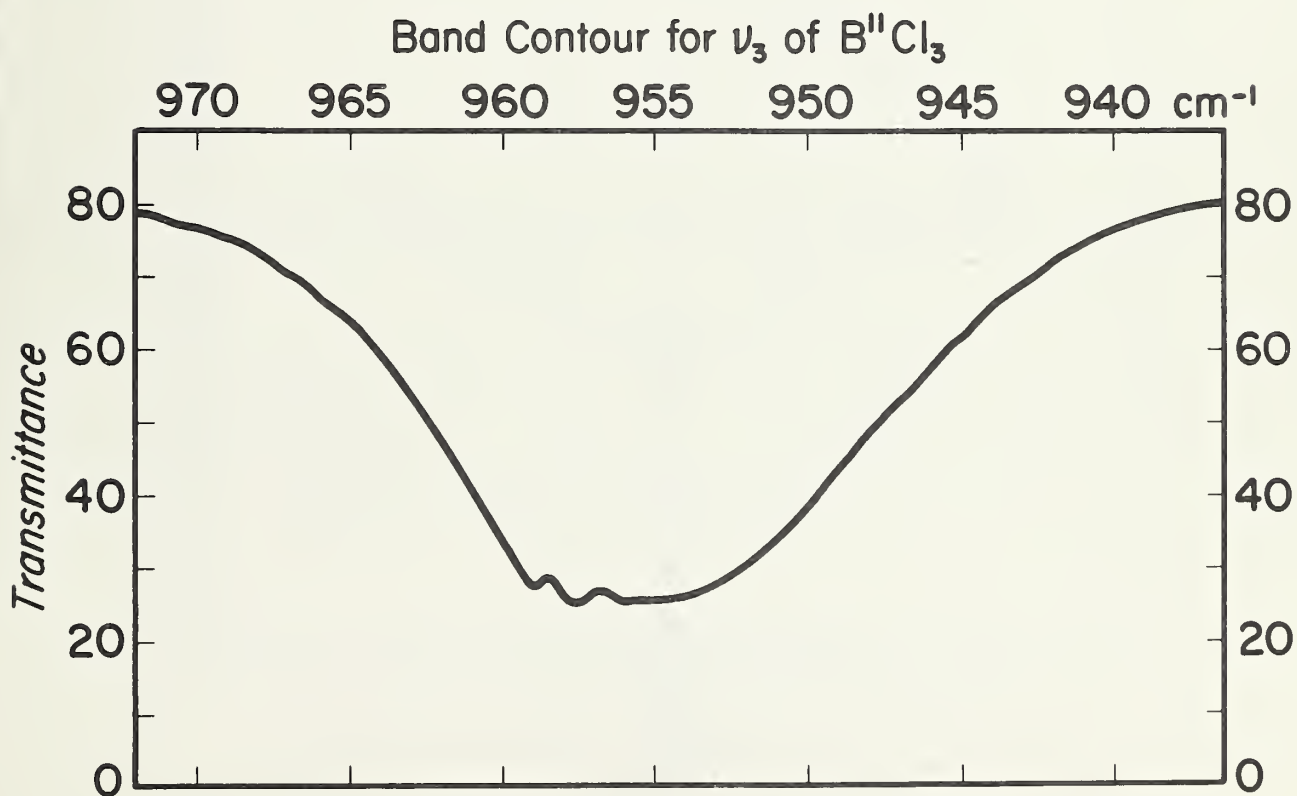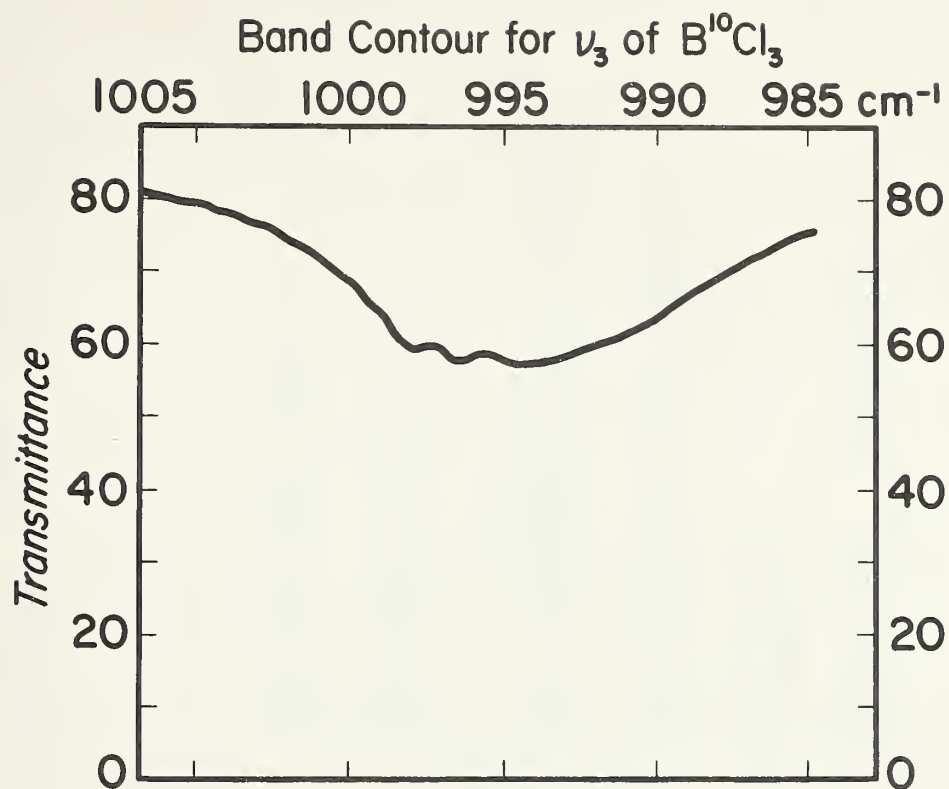
Fig. 3. Observed infrared gas phase contours
for the ν_3 modes of BCl_3.

SYMMETRY COORDINATES

E Species

$$S_{3a} = \frac{1}{\sqrt{6}}\left(\Delta r_2 + \Delta r_3 - 2\Delta r_1\right)$$

$$S_{4a} = \frac{r_0}{\sqrt{6}}\left(\Delta\alpha_{13} + \Delta\alpha_{12} - 2\Delta\alpha_{23}\right)$$

$$S_{3b} = \frac{1}{\sqrt{2}}\left(\Delta r_2 - \Delta r_3\right)$$

$$S_{4b} = \frac{r_0}{\sqrt{2}}\left(\Delta\alpha_{13} - \Delta\alpha_{12}\right)$$
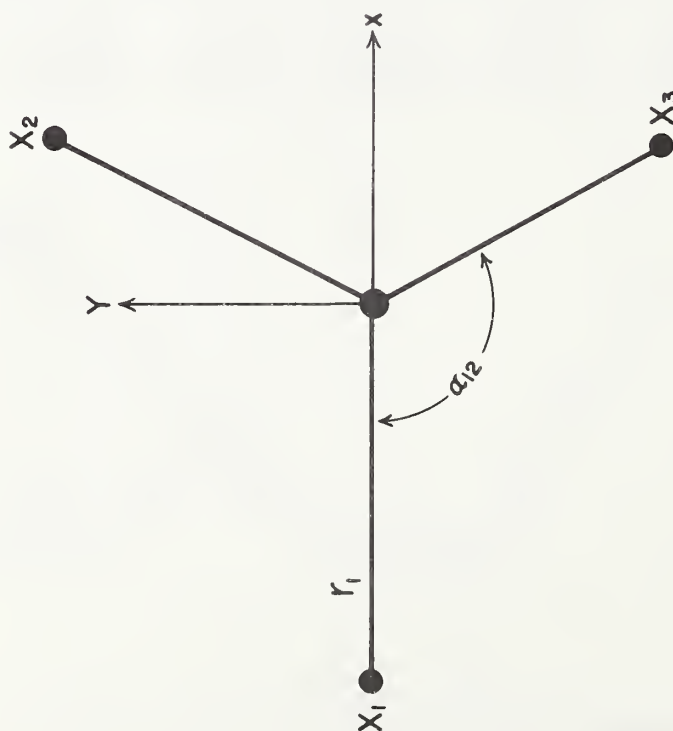
Fig. 4. Symmetry coordinates for the BX_3 molecules.
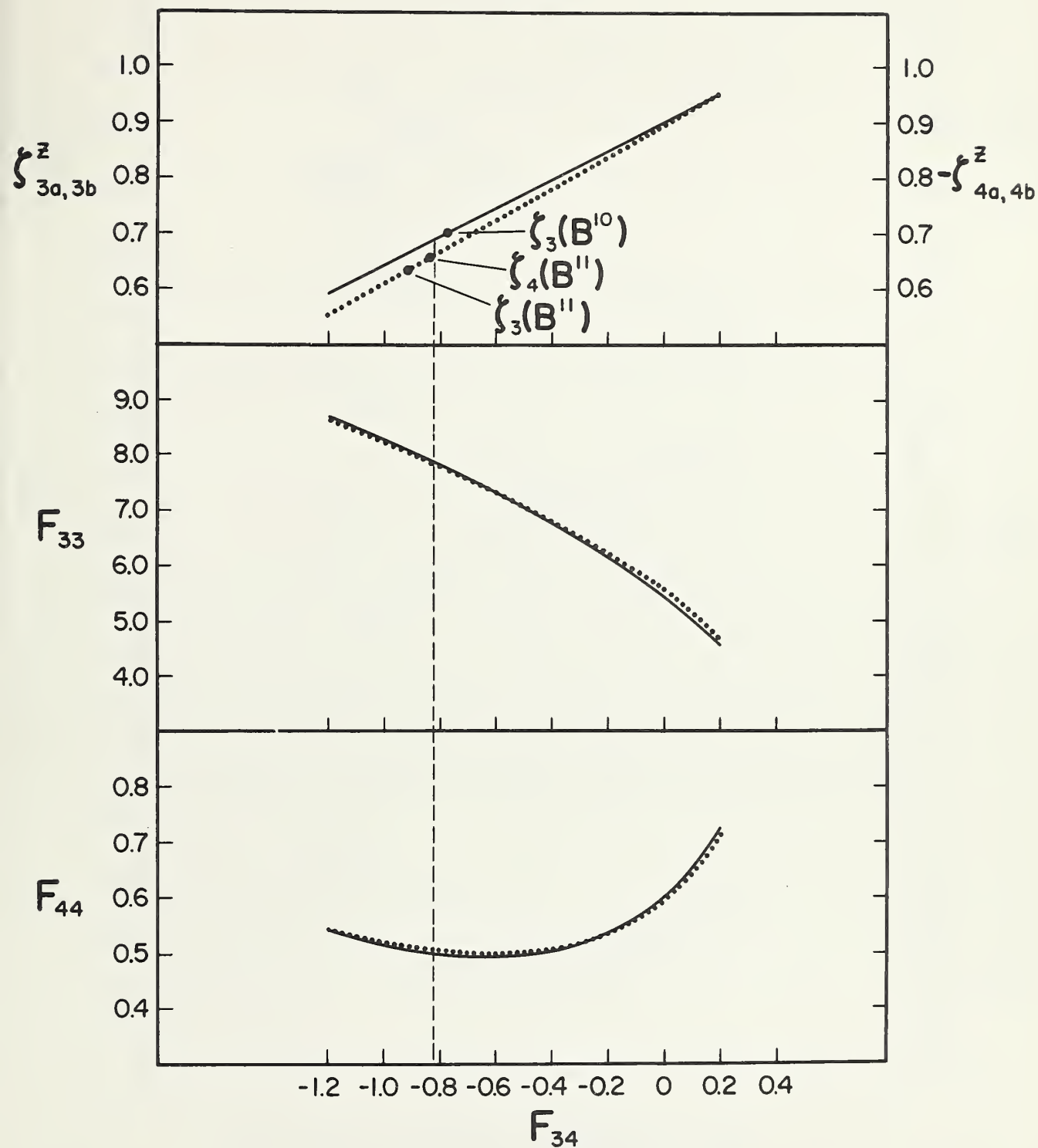
Fig. 5. Plots of F_{33}, F_{44}, $\zeta_{3a,3b}^z$, and $-\zeta_{4a,4b}^z$ as a function of F_{34} for the E symmetry species of the BX_3 molecules. The solid and dotted lines represent the B^{10} and B^{11} isotopes, respectively.

37
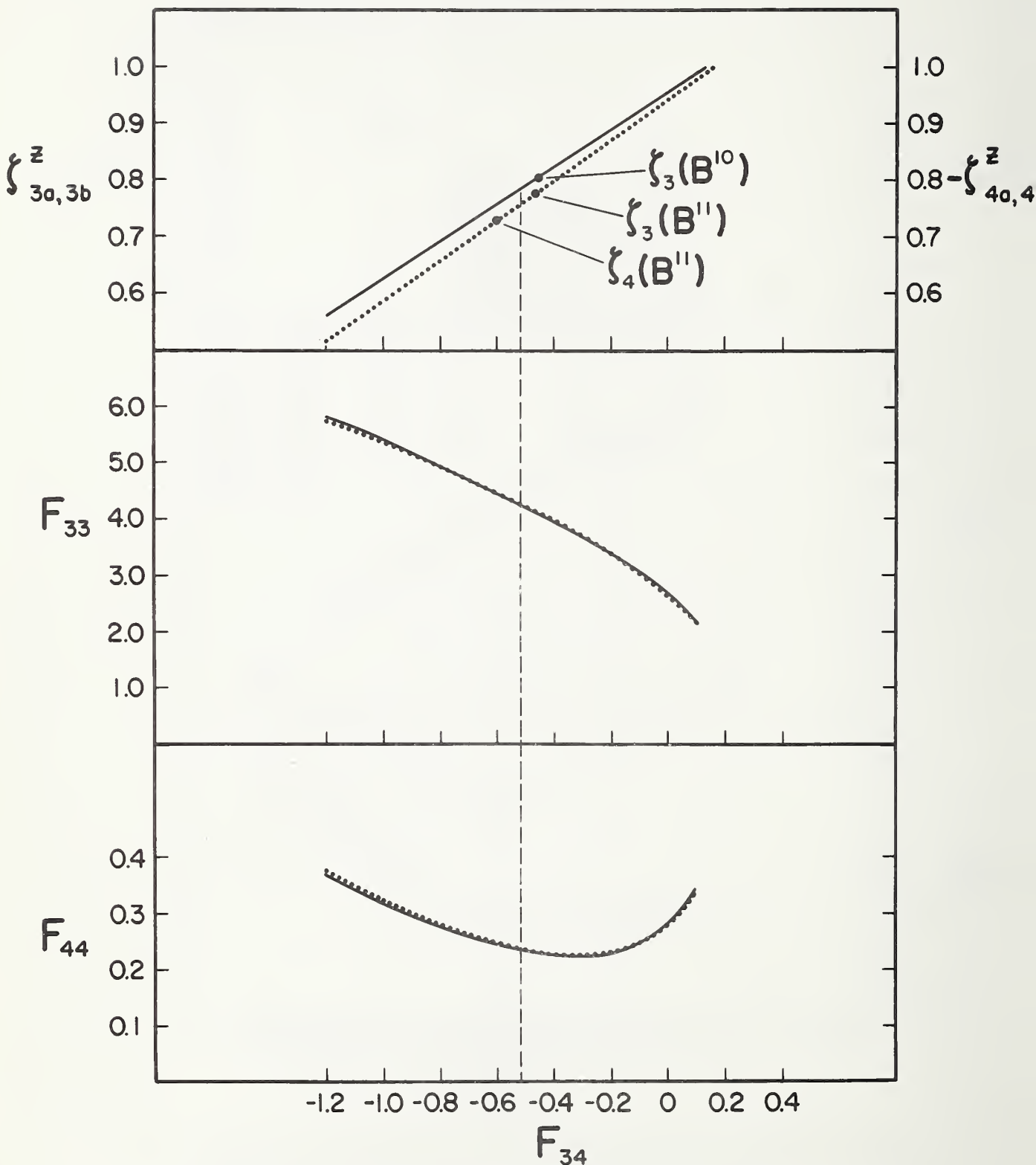
Fig. 6. Plots of F_{33}, F_{44}, $\zeta^z_{3a,3b}$, and $-\zeta^z_{4a,4b}$ as a function of F_{34} for the E symmetry species of the BX_3 molecules. The solid and dotted lines represent the B^{10} and B^{11} isotopes, respectively.
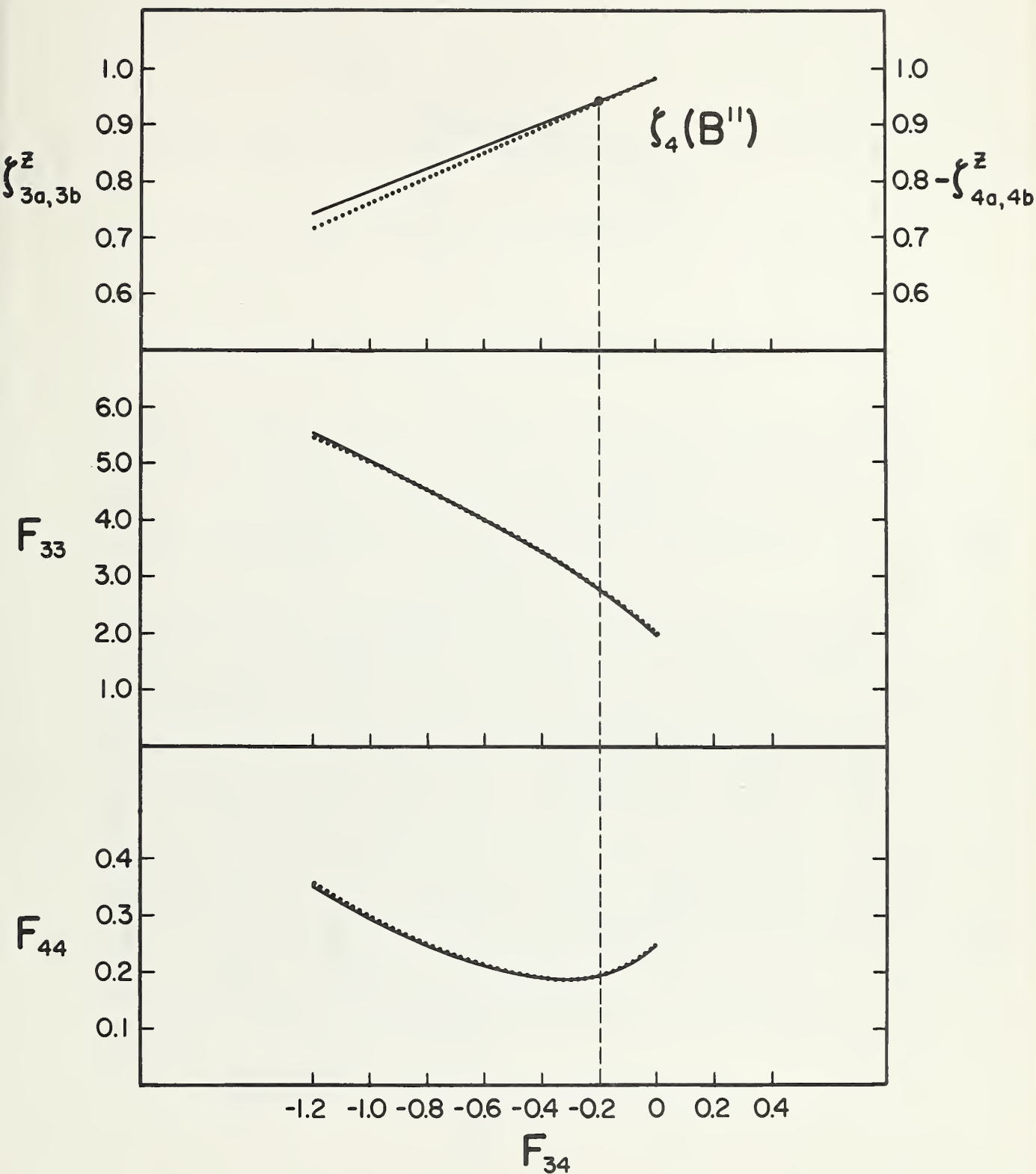
Fig. 7. Plots of F_{33}, F_{44}, $\zeta_{3a,3b}^{z}$, and $-\zeta_{4a,4b}^{z}$ as a function of F_{34} for the E symmetry species of the BX_3 molecules. The solid and dotted lines represent the B^{10} and B^{11} isotopes, respectively.
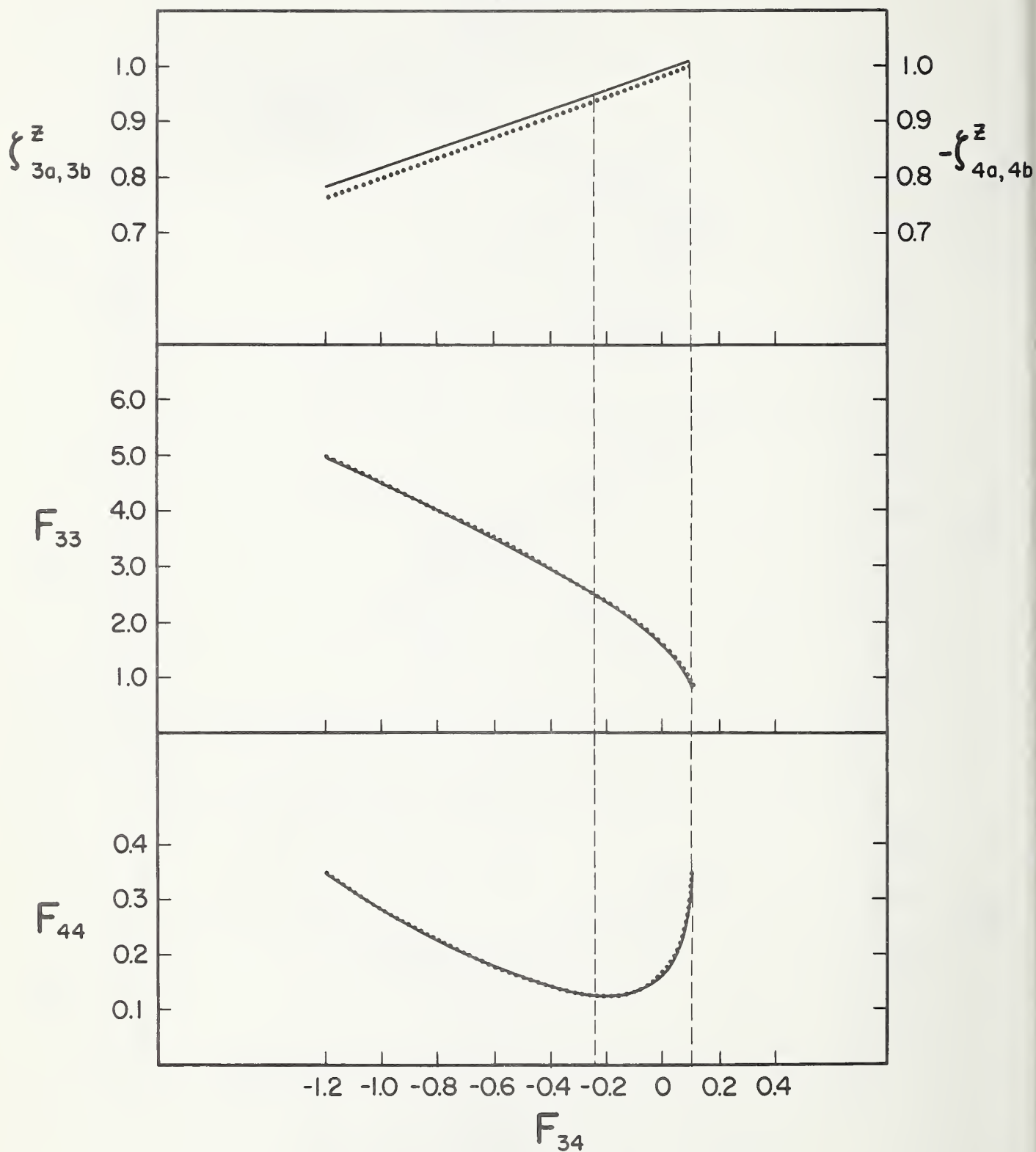
Fig. 8. Plots of F_{33}, F_{44}, $\zeta^z_{3a,3b}$, and $-\zeta^z_{4a,4b}$ as a function of F_{34} for the E symmetry species of the BX molecules. The solid and dotted lines represent the B^{10} and B^{11} isotopes, respectively.

40

Chapter 3

ISOTOPIC EFFECTS IN THE ν_3 FUNDAMENTAL OF MATRIX ISOLATED BCl_3

J. J. Comeford and S. Abramowitz
National Bureau of Standards, Washington, D. C.   20234

and

I. W. Levin
National Institutes of Health, Bethesda, Maryland   20014

The infrared spectrum of matrix isolated BCl_3 has been observed at 14 and 20°K in the region of the ν_3 fundamental under conditions of moderate resolution (~ 0.6 cm^{-1}). Two separate broad bands assigned to ν_3 of $B^{10}Cl_3$ and $B^{11}Cl_3$ are in turn broken up into several bands due to the chlorine isotope effect. It is the object of this note to explain quantitatively this chlorine isotopic effect making use of a recently derived force field.[1]

Normal boron trichloride consists of about 80% $B^{11}Cl_3$ and 20% $B^{10}Cl_3$. The boron isotope effect on the ν_3 vibration is fairly large (~ 40 cm^{-1}) and is well understood.[2] For each boron isotope the natural abundances of the chlorine isotopes are 42.2% BCl_3^{35}, 42.2% $BCl_2^{35}Cl^{37}$, 14.1% $BCl^{35}Cl_2^{37}$ and 1.6% BCl_3^{37}. Substitution of Cl^{37} for Cl^{35} not only tends to lower the vibrational frequency but reduces the symmetry, which leads to a splitting of degeneracies. The vibrational frequencies of the various isotopic species of BCl_3 were calculated from a general force field which was derived from the boron isotopic frequency data and the Coriolis coupling constants. The use of these zeta constants which were obtained by infrared gas phase band contour measurements uniquely specifies the force constants for the E vibrational mode.[1] The calculated separations of the components of BCl_3 due to isotopic splittings is given in Table 1. The expected relative intensities can be estimated by assuming that each component has the same inherent absorptivity and has a concentration determined by the natural abundance of Cl^{37}(24.6%). Indirect evidence for such an approach was obtained in the case of CCl_4.[3]

The matrix spectrum is shown in Fig. 1. With a thin film, ν_3 of $B^{11}C\ell_3$ is split into four components and appears similar to ν_3 of $B^{10}C\ell_3$. The observed separations are given in Table 1 together with the calculated shifts. The accidental degeneracy of ν_3' a produces the strongest band in the spectrum with a relative intensity of 9 followed by bands of relative intensity 1, 3 and 1. ν_3'' due to its low intensity and near accidental degeneracy with ν_3'' b tends to be obscured. The excellent agreement between the calculated and observed shifts lends support to the force field us᠎.

The fact that the observed effect does not change either with temperature (14 or 20°K) or with concentration, coupled with the excellent agreement between the computed and observed spectra rules out matrix effects as a cause of the splitting. The spectra were recorded using a prism–grating spectrophotometer with a conventional low temperature dewar.

References

1. I. W. Levin and S. Abramowitz (to be published).

2. G. Herzberg, "Molecular Spectra and Molecular Structure. II. Infrared and Raman Spectra of Polyatomic Molecules", D. Van Nostrand Co., Inc. Princeton, N. J., 1945.

3. S. Abramowitz and R. P. Bauman, J. Chem. Phys. 39, 2757 (1963).

Table 1

Species	Abundance[*] (1%)	Vibration	Relative Intensity (calculated)	Calculated Shift	Observed Shift
$B^{10}Cl_3^{35}$	42.2	ν_3	9 ⎱	0	0
$B^{10}Cl_2^{35}Cl^{37}$	42.2	ν'_{3a}	⎰	0	0
		ν'_{3b}	3	3.2	2.8
$B^{10}Cl_2^{37}Cl^{35}$	14.1	ν''_{3a}	1	1.6	1.4
		ν''_{3b}	1	4.8	3.9
$B^{10}Cl_3^{37}$	1.6	ν'''_3	0.2	4.8	–
$B^{11}Cl_3^{35}$	42.2	ν_3	9 ⎱	0	0
$B^{11}Cl_2^{35}Cl^{37}$	42.2	ν'_{3a}	⎰	0	0
		ν'_{3b}	3	3.4	2.7
$B^{11}Cl_2^{37}Cl^{35}$	14.1	ν''_{3a}	1	1.7	1.4
		ν''_{3b}	1	4.8	4.1
$B^{11}Cl_3^{37}$	1.6	ν'''_3	0.2	5.1	–

[*] The B^{10} and B^{11} isotopes are treated separately since the boron isotope shift is much greater (~ 40 cm^{-1}) than the chlorine isotope effect.
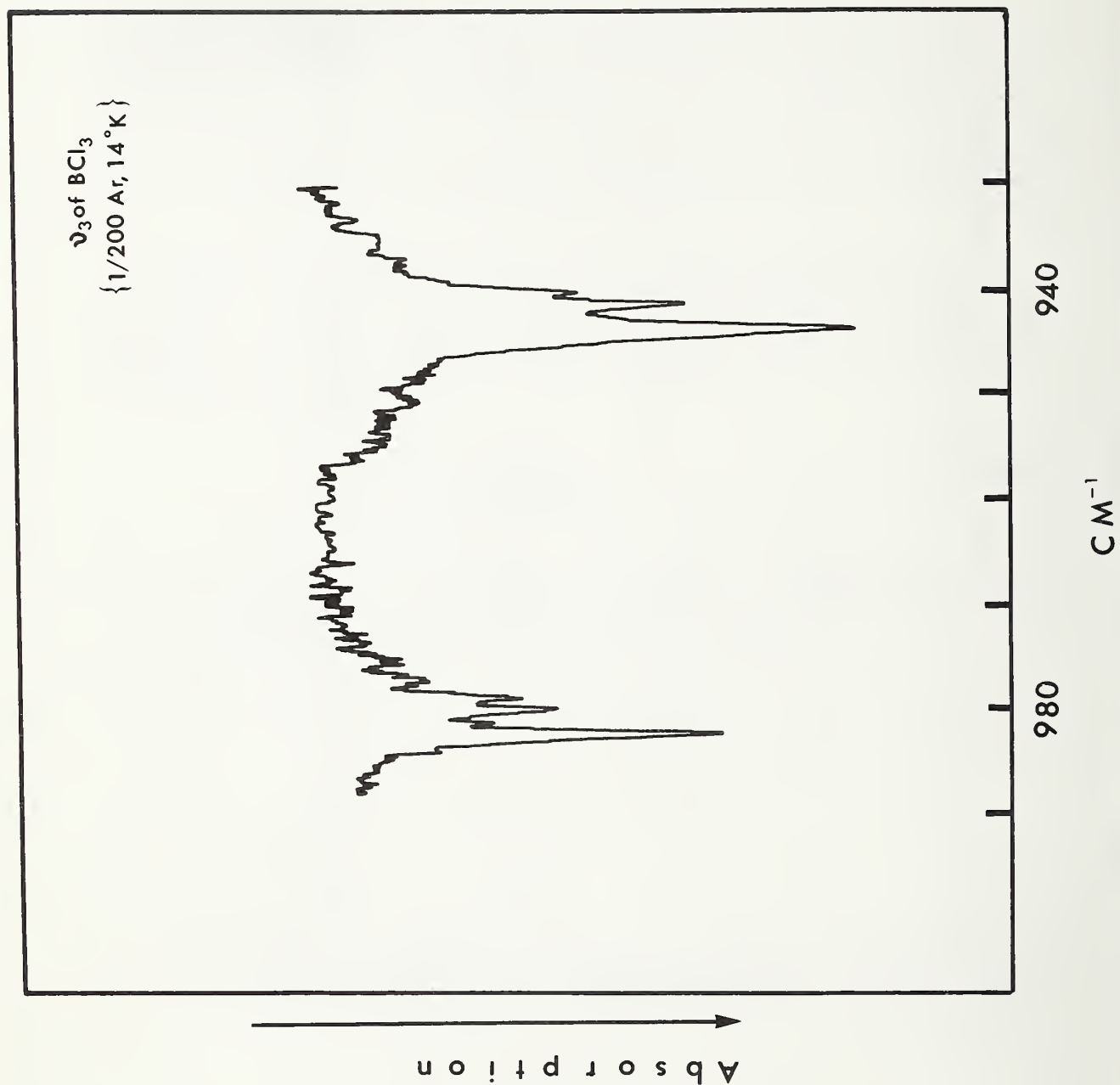
Fig. 1 – ν_3 of matrix isolated $BC\ell_3$.

44

Chapter 4

HEAT CAPACITY AND THERMODYNAMIC PROPERTIES OF
BERYLLIUM 1:3-ALUMINATE[a], BeO·3Al$_2$O$_3$, FROM 15 TO 390°K

Key Words:

Heat Capacity, Thermodynamic Properties, Entropy,
Gibbs Energy, Enthalpy, Low Temperature Calorimetry,
Beryllium 1:3-Aluminate

George T. Furukawa and William G. Saba

1. Introduction

The results of the heat-capacity measurements on beryllium
1:3-aluminate[a], BeO·3Al$_2$O$_3$, from 15 to 380°K presented herein have
been obtained as a part of the program at the National Bureau of
Standards to provide accurate thermodynamic data on "light-element"
compounds. Earlier measurements on the BeO-Al$_2$O$_3$ system that have
been reported from this laboratory are aluminum oxide (corundum),
Al$_2$O$_3$ [3][b], and beryllium 1:1-aluminate (chrysoberyl), BeO·Al$_2$O$_3$ [6].
Measurements on beryllium oxide, BeO, of relatively small crystal
size have recently been completed [4] and will be reported in a
future paper.

2. Sample

Lang et al. [9] reported "practically all BeO·3Al$_2$O$_3$" and
"all BeO·3Al$_2$O$_3$" for the results of petrographic and x-ray examinations,
respectively, on a sample prepared by fusing a mixture of 1 to 3 molal
ratio of BeO to Al$_2$O$_3$. Semi-Elements, Inc. prepared, on request, the
sample accordingly for the heat-capacity measurements presented. The
preparation procedure was as follows: stoichiometric amounts of dried
BeO and Al$_2$O$_3$ powder were thoroughly mixed and fused in an arc
furnace. To avoid contamination a fused mass was formed within a
relatively large charge of the mixture so that the unfused mixture
would serve as the container for the fused portion of the material.
The fused material was slowly cooled to room temperature, freed of
any unfused material, and crushed and sieved to collect particle sizes
between 0.3 and 2 mm (10 and 50 mesh) on the edge.

[a] The numbers indicate base to acid anhydride ratio.

[b] Figures in brackets indicate references listed at the end of this
paper.

Some of the particles in the sample that was received appeared gray, presumably from occlusion of traces of carbon from the graphite electrodes used in the arc fusion preparation. Qualitative spectrochemical analysis of the material by the Spectrochemical Analysis Section of the National Bureau of Standards showed the limits of percentage impurities given in Table 1.

A petrographic (microscopic) examination of the $BeO \cdot 3Al_2O_3$ sample was made in the Crystallography Section of the National Bureau of Standards. The crystal size was found to be on the average about 300μ. Since the sample was ground for the microscopic examination, the crystal size of the original 10 to 50 mesh polycrystalline material on which the heat-capacity measurements were made is considered to be larger than 300μ. The crystals were clear with some voids and growth defects resulting from too rapid cooling. There was some evidence of another phase present, possibly up to about 5 percent. No BeO phase was detected.

X-ray diffraction examination of the $BeO \cdot 3Al_2O_3$ sample was also made in the Crystallography Section of the National Bureau of Standards. The pattern obtained is in agreement with published values for $BeO \cdot 3Al_2O_3$ [1,2,7] with some possible impurity lines close to $BeO \cdot Al_2O_3$ and α-Al_2O_3 but without presence of all strong lines of these substances. A few unidentified lines were also found. The patterns corresponding to graphite, BeO, and $3BeO \cdot Al_2O_3$ were absent.

Optical properties of $BeO \cdot Al_2O_3$ and $BeO \cdot 3Al_2O_3$ have been found to be very similar [2,7,9,10]. It seems, therefore, that the impurity phase observed petrographically in the sample investigated is probably not $BeO \cdot Al_2O_3$. If the undetectable $BeO \cdot Al_2O_3$ is present, then the excess Al_2O_3 should be observed as α-Al_2O_3 or there is an unidentified compound of BeO and Al_2O_3 of ratio greater than 1 to 3. The x-ray pattern obtained does not definitively indicate the presence of α-Al_2O_3.

Distinctive x-ray diffraction patterns have been reported for $BeO \cdot Al_2O_3$ and $BeO \cdot 3Al_2O_3$ [1,2,7]. Lang et al. [9] observed an unidentified phase of high refractive index in mixtures that have been heated to melting temperatures, having compositions between $BeO \cdot Al_2O_3$ and Al_2O_3. These investigators also found another unidentified phase in x-ray diffraction patterns of fused mixtures of composition between $BeO \cdot Al_2O_3$ and BeO. The major d-spacings observed for the latter impurity phase cannot be identified with the d values reported for the more recently found $3BeO \cdot Al_2O_3$ phase [7]. Lang et al. [9] could not determine the presence of both of the unidentified phases in the same specimen or any similarity, if any, in the phases. They were not able

to identify either phase in the same specimen by both petrographic and x-ray methods. These results seem to indicate that yet un-identified phases exist in the BeO-$A\ell_2O_3$ system or additional careful study of the known phases is needed.

Chemical analysis of the BeO·$A\ell_2O_3$ sample was performed in the Analysis and Purification Section of the National Bureau of Standards. Two 0.5 gram samples were dissolved in $HC\ell$ by heating the mixture sealed in tubes at 250°C for 16 hours. A known mixture of BeO and $A\ell_2O_3$ was treated in the same manner as a control on the analysis. The treatment of the resulting solution and the analysis for Be and $A\ell$ were the same as those described for BeO·$A\ell_2O_3$ [6]. The results of the chemical analysis, summarized in Table 2, show the beryllium and aluminum composition to have the theoretical stoichiometric ratio within the precision of the analytical method. The amount of graphite impurity was considered insignificant, and the sample was taken to be 100 percent BeO·$3A\ell_2O_3$ in the processing of the heat-capacity data obtained.

Although BeO·$3A\ell_2O_3$ is considered to be inert, the sample was handled and poured into the calorimeter vessel in a controlled-atmosphere box containing dry argon gas (dew-point of about -80°C). The calorimeter vessel was provided with a screw-cap and gasket closure and a "pump out" tube with a valve previously described [5]. The vessel containing the sample was pumped to a high vacuum and purged with dry helium gas several times and finally sealed with 60.5 torr pressure of helium gas. The mass of sample investigated was 252.1429 g.

3. Apparatus and Method

The heat-capacity measurements on BeO·$3A\ell_2O_3$ were made in an adiabatic calorimeter similar in principle and design to that described previously [11]. The calorimeter, sample container, and the adjuvant instruments were the same, except for the bridge, as those used with the recently published measurements on BeO·$A\ell_2O_3$ [6]. Description of methods and procedures used for the measurements of temperature, power, and time interval of heating, and the calibration information on the temperature scale and electrical instruments are given in the reference.

An automatic Mueller bridge, capable of resistance measurements up to almost 500 ohms to the nearest 0.00001 ohm, was used with the platinum-resistance thermometer for most of the temperature measure-ments. The performance of this automatic bridge was found comparable to the high-precision manually-operated Mueller bridge used exclusively in the measurements with BeO·$A\ell_2O_3$ [6]. The bridge readings were

automatically recorded on punch cards and subsequently processed
on the high-speed digital computer to obtain the temperatures
associated with each heating interval.

The 1961 atomic weights based on carbon-12 were used for con-
verting the mass of sample investigated to gram formula weight
basis [8]. The energy measurements were made in terms of the cgs
unit of energy joule. Wherever conversion to the energy unit calorie
was made, the following relation was used:

$$1 \text{ defined calorie} = 4.1840 \text{ J}$$

4. Heat-Capacity Measurements and Results

Measurements totaling 147 heat-capacity "points" were obtained
on the calorimeter vessel plus sample from about 15 to 390°K and
87 points were obtained subsequently on the empty vessel in the same
temperature range. Smoothed values of heat capacity at closely and
regularly spaced integral temperatures were calculated for the two
series of measurements using high-speed digital computer methods.
The heat capacity of the sample was then obtained by differencing the
smoothed values from the two series of measurements at the corre-
sponding regular temperatures. The values of heat capacity for the
$BeO \cdot 3Al_2O_3$ below 15°K were obtained by extrapolating the smoothed
experimental values at the lower temperatures in accordance with a
T^3 relation.

Briefly, the procedures used in analyzing the experimental
observations on the IBM 7094 computer were as follows. Since the data
could not be adequately represented over the complete temperature
range in terms of a single heat-capacity equation, a number of poly-
nomials of varying degrees of complexity were fitted by the method of
least squares to the data over different temperature ranges. To avoid
curvature corrections the analysis was formulated according to the
relation:

$$Q_{T_2, T_1} = \int_{T_1}^{T_2} C(T) dT,$$

where Q_{T_2, T_1} is the input energy, T_1 and T_2 the corresponding initial
and final temperatures, respectively, for each of the points, and $C(T)$
is the polynomial for which the coefficients were obtained by the
least-squares method. Three or four polynomials were selected from
the group on the basis of their fit over the complete temperature
range of observations and for their agreement where the temperatures
overlap. The polynomials were evaluated at closely spaced regular
temperatures and joined at temperatures where the values of heat capacity

and their first and second derivatives showed the best agreement.
A numerical smoothing analysis was performed on these tabular values
using the computer to test the smoothness of the joining process.
Since the values were adequately smooth, they were changed insignifi-
cantly by the computer smoothing program.

The deviations of the observed values of heat capacity for the
calorimeter-vessel-plus-sample and for the empty-vessel measurements
from the final smoothed tabular values for the two series of measure-
ments are plotted in Figures 1 and 2, respectively. Except below
about 50°K, all of the observations are well within the ±0.1 percent
limit of the net heat capacity of the $BeO \cdot 3Al_2O_3$ sample.

The final smoothed values of heat capacity of $BeO \cdot 3Al_2O_3$ given
in Table 4 were obtained by differencing at corresponding temperatures
the smoothed values for the above two series of measurements and
correcting for the contribution of the helium exchange gas wherever
significant. The smoothness of the resulting tabular values was
checked on the computer and converted to molal values.

The smoothed values at the lower temperatures were plotted as
C/T versus T^2 and extrapolated linearly to 0°K to obtain values below
15°K, the lower temperature limit of the experimental measurements.
The slope of the line used was 4.025×10^{-5} J deg^{-4} mol^{-1}, which
corresponds to an effective Debye characteristic temperature of
936°K (assuming $C_V = C_p$).

The "observed molal heat capacity" is shown in Figure 3 and
listed in Table 3 in the chronological order of the measurements
made. These values were obtained by subtracting the smoothed heat
capacity of the empty vessel from that of the calorimeter vessel
plus sample at the observed temperatures (mid-temperatures of the
heating intervals). The heat-capacity values of the empty vessel
at the corresponding observed temperatures were obtained by interpo-
lation in the table of smoothed values described earlier. Correc-
tions were made for the heat capacity of helium gas and for curva-
ture wherever significant and the net heat capacity converted to
the molal observed values.

5. Reliability of the Results

In addition to the imprecision of the measurements shown in
Figures 1 and 2, the purity of the sample, the accuracy of calibra-
tion of the instruments used, and the possible sources of systematic
errors were examined to estimate the uncertainties in the final values
of heat capacity of $BeO \cdot 3Al_2O_3$. The estimated uncertainty in the
values given in Table 4 between 80 and 390°K is ±0.1 percent. Below

49

about 80°K, the uncertainty increased, because of the decrease in the contribution of the sample to the gross heat capacity. At 300°K the heat capacity of the sample was 81 percent of the gross; at 80°K, 46 percent; at 50°K, 29 percent; 20°K, 14 percent; and at 13°K, only 10 percent. In addition, the sensitivity dR/dT of the platinum resistance thermometer began to decrease significantly below about 40°K. Considering these factors, the estimated uncertainty is ±0.2 percent at 50°K, ±1 percent at 20°K, and ±3 percent at 13°K.

6. Thermodynamic Functions and Discussion of the Results

The thermodynamic functions for BeO·3Al$_2$O$_3$ were derived, using their usual relations with respect to heat capacity, from the smoothed tabular values. The thermodynamic relations were evaluated on the computer by numerical integration procedures with four-point Lagrangian integration coefficients [12]. The thermodynamic functions are given in Table 4 from 0° to 390°K.

Acknowledgements

7. References

[1] P. P. Budnikov, V. G. Avetikov, E. I. Dudavsky, and A. A. Zvyagilsky, Doklady Akad. Nauk SSSR 68, 313 (1949).

[2] W. R. Foster and H. F. Royal, J. Am. Ceram. Soc. 32, 26 (1949).

[3] G. T. Furukawa, T. B. Douglas, R. E. McCoskey, and D. C. Ginnings, J. Research NBS 57, 67 (1956) RP2694.

[4] G. T. Furukawa and M. L. Reilly, unpublished measurements.

[5] G. T. Furukawa, M. L. Reilly and J. H. Piccirelli, J. Research NBS 68A, (Phys. and Chem.) No. 4, 381 (1964).

[6] G. T. Furukawa and W. G. Saba, J. Research NBS 69A, (Phys. and Chem.) No. 1, 13 (1965).

[7] F. Ya. Galakov, Izvest. Akad. Nauk SSSR, Otdel. Khim. Nauk, No. 9, 1035 (1957); Bull. Acad. Sci. USSR, Div. Chem. Sci., No. 9, 1062 (1957).

[8] IUPAC Revises Atomic Weight Values, Chem. Eng. News 39, 42 (1961).

[9] S. M. Lang, C. L. Fillmore, and L. H. Maxwell, J. Research NBS 48, 298 (1952) RP2316.

[10] C. Palache, H. Berman, and C. Frondel, "The System of Mineralogy", Vol. 1, p. 718 (J. Wiley and Sons, New York, 1944).

[11] R. B. Scott, C. H. Meyers, R. D. Rands, Jr., F. G. Brickwedde, and N. Bekkedahl, J. Research NBS 35, 39 (1945) RP1661.

[12] Tables of Lagrangian Interpolation Coefficients (Columbia University Press, New York, N. Y., 1944).

Table 1

Spectrochemical Analysis
of Beryllium 1:3-Aluminate $(BeO \cdot 3Al_2O_3)$[a]

Element	Percentage Limit	Element	Percentage Limit
Ag	< 0.0001	Mg	0.001 – 0.01
B	0.001 – 0.01	Mn	0.0001 – 0.001
Ca	0.001 – 0.01	Na	0.01 – 0.1
Cu	< 0.0001	Si	0.01 – 0.1
Fe	0.01 – 0.1	Zr	0.001 – 0.01

[a] Analyzed by Elizabeth K. Hubbard
    Spectrochemical Analysis Section

Table 2

Chemical Analysis of
Beryllium 1:3-Aluminate $(BeO \cdot 3Al_2O_3)$[a]

| Sample | Percentage by Weight | | Mol Ratio |
	Al	Be	BeO/Al_2O_3
1	48.96	2.71[b]	3.017
		2.74[b]	2.984
2	48.93	2.72	3.004
Theoretical	48.92	2.72	

[a] Analysis by E. J. Maienthal,
   Analysis and Purification Section

[b] Duplicate aliquots

TABLE 3

OBSERVED HEAT CAPACITY OF BERYLLIUM 1:3-ALUMINATE (BEO.3AL$_2$O$_3$)

GRAM MOLECULAR WT.=330.8952 GRAMS   1 CAL=4.1840 ABS J

T DEG K = 273.15 + T DEG C

T	c_p	T	c_p	T	c_p
DEG K	J DEG^{-1}MOL^{-1}	DEG K	J DEG^{-1}MOL^{-1}	DEG K	J DEG^{-1}MOL^{-1}
RUN 1		**RUN 6**		**RUN 11 CONT.**	
82.8203	28.964	18.4505	0.250	259.3612	233.673
88.0822	34.227	21.0068	0.381	266.5257	239.939
93.6560	40.027	23.3504	0.532	273.6103	246.048
99.4640	46.435	26.8876	0.827	280.6552	251.690
105.1819	53.076	30.7964	1.270	287.9167	257.439
110.8937	59.946			295.3757	263.122
116.2799	66.639	**RUN 7**		302.7188	268.501
121.5671	73.341			309.9404	273.633
126.9319	80.234	14.7135	0.107	317.0493	278.493
		19.0305	0.279	324.0556	283.101
RUN 2		21.4966	0.414		
		24.9047	0.654	**RUN 12**	
83.4430	29.619	28.9755	1.047		
93.1378	39.520			199.6885	172.558
102.3438	49.768	**RUN 8**		209.5623	183.776
110.0670	58.972			220.4510	195.579
117.2945	67.939	25.6653	0.718	230.4099	205.954
123.8566	76.279	29.7872	1.147	241.5414	217.011
129.9306	84.191	33.8800	1.737	253.8218	228.599
135.6114	91.641	38.4138	2.618	265.6168	239.092
		42.7876	3.715	277.0019	248.759
RUN 3		46.9192	5.045		
		51.3870	6.817	**RUN 13**	
132.6454	87.716	56.0607	9.017		
138.1908	95.032			198.0565	170.655
143.4155	101.938	**RUN 9**		201.9686	175.189
148.3858	108.477			207.2721	181.202
150.3864	111.090	53.0258	7.546		
155.0609	117.220	57.5249	9.794	**RUN 14**	
159.5568	123.071	61.8323	12.339		
163.8977	128.677	66.0923	15.097	275.0636	247.116
167.4038	133.143	70.4018	18.206	278.9339	250.319
171.4439	138.297	74.9699	21.849	285.8983	255.860
177.6536	146.111	79.9109	26.210	293.6534	261.865
184.5438	154.587	85.1544	31.264	301.7499	267.778
191.1511	162.544			311.7800	274.892
197.5135	170.039	**RUN 10**		322.8485	282.271
199.9364	172.860			333.3522	288.997
206.0172	179.794	53.4833	7.764	343.2091	294.909
212.9353	187.490	58.9604	10.617	352.1076	300.070
220.6606	195.831	64.5559	14.102	361.4226	305.043
228.1316	203.644	70.6195	18.435	371.2744	310.239
235.3762	210.991	77.0761	23.717	380.9849	315.212
242.4181	217.892	83.3997	29.590		
249.2865	224.433	89.8264	36.063	**RUN 15**	
255.9950	230.597	96.1066	42.727		
		102.1024	49.512	277.8938	249.497
RUN 4		107.8188	56.257	284.1183	254.451
		113.3406	63.011	290.9840	259.825
54.4277	8.188	119.0752	70.194	298.9705	265.799
57.6286	9.833			307.2420	271.725
60.6838	11.611	**RUN 11**		319.3254	279.963
64.0585	13.748			331.2745	287.670
68.1789	16.598	196.3894	168.737	339.1056	292.530
		200.5662	173.578	346.9111	297.086
RUN 5		206.1477	179.973	354.6113	301.477
		212.0283	186.512	362.3108	305.570
21.9906	0.446	218.3673	193.399	369.8374	309.529
25.3842	0.691	224.7804	200.188	377.2870	313.293
28.5606	1.002	231.5555	207.161		
32.1099	1.452	238.6756	214.253	**RUN 16**	
35.5483	2.025	245.6172	220.957	307.6850	272.065
		252.3915	227.307	315.9765	277.803

TABLE 4

THERMODYNAMIC FUNCTIONS FOR BERYLLIUM 1:3-ALUMINATE (BEO·3AL$_2$O$_3$)
SOLID PHASE

GRAM MOLECULAR WT.=330.8952 GRAMS　　　　　　　　　1 CAL=4.1840 ABS J

T DEG K = 273.15 + T DEG C

T	C_p^0	$(H_T^0-H_0^C)$	$(H_T^0-H_0^C)/T$	$(S_T-S_0^C)$	$-(G_T^0-H_0^C)$	$-(G_T^0-H_0^C)/T$
DEG K	$\dfrac{J}{\text{DEG MOLE}}$	$\dfrac{J}{\text{MOLE}}$	$\dfrac{J}{\text{DEG MOLE}}$	$\dfrac{J}{\text{DEG MOLE}}$	$\dfrac{J}{\text{MOLE}}$	$\dfrac{J}{\text{DEG MOLE}}$
0.00	0.000	0.000	0.000	0.000	0.000	0.000
5.00	0.005	0.006	0.001	0.002	0.002	0.000
10.00	0.040	0.101	0.010	0.013	0.034	0.003
15.00	0.135	0.509	0.034	0.045	0.170	0.011
20.00	0.326	1.611	0.081	0.107	0.536	0.027
25.00	0.656	4.002	0.160	0.213	1.316	0.053
30.00	1.167	8.470	0.282	0.374	2.757	0.092
35.00	1.919	16.072	0.459	0.607	5.177	0.148
40.00	2.973	28.165	0.704	0.928	8.975	0.224
45.00	4.387	46.405	1.031	1.357	14.639	0.325
50.00	6.208	72.717	1.454	1.909	22.748	0.455
55.00	8.468	109.22	1.986	2.603	33.968	0.618
60.00	11.196	158.18	2.636	3.454	49.043	0.817
65.00	14.358	221.91	3.414	4.472	68.786	1.058
70.00	17.910	302.41	4.320	5.664	94.053	1.344
75.00	21.885	401.72	5.356	7.032	125.72	1.676
80.00	26.294	521.98	6.525	8.583	164.68	2.059
85.00	31.114	665.35	7.828	10.320	211.86	2.492
90.00	36.197	833.56	9.262	12.242	268.19	2.980
95.00	41.483	1027.7	10.817	14.339	334.57	3.522
100.00	47.050	1248.9	12.489	16.607	411.87	4.119
105.00	52.858	1498.5	14.272	19.043	500.92	4.771
110.00	58.859	1777.8	16.161	21.639	602.56	5.478
115.00	65.021	2087.4	18.151	24.391	717.57	6.240
120.00	71.326	2428.2	20.235	27.291	846.72	7.056
125.00	77.740	2800.8	22.407	30.332	990.72	7.926
130.00	84.236	3205.8	24.660	33.508	1150.3	8.848
135.00	90.790	3643.3	26.987	36.810	1326.0	9.822
140.00	97.375	4113.7	29.384	40.230	1518.6	10.847
145.00	103.97	4617.1	31.842	43.763	1728.5	11.921
150.00	110.55	5153.4	34.356	47.398	1956.4	13.042
155.00	117.11	5722.5	36.920	51.130	2202.6	14.211
160.00	123.62	6324.4	39.527	54.951	2467.8	15.424
165.00	130.07	6958.6	42.173	58.854	2752.3	16.681
170.00	136.46	7625.0	44.853	62.832	3056.5	17.979
175.00	142.77	8323.1	47.560	66.879	3380.7	19.318
180.00	148.99	9052.5	50.292	70.988	3725.4	20.696
185.00	155.13	9812.9	53.042	75.154	4090.7	22.112
190.00	161.16	10604.	55.808	79.372	4477.0	23.563
195.00	167.10	11424.	58.586	83.635	4884.5	25.049
200.00	172.93	12274.	61.372	87.939	5313.4	26.567
205.00	178.65	13153.	64.163	92.280	5763.9	28.117
210.00	184.26	14061.	66.956	96.652	6236.3	29.696
215.00	189.75	14996.	69.748	101.05	6730.5	31.305
220.00	195.14	15958.	72.536	105.48	7246.8	32.940
225.00	200.41	16947.	75.320	109.92	7785.3	34.601
230.00	205.57	17962.	78.095	114.38	8346.1	36.287
235.00	210.62	19002.	80.862	118.86	8929.2	37.996
240.00	215.56	20068.	83.616	123.34	9534.7	39.728
245.00	220.38	21158.	86.359	127.84	10163.	41.480
250.00	225.10	22272.	89.086	132.34	10813.	43.252
255.00	229.71	23409.	91.799	136.84	11486.	45.043
260.00	234.21	24568.	94.494	141.35	12181.	46.852
265.00	238.61	25751.	97.172	145.85	12899.	48.677
270.00	242.90	26954.	99.831	150.35	13640.	50.518
273.15	245.55	27724.	101.50	153.18	14118.	51.686
275.00	247.09	28179.	102.47	154.84	14403.	52.374
280.00	251.17	29425.	105.09	159.33	15188.	54.244
285.00	255.16	30691.	107.69	163.81	15996.	56.127
290.00	259.05	31977.	110.26	168.29	16827.	58.023
295.00	262.84	33281.	112.82	172.75	17679.	59.929
298.15	265.19	34113.	114.42	175.55	18228.	61.136
300.00	266.54	34605.	115.35	177.20	18554.	61.847
305.00	270.15	35947.	117.86	181.63	19451.	63.774
310.00	273.67	37306.	120.34	186.05	20370.	65.711
315.00	277.11	38683.	122.80	190.46	21312.	67.656
320.00	280.46	40077.	125.24	194.85	22275.	69.609
325.00	283.72	41488.	127.65	199.22	23260.	71.569
330.00	286.90	42914.	130.04	203.58	24267.	73.537
335.00	290.00	44356.	132.41	207.92	25296.	75.510
340.00	293.02	45814.	134.75	212.24	26346.	77.489
345.00	295.96	47287.	137.06	216.54	27418.	79.473
350.00	298.82	48774.	139.35	220.81	28512.	81.461
355.00	301.60	50275.	141.62	225.07	29626.	83.454
360.00	304.32	51789.	143.86	229.31	30762.	85.451
365.00	306.98	53318.	146.08	233.53	31919.	87.450
370.00	309.59	54859.	148.27	237.72	33097.	89.452
373.15	311.21	55837.	149.64	240.35	33850.	90.715
375.00	312.15	56413.	150.44	241.89	34296.	91.457
380.00	314.68	57981.	152.58	246.04	35516.	93.464
385.00	317.19	59560.	154.70	250.17	36757.	95.472
390.00	319.69	61152.	156.80	254.28	38018.	97.482

H_0^C AND S_0^C APPLY TO THE REFERENCE STATE OF THE SOLID AT ZERO DEG K
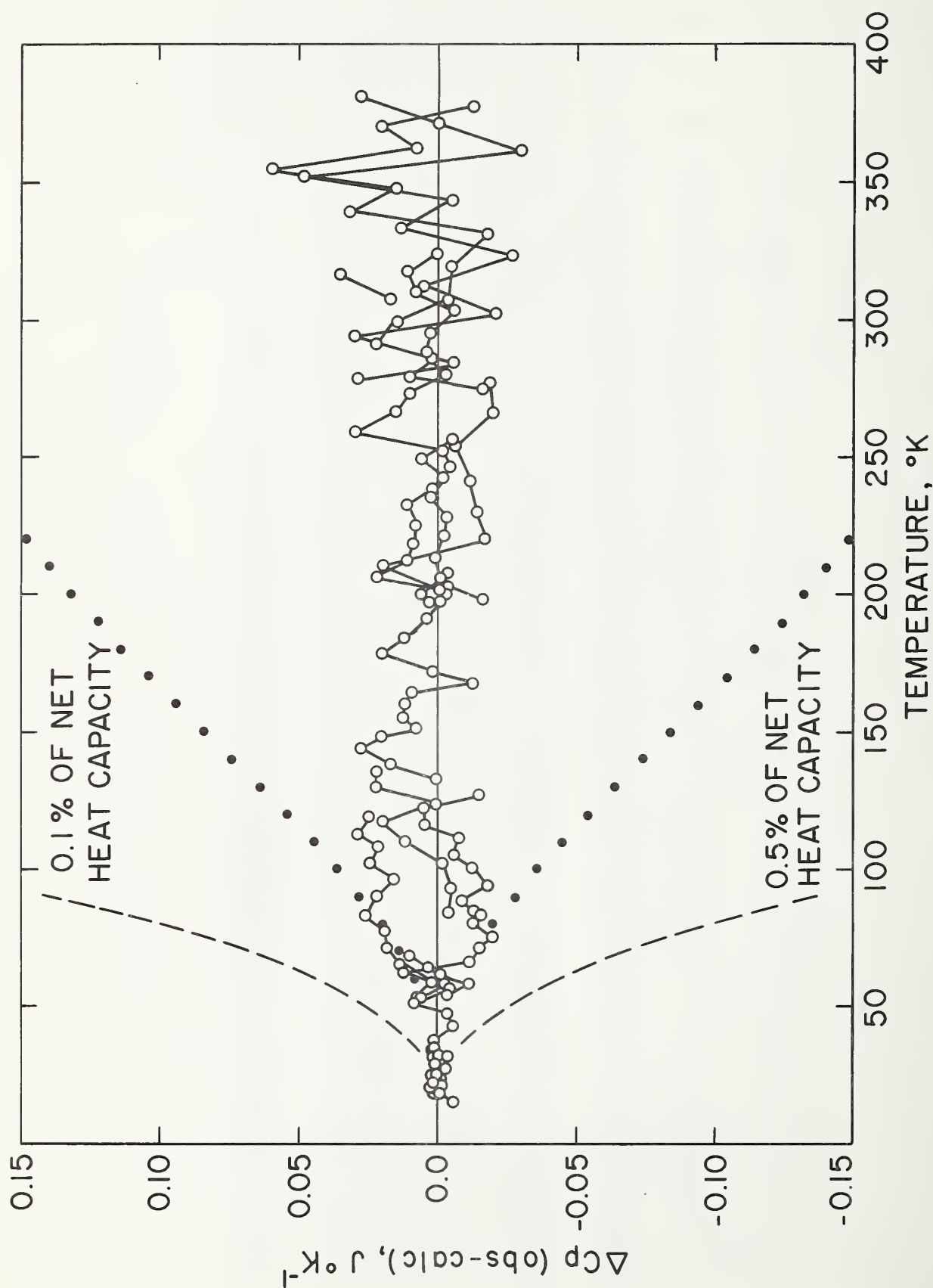
Figure 1. Deviations of the heat-capacity measurements on calorimeter vessel plus beryllium 1:3-aluminate, $BeO \cdot 3Al_2O_3$.
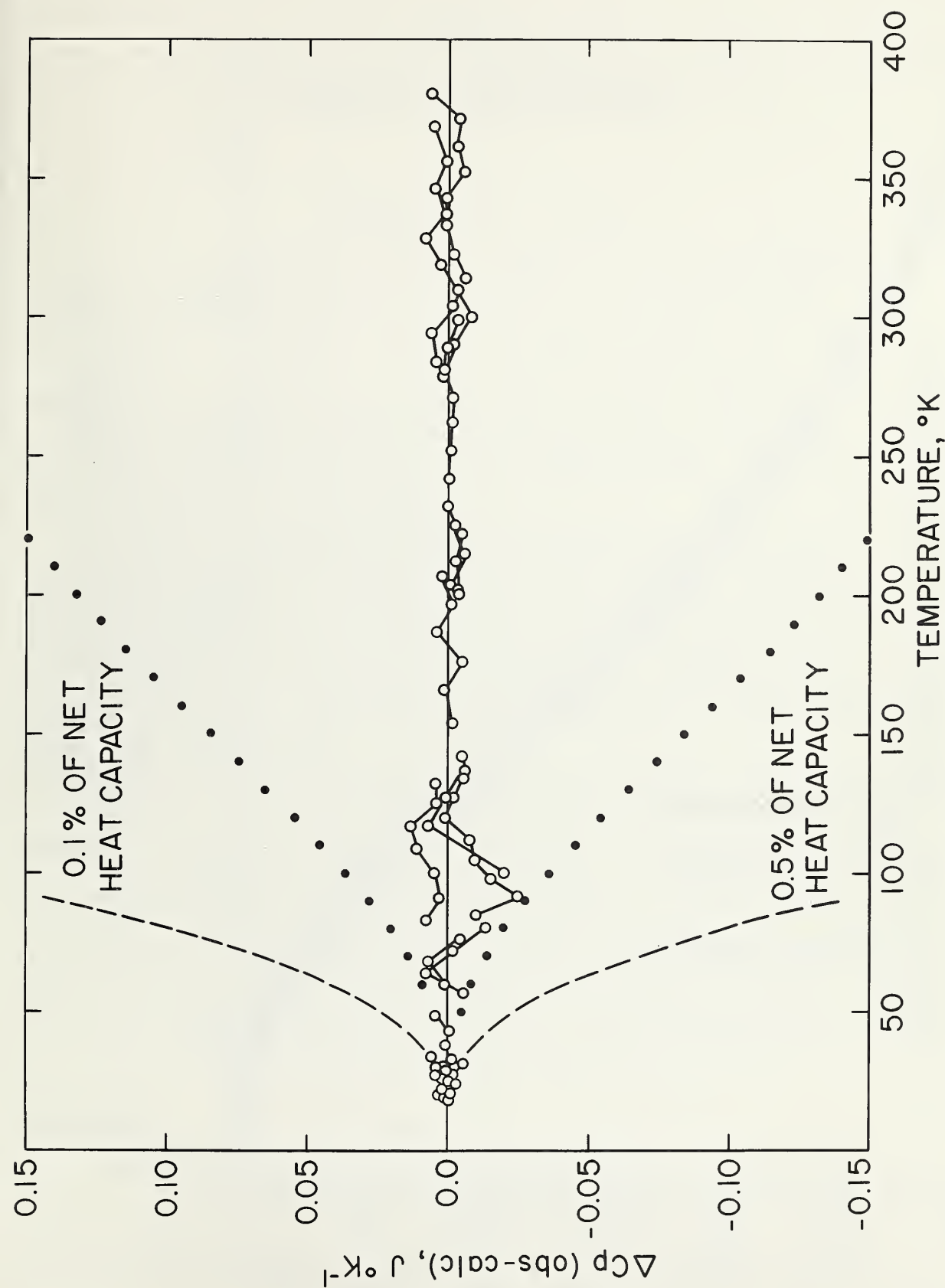
Figure 2. Deviations of the heat-capacity measurements on the empty calorimeter vessel used with beryllium 1:3-aluminate, $BeO \cdot 3Al_2O_3$.

57
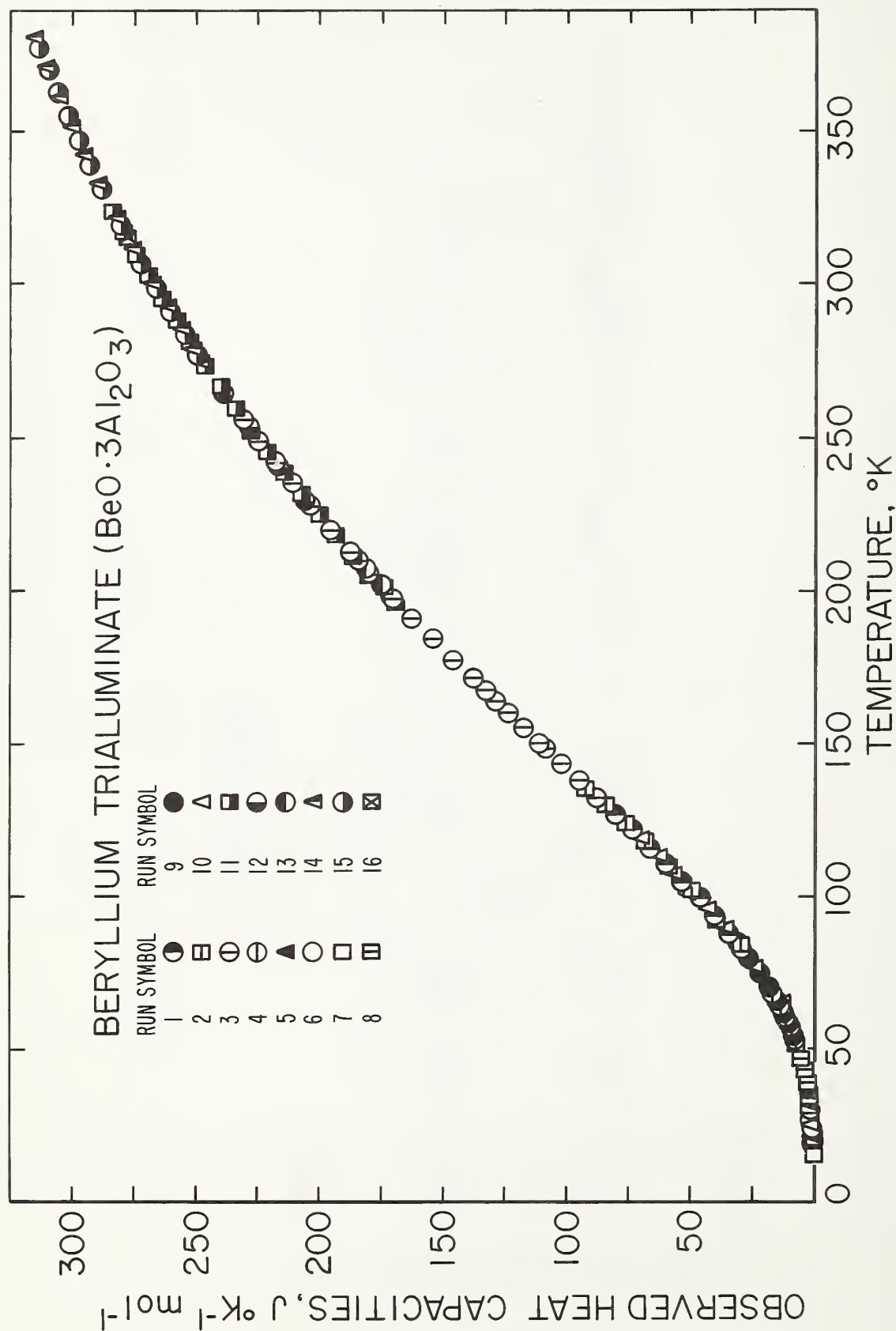
Figure 3. Observed values of the molal heat capacity of beryllium 1:3-aluminate, $BeO \cdot 3Al_2O_3$, as a function of the temperature. (Numerical values are given in Table 3.)

HIGH TEMPERATURE MASS SPECTROMETRIC STUDY OF THE COMPOUND, $Al_2O_3 \cdot BeO$. REVISION

by

J. Efimenko and W. S. Horton

The data presented in Table 1, Chapter 6, Report No. 8628 were recalculated employing relative sensitivities through the following relationship: $p_i = I_i^+/S_i$. The corrected data, containing all the original data points are reproduced in Table 1 below. (Tables are numbered here to correspond with those in Report No. 8628. Table 2, which is unchanged, is not repeated.)

By means of OMNITAB programing (1), ΔH_0^O values were obtained for reactions 1, 2, 3, 4 and analyzed. Using the criteria for extreme mean (2) some points were discarded leaving twelve temperature datum points for subsequent computations. The excluded data were for temperatures 2205°, 2211°, 2152°K.

The twelve selected temperature-pressure data points were programed to give $\ln K$ vs $\frac{1}{T}$ values for reactions 1, 2, 3 and 5. Reaction enthalpies were obtained from the slopes. Reaction enthalpies at absolute zero were obtained also for these reactions from free energy functions and a summary is tabulated in Table 3A. No free energy functions are available for $Al_2O_3 \cdot BeO$ liquid at present.

Discussion

The results (Table 3A) for oxygen dissociation, reaction 4, may indicate that equilibrium in the gas phase was closely approached. The enthalpy for dissociation of O_2 (g) shown here, 57 ±1 kcal/mol agrees

well with the accepted value, 58.983 kcal/mol (NBS Report No. 8504, p. 165, July, 1964). Reaction (2) has been studied mass spectrometrically by others: R. F. Porter, P. Schissel and M. G. Inghram, J. Chem. Phys. 23, 399 (1955), ΔH_0^0 = -254 ±7 kcal/mol; and J. Drowart, G. de Maria, R. P. Burns and M. G. Inghram, J. Chem. Phys. 32, 1372 (1960), ΔH_0^0 = -243.4 ±7 kcal/mol. The value reported here is in reasonable agreement with these.

From an algebraic view, reaction (3) is not independent but is the difference between reactions (1) and (2). Table 3A shows that the enthalpy for (3) is consistent with this requirement for the slope method and for the free-energy-functions method. However, the two methods do not produce enthalpy values that agree with each other. Reactions (2) and (3) show this kind of discrepency but reaction (1) shows good agreement. Examination of the tabulated ΔH_0^0's for reaction (2) from free energy functions also shows a small but definite temperature dependence. Such a trend may arise from at least two possible sources, (i), poor quality data in the intensities of $Al_2O(g)$; (ii), error in the free energy functions for $Al_2O(g)$. It appears likely that the difficulty lies with Al_2O rather than any other molecule because it is the only one involved in reaction (2) which is not in reaction (1). The good agreement for reaction (1) lends strength to the estimated free energy functions for AlOBe. A new set of experimental data will be obtained for the $Al_2O_3 \cdot BeO$ compound to supplement the present results.

A tentative value for the standard heat of formation for the specie, AlOBe(g), is obtained through reaction (1). Using the reaction

60

enthalpy based on free energy functions and standard heats of formation (NBS 6928, Table C1) one obtains $\Delta H^\circ_f(AlOBe) = -6.2$ kcal/mol at $0°K$.

The identification of the AlOBe specie is chiefly through its m/e position and a positive shutter behavior, but in a complex experimental system this method often is not conclusive. Chromium also has an isotope of mass 52, the most abundant of its four isotopes and this element is a component of stainless steel used in parts of the Knudsen cell support structure. Whether the mass peak 52 is due to chromium or the specie AlOBe can be determined by comparing the enthalpies of sublimation. From the data of Table 1, a Clausius-Clapeyron plot for m/e value 52 was made and from the slope the enthalpy value below was obtained. The large difference, when compared to a literature value, argues against assigning the 52 peak to chromium. There are no other stable elemental isotopes to account for this mass.

m/e	ΔH°_0, subl.
52	151.4 kcal/mol
Cr_{52}	94.8 kcal/mol (3)

Another possible specie having mass 52 is $(CN)_2{}^+$ but it is not likely to be formed as a beam and show a positive shutter effect.

Table 1

Mass Spectrometric Temperature - Partial Pressure Values

Atmospheres

$T^\circ K$	P_{Be}	P_O	P_{Al}	P_{AlOBe}	P_{Al_2O}	P_{O_2}
2567	1.22×10^{-5}	2.29×10^{-5}	2.02×10^{-5}	9.41×10^{-8}	3.14×10^{-7}	2.17×10^{-7}
2518	8.20×10^{-6}	1.61×10^{-5}	1.44×10^{-5}	8.41×10^{-8}	3.12×10^{-7}	4.68×10^{-7}
2470	5.84×10^{-6}	9.36×10^{-6}	8.33×10^{-6}	4.18×10^{-8}	1.71×10^{-7}	2.46×10^{-7}
2417	3.48×10^{-6}	5.15×10^{-6}	4.73×10^{-6}	2.21×10^{-8}	8.88×10^{-8}	1.43×10^{-7}
2343	1.61×10^{-6}	2.29×10^{-6}	1.89×10^{-6}	8.36×10^{-9}	3.44×10^{-8}	
2290	8.58×10^{-7}	1.14×10^{-6}	8.89×10^{-7}	3.24×10^{-9}	1.32×10^{-8}	
2290	8.58×10^{-7}	1.18×10^{-6}	9.23×10^{-7}	3.23×10^{-9}	1.45×10^{-8}	
2337	1.42×10^{-6}	2.03×10^{-6}	1.67×10^{-6}	6.85×10^{-9}	2.88×10^{-8}	
2279	7.21×10^{-7}	9.79×10^{-7}	7.35×10^{-7}	2.57×10^{-9}	1.01×10^{-8}	
2226	3.76×10^{-7}	4.98×10^{-7}	2.38×10^{-7}	8.46×10^{-10}	4.14×10^{-9}	
2179	2.23×10^{-7}	2.51×10^{-7}	1.73×10^{-7}	3.00×10^{-10}	1.68×10^{-9}	
2290	9.79×10^{-7}	1.30×10^{-6}	1.05×10^{-6}	3.82×10^{-9}	1.69×10^{-8}	
*2152	1.84×10^{-7}	2.32×10^{-7}	1.50×10^{-7}	8.82×10^{-11}	1.09×10^{-9}	
*2205	3.17×10^{-8}	4.11×10^{-8}	2.77×10^{-7}	5.32×10^{-10}	3.29×10^{-9}	
*2211	4.09×10^{-8}	5.72×10^{-7}	3.64×10^{-7}	9.16×10^{-10}		

* Data not used in computation of enthalpies.

Table 3

Enthalpy Changes from Free Energy Functions

Reaction T°K	1 $-\Delta H_0^0$ kcal/mol	2 $-\Delta H_0^0$ kcal/mol	3 $+\Delta H_0^0$ kcal/mol	4 $+\Delta H_0^0$ kcal/mol
2567	219.0	234.6	15.6	54.3
2518	219.6	235.4	15.8	56.9
2470	218.8	235.6	16.7	56.9
2417	219.0	235.6	16.5	57.2
2343	219.2	236.1	16.9	
2290	219.3	236.3	17.0	
2290	219.0	236.2	17.3	
2337	219.5	236.4	16.9	
2279	219.5	236.3	16.8	
2179	217.5	236.3	18.9	
2290	218.1	235.3	17.2	
2226	220.2	239.8	19.5	

Table 3A

Standard Enthalpy Changes, ΔH_0^0

Reaction	van't Hoff Equation (slope)	Free Energy Functions
	kcal/mol	kcal/mol
(1)	-216.3 ±4.6	-219.0 ±0.2
(2)	-252.2 ±3.3	-236.2 ±0.4
(3)	+ 36.2 ±4.0	+ 17.1 ±0.3
(4)		+ 57 ±1.0
(5)	+952 ±71 (ΔH_{2350}°)	

Note: (a) The ± values listed are the standard errors

(b) Reactions considered:

(1) $Al(g) + Be(g) + O(g) \rightleftarrows AlOBe(g)$

(2) $2Al(g) + O(g) \rightleftarrows Al_2O(g)$

(3) $Al_2O(g) + Be(g) \rightleftarrows AlOBe(g) + Al(g)$

(4) $\frac{1}{2}O_2(g) \rightleftarrows O(g)$

(5) $Al_2O_3 \cdot BeO(1) \rightleftarrows 2Al(g) + Be(g) + 4O(g)$
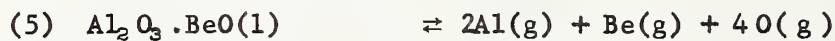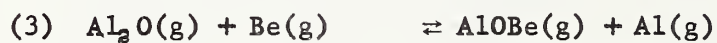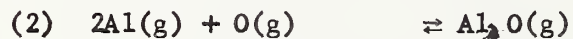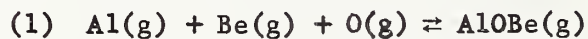
References

(1) J. Hilsenrath, G. G. Ziegler, C. G. Messina, P. J. Walsh and R. J.
     Herbold, "A General-Purpose Interpretive Program for the
     Calculation of Tables of Functions and Statistical and Numerical
     Analysis," NBS Handbook 101 (1965), to be published.

(2) W. J. Dixon and F. J. Massey, Jr., "Introduction to Statistical
     Analysis," McGraw-Hill Book Co. (1957). p. 412.

(3) D. S. Dickson, J. R. Myers, R. K. Saxer, J. Phys. Chem. $\underline{69}$, 4045
     (1965).

Chapter 6

VAPORIZATION OF REFRACTORY MATERIALS:
ARC-IMAGE RESEARCH

by

J. J. Diamond and A. L. Dragoo

Vapor-Deposited Oxides

DTA studies were carried out from 50° to 1000°C on three samples

of amorphous alumina, on a sample of amorphous alumina contaminated with

silica and on BeO. All samples were produced by vapor-deposition on the

glass envelope of the vacuum chamber from samples melted with the arc-

image furnace. The alumina samples initially gave no x-ray diffraction

lines and no electron diffraction rings. In addition, DTA was performed

on an amorphous alumina sample heated from 50° to 450°C and then cooled

to 200°C. The DTA apparatus was set for a rise rate of 10°/min., and

all runs were performed in air. The amorphous alumina gave exothermal

peaks at about 320° and 860°C, and the final product gave only two diffuse

x-ray diffraction lines at d = 1.98A and 1.39A, corresponding to a poorly

formed γ-alumina. The contaminated alumina yielded an exothermal peak

at 860°C and its product yielded a similar x-ray pattern; however, the

DTA curve was affected by electronic noise. No DTA peaks were obtained

during cooling for any of the aluminas.

The final alumina form obtained from the DTA experiment corresponds

to the product reported earlier (Report 8628) at temperatures between

570° and 670°C after annealing periods of 8 hours and longer. However,

the exothermal peak at 320°C remains to be explained.

One possible explanation is that transformation occurs at this temperature. However, amorphous alumina annealed at 330°C for 360 hours still gave an amorphous pattern.

TGA of two amorphous alumina samples, one in air and the other in vacuum, from room temperature to 700°C showed weight losses of 3.5 and 3.3 per cent, respectively, which were linear with respect to time. If there were uncombined Al or suboxides present in the sample, these could give rise to the exothermal DTA peak at 320°C and would result in a lower weight loss in air than in vacuum when heated. The presence of essentially equivalent weight losses excludes the possibility of uncombined aluminum or of suboxides.

A third possible cause for this DTA peak is the release of strain energy at 320°. The film as produced is highly strained and tends to curl on heating.

The BeO film initially gave an x-ray diffraction pattern with only a broad hump at d ≈ 2.34A. The film gave only diffuse rings when examined by electron diffraction, which were inseparable from those of the formvar substrate. The DTA curve contained two large endothermal peaks at about 100° and 200°C, probably due to loss of water, but no other peaks. The product from the DTA heating yielded the three strong diffraction lines of the common hexagonal BeO (bromellite).

The absence of any exothermal DTA peak, corresponding to a transition to a more highly ordered BeO form, indicates that the film is probably deposited as very small crystallites of hexagonal BeO, no larger than a few unit cells. The absence of distinct electron diffraction rings probably results from secondary scattering from the thick films.

Kerr [1] obtained BeO films by treating $BeSO_4$ solutions with Na_2CO_3, $(NH_4)_2CO_3$ or NH_3 which he studied by electron diffraction. Crystal sizes were estimated from the ring breadths. As formed the crystal sizes were about 10A. Upon heating to 500° for one-half hour they increased to about 100A. Since the haloes for the film fell near prominent sharp rings of beryllium oxide, he concluded that the diffuse rings were probably due to the BeO crystals.

Vaporization of Molten Alumina

Measurements of the rate of vaporization of molten alumina were repeated using an automatic pyrometer instead of a visual pyrometer. The vapor pressures and standard heats of vaporization were calculated for the two cases: (1) the surface of the drop was assumed to be a spherical segment and (2) the surface was assumed to be an ellipsoidal segment. Virtually, the same average values of $\Delta H^{\bullet}_{298}$ were obtained (approximately 725 kcal mole^{-1}); however, the individual values showed a significant upward trend with temperature. Values obtained for $\Delta H^{\bullet}_{298}$ using the visual pyrometer show no discernible trend with temperature.

One possibility is that because the automatic pyrometer has a different sensitivity to the spectrum than the human eye, the drop may be more transparent at the effective wavelength λ_T of the pyrometer than at the λ_T of the visual pyrometer. However, this possibility would only account for the heats which are too low.

Another possibility, suggested by a recent paper by Finkel'shtein [2], is that the surface of the liquid cools perceptibly when the

cross-over point chopper is interposed between the arc and the sample.
Using Finkel'shtein equations and data from his tables, the maximum
cooling is estimated to be -29° at 2500°K and -34° at 2600°C, assuming
a total emissivity of 1.0. The pyrometer samples the temperature of
the drop only when the arc radiation is cut off by the chopper. Since
the pyrometer measures the temperature of a finite volume of the liquid
beneath the surface, the measured temperature would be between the tempera-
ture which the drop attains during heating by the arc and the surface
when the arc radiation is cut off by the chopper. Furthermore, the
total emissivity is probably less than 1.0, so that the error due to
cooling of the surface is reduced further. Moreover, the surface cooling
error is present to about the same extent when the visual pyrometer is
used (i.e., cooling times are nearly the same). Consequently, it appears
that cooling of the surface of the drop during the time that temperatures
are measured is not the source of error in the heats.

Finally, since the spectral emissivity is nearly constant up to
angles of 55° from the normal and since the area of the surface sampled
by the automatic pyrometer is well within this for a 0.64 cm diameter
drop, the spectral emissivity is nearly constant with respect to
direction of incidence for all measurements.

None of these three possibilities offer an adequate explanation
of the trend in the third law heats. Further investigation of the
characteristics of the automatic pyrometer will have to be made before
it can be used effectively in making vapor pressure measurements.

References

[1] I. S. Kerr, Acta Cryst. $\underline{9}$, 879 (1956).

[2] V. E. Finkel'shtein, High Temp. $\underline{3}$ [1], 120 (1965), transl. of
     Teplofiz. Vysokikh Temperatur $\underline{3}$ [1], 134 (1965).

A CALORIMETRIC DETERMINATION OF THE ENTHALPY
OF SOLID AND LIQUID ALUMINUM OXIDE TO 2500°K

by E. D. West and S. Ishihara

Data for the enthalpy of aluminum oxide at high temperatures are essential for thermodynamic calculations involving fuels which contain aluminum compounds. But data on Al_2O_3 have a much broader significance because Al_2O_3 is generally used for intercomparison of apparatus. From such intercomparisons, decisions can be made on the inclusion or weighting of data from different sources in tables of thermodynamic data. From this standpoint, measurements reported below bear on the use to be made of all high temperature data originating in the USSR and elsewhere.

Materials

Several different specimens of Al_2O_3 were used, all single crystals in the form of ground rods obtained from the Linde Division of the Union Carbide Corp. The polished specimens were observed to be transparent "white sapphire" with no inclusions. All specimens were washed in CCl_4 and hot 50% HCl, then heated to red heat in a platinum container. Analyses are not yet available.

Apparatus

The apparatus used for this work has been described briefly [1]. Essentially, it consists of a furnace in which the sample is held at various high temperatures and a calorimeter, operating near room temperature, which measures the heat given up when the hot sample is lifted into it.

The principal errors in this type of measurement are: (1) measuring the true sample temperature, (2) accounting for changes in weight of the sample at high temperatures, (3) accounting for heat loss from the capsule as it is transferred to the calorimeter and for heat radiated directly from the furnace into the calorimeter during this transfer. Available calorimetric techniques are more than adequate for this type of work, although they are sometimes allowed to impair the accuracy of the measurements. The calorimeter used in this work is an adiabatic calorimeter. Its energy equivalent has been determined electrically with a standard deviation of 0.006 percent, approximately two orders of magnitude better than the overall enthalpy results so that the calorimeter does not contribute significant uncertainty.

In our apparatus the capsule is suspended on a wire to facilitate repeating measurements. The difficulty of this technique has apparently prevented its previous use at these high temperatures, yet it is essential for analyzing the results obtained. Our method of operation alternates experiments on an empty capsule with experiments on the capsule plus sample. The difference is the enthalpy of the sample and, with care, corrects directly for item (3) above. The capsule also protects the sample chemically and mechanically from the environment, so that item (2) can be kept well within bounds. This method of operation, which obtains in one day all the data necessary for calculating the enthalpy at one furnace temperature, has several advantages. Subsequent accidents with either sample or capsule do not affect the work already done. If, for example, the capsule gradually changes weight, only the relatively small change during a single day affects the data. Another advantage is that capsule and sample may be changed to suit the temperature range or other experimental conditions. This flexibility has been quite useful in measurements on Al_2O_3. A third advantage is that, in duplicating an experiment, e.g., the empty capsule, at the beginning and end of the day, many of the changes during the day are accounted for in the data.

Measuring the true temperature of a sample has proved to be more difficult. The problems here can be further subdivided: (1) errors in the temperature measuring instruments – optical pyrometer in our high temperature range. These errors include errors in emittance or emittance corrections which we have kept small by using a furnace which is very nearly a black body. (2) The sample may not be at a uniform temperature because of a steady-state temperature gradient in the furnace, or a transient temperature gradient in the furnace due to changing furnace temperature. (Another error is possible due to a transient temperature in the sample because it is not held in the furnace long enough so that its interior is too cold. Such an error results only from poor technique and is mentioned mainly to indicate our awareness of it.)

Transient effects due to changing furnace temperature are made negligible in our apparatus by controlling the furnace temperature directly and holding it constant for several hours before the first experiment. The steady-state gradient in the furnace has been made quite small by insulating the furnace with fine powder and distributing the heat input so that a little more heat is provided at the ends of the furnace. The effectiveness of the insulation is shown by the power requirement of 980 watts at 2500°K, which is quite small for a hot zone 5/8" in diameter and 16" long. Evidence for the adequacy of these measures is that the measured enthalpy for an experiment at 1500°K with the pyrometer focussed on a furnace wall agrees to 0.02 percent with an experiment with the pyrometer focussed directly on the capsule.

The principal difficulty with the temperature measurements has proved to be in the temperature measuring instrument itself. The instrument used is an automatic photoelectric optical pyrometer which gives a continuous output for both control and observation. This instrument has aided the control problem and eliminated the observer bias associated with visual instruments. As a result of analysis for the source of diurnal changes in the Al_2O_3 data, we found the pyrometer to change significantly with room temperature. Some of the change can be eliminated by balancing the electronics for each lamp current, but there is a residual effect which will require better control of room temperature or direct control of the pyrometer temperature.

Results

The corrected experimental data for the enthalpy of solid aluminum oxide are shown in Table 1. In the solid range, three kinds of capsules and five different samples were used. A pyrolytic graphite capsule was used up to 1406°K, a molybdenum capsule from 1493 to 2110°K, and tungsten capsules above 2110°K. The samples were single crystal "white sapphire" rods, selected or cut to fit the particular capsule. Most were optical quality "windows" with ends polished. More capsules and samples were required above 2200°K due to greater experimental difficulties in this range.

The temperature of the capsule in the furnace was measured with a Leeds and Northrup automatic photoelectric pyrometer. The temperature has been corrected for the loss of radiation in the prism and also for changes in room temperature. The pyrometer was calibrated at room temperatures of 25 and 28°C by the NBS Pyrometry Section. Corrections were then applied for variations in our laboratory temperature. The trend of the data – e.g., on 10-27-65 – indicate something amiss. Measurements at 1500 degrees sighting on the furnace wall agree with similar measurements sighting directly on the capsule. This observation and the fact that not all measurements have a diurnal trend indicate that the cause of the diurnal trend is not to be found in the changing temperature gradient in the furnace as was formerly thought [1]. Elimination of this possibility left as the most likely source of error some variation due to the pyrometer itself. This was later verified by experiments with a tungsten strip lamp varying the temperature of the room. In our laboratory where the temperature may vary from 21 to 31°C the possible temperature measurement error due to this effect amounts to a maximum of about three tenths of a percent in the high range.

The quantity of heat in column 2 of Table 1 includes corrections for the enthalpy of the capsule and contents between the actual calorimeter temperature and 298.15, for occasional small changes in the furnace temperature, and for any small weight changes during the day. The data for the enthalpy correction to 298.15 are based on tables given by Stull and Sinke [2] for tungsten, molybdenum, and tantalum, and on tables given by Furukawa, et. al. [3] for aluminum oxide. The largest change in weight of the sample occurred at 2300°K and amounted to 0.1 percent for the entire day.

The number of moles of aluminum oxide, given in column 3, were calculated from weight in vacuo, using a molecular weight of 101.9612. The small decreases in the weight of the aluminum oxide samples were assumed to be simply loss of aluminum oxide.

The calculated molar enthalpy for each temperature is shown in the column 4. The data for the solid were fit by the method of least squares to obtain the following equation for the enthalpy in Joules per mole for temperatures between 1170°K and the melting point:

$$H_T - H_{298.15} = 121.0504T + 0.00618697T^2 - 23300.5 \log_{10} T$$

$$+ 21014.3 , \qquad (1)$$

which fit the data with a standard deviation of 0.22 percent. Deviations for the experimental values from eq. (1) are shown in the last column.

Liquid aluminum oxide presents a different container problem from the solid. Kantor, et. al. [4] cites the need for sealing the aluminum oxide container. In their work on the melting point of aluminum oxide, Chekovskoi and Petrov [5] found no need for sealed ampoules. We find some validity in both points of view. Our first experiments in the liquid range were made with an aluminum oxide sample placed directly in an unsealed capsule. The data obtained are not very reliable because experiments were carried out on only one empty and one full capsule. (The Al_2O_3 cannot be removed from the tungsten capsule after melting.) We were unable to repeat these experiments. In all subsequent experiments, liquid Al_2O_3 oozed out the top of the capsules and the balance of the measurements were made with the sample sealed by welding in a tungsten inner container which could be inserted into the tungsten capsule and removed to check for weight changes. This method has the advantage of close check on the weight, but the disadvantage that the enthalpy of tungsten must be known in order to obtain the enthalpy of aluminum oxide. The inner container (0.4" dia. x 1.1" long) was welded in vacuum with an electron-beam. This technique gives

74

intense local heating and avoids melting more than a very small region of tungsten. The container cools rapidly by radiation so that the temperature decreases rapidly with distance from the weld. The Al_2O_3 was kept about 7/16" below the weld in order to avoid vaporizing any of it. The total weight loss in welding was 4.7 mg, all of which was assumed to be tungsten. A light film was deposited on the window of the vacuum chamber during the welding. This appeared to be "tungsten blue". The container cracked and leaked Al_2O_3 when heated to 2600°K.

Table 2 shows the experimental data for liquid aluminum oxide plus the tungsten inner container. For comparison, the last two lines show the same quantity calculated from the experiments on an unsealed capsule. The data were fit by the method of least squares to obtain the enthalpy in joules per 0.018095 moles of aluminum oxide plus 0.062702 moles of tungsten:

$$H_T - H_{298.15} = 5.21799T - 1555.7 \tag{2}$$

Deviations of experimental enthalpies from this curve are shown in the 3rd column of Table 2. The enthalpy of liquid Al_2O_3 calculated from the experimental data in column 3 and the tungsten data of [6] are shown in column 4 of the table.

Discussion

At 1200°, equation (1) gives a value for the enthalpy 0.19 percent above the earlier and more reliable work reported by Furukawa, Douglas, McCoskey, and Ginnings [3]. This is considered good agreement in view of the problems with optical pyrometry.

Chekhovskoi [7] has recently reviewed and smoothed enthalpy data for solid aluminum oxide. In the high temperature region, his formulation is based on two papers, both originating in the USSR [4,7], with implications for the quality of corresponding work in this country. The values for the enthalpy calculated from his formulation are less than those calculated from eq. (1) by about 0.1 percent at 1400°K, increasing to 1 percent at 2300°K. Considering the precision of their data the agreement is quite good. Our data agree somewhat better with the data of reference [4] which are somewhat more precise than those of reference [7]. It is indicated in reference [4] that a better pyrometer was used than in reference [7]. The agreement of our work with Chekhovskoi's formulation substantiates the acceptable accuracy of data from these two groups in the USSR. In conjunction with reference [7], the reliability of data from a large number of sources can be roughly evaluated from their measurements on Al_2O_3. Agreement on results Al_2O_3 are necessary (but not a sufficient) indication of the accuracy of

results on other materials. For example, reference [7] cites difference of differences of 1.5 to 2.3 percent from another experimental group on aluminum oxide, but differences of 1 to 3 percent on tungsten in the same temperature range.

Our experimental results in the liquid range cannot be reduced to enthalpy data for Al_2O_3 until we obtain satisfactory data for the enthalpy of tungsten. Considering our agreement on Al_2O_3 at just below the melting point with Chekhovskoi's compilation, the tungsten data of Kirillin, Sheindlin, Chekhovskoi and Petrov [8] are to be preferred over the tungsten data in JANAF tables. Using these data to calculate a comparison for our one unsealed capsule experiment, gives a result roughly 1 percent below our observed enthalpy for the tungsten plus Al_2O_3. This corresponds very closely to the deviation of Chekhovskoi's compilation for Al_2O_3 from our data just below the melting point. Our data, corrected with Kirillin's tungsten data, lie 1.9 to 2.6 percent above the data of Kantor, et. al. [4] which we might expect on the basis of our agreement on solid aluminum oxide. The data from the unsealed experiment give a result 0.6 percent above their data.

A similar effect is present in the data for the heat of fusion. Using the data of Kirillin [8] we obtain 29.7 kcal/mole for the heat of fusion. If we assume these tungsten data are 1 percent too low based on the relative measurements on Al_2O_3 we obtain 29.2 kcal/mole, compared to 28.3 ±0.55 obtained by Kantor, et. al., and 26.0 kcal/mole estimated from phase studies and included in earlier reports of this series.

Conclusions

Agreement between our work and the compilation by Chekhovskoi indicate that the high temperature enthalpy of aluminum oxide is known from 1200°K to the melting point within 1 percent which is adequate for most engineering calculations. Measurements from other laboratories on other materials can be judged roughly by how well their Al_2O_3 results agree with the compilation of Chekhovskoi although differences of the order of 1 percent cannot be accorded any significance.

In the liquid range, the data of Kantor, et. al appear in reasonable agreement with what we will get if the present tungsten data are too low. Until we complete measurements on tungsten we recommend use of their liquid enthalpy data, including the heat of fusion.

References

[1] E. D. West and S. Ishihara, in "Advances in Thermophysical Properties at Extreme Temperatures and Pressures", Am. Soc. Mech. Engr. (1965) p. 146.

[2] D. R. Stull and G. C. Sinke, Thermodynamic Properties of the Elements, American Chemical Society, Washington (1956).

[3] G. T. Furukawa, T. B. Douglas, R. E. McCoskey, and D. C. Ginnings, J. Res. Natl. Bur. Standards 57, 67 (1956).

[4] P. B. Kantor, L. S. Lazareva, V. V. Kandyba, and A. N. Fomichev, Ukr. fiz. zh. 7, (1962).

[5] V. Ya. Chekhovskoi and V. A. Petrov, Measurement Techniques, 751 (1963), translated from Izmeritel'naya Tekhnika p. 26 (1963).

[6] V. A. Kirillin, A. E. Sheindlin, V. Ya. Chekhovskoi, Inzh-fiz Zhurn. 4, (1961)

[7] V. Ya. Chekhovskoi, High Temperature 2, 264 (1964, translated from Teplofizika Vysokikh Temperatur 2, 296 (1964).

[8] V. A. Kirillin, A. E. Sheindlin, V. Ya. Chekhovskoi, and V. A. Petrov, Zh. Fiz. Khimii 37, (1963).

Table 1

Experimental Data for Solid Al_2O_3

Furnace Temperature °K, and Date	Heat to Calorimeter at 298.15°K	Moles Al_2O_3	$H_T-H_{298.15}$ and % above Eq.
1171.4 4-14-65	13813.0 J 13818.1 2946.6 2946.2 2944.6 13813.7	.108932	99779.4 J/gfw − .02
1307.0 4-16-65	3520.9 16290.5 16290.3	.108932	117223.6 + .04
1406.0 4-23-65	18107.5 3949.7 3948.0 18114.7	.108932	130009.0 − .07
1493.6 5-10-65	2880.5 2880.0 9330.4 9332.1 2883.0	.045471	141850 + .14
1587.2 5-12-65	10141.0 3129.6 3130.7 10139.3	.045471	154160 + .01
1712.8 5-14-65	3471.0 3471.2 11254.9 11254.8 3475.0	.045471	171150 .00
1806.2 5-17-65	12083.8 3734.7 3737.0 3738.3 12090.2	.045470	183640 − .17
1914.6 5-26-65	4095.5 13137.2 13138.4 4096.1	.045462	198890 − .05
2011.4 6-1-65	14042.1 4396.6 4399.2 14051.1	.045433	212370 − .09
2110.1 6-4-65	4685.3 14969.8 14971.2 4686.2	.045394	226570 + .02
2219.9 6-7-65	6226.0 6223.6 17257.7 17269.1 6243.7	.045345	243300 + .43
2225.2 10-27-65	16226.5 16260.5 5160.3 5169.6	.045467	243660 + .27
2293.5 6-9/11-65	18010.1 18020.7 6568.3 6577.7	.045300	252590 − .12
2296.4 9-7/8-65	17847.9 6378.4 6384.2 17845.0	.045441	252310 − .39

78

<div align="center">

Table 2

Enthalpy of Liquid Aluminum Oxide

</div>

Furnace Temperature °K, and Date	Heat to Calorimeter at 298.15°K Joules	$H_T-H_{298.15}$ for $Al_2O_3 + W$ Joules Deviations, %	$H_T-H_{298.15}$ $Al_2O_3(\ell)$ J/mole
2316.5 9-10-65	16257.5 5811.3	10446 -0.82	373960[*]
2338.8 9-29-65	5504.7 16204.6	10700 -0.48	385770[*]
2338.8 9-29-65	16077.2 5480.2	10597 +0.48	380080[*]
2374.6 9-17-65	6255.8 17135.6 17096.6	10860 +0.24	390360[*]
2425.1 9-21-65	17530.4 6500.3 6555.8	11002 -0.87	392280[*]
2487.6 9-24-65	7031.3 18630.1	11599 +1.50	417820[*]
2387.9 5-28-65	7589.7 14284.0	10800[*] -1.1	385440

[*] Calculated using enthalpy of tungsten from Kirillin, et. al. [6].

Chapter 8

$BeO \cdot Al_2O_3$ AND $BeO \cdot 3Al_2O_3$: NEW MEASUREMENTS OF RELATIVE ENTHALPY
BETWEEN 273 AND 1173°K. TABULATED THERMODYNAMIC FUNCTIONS, 0-2150°K

by David A. Ditmars and Thomas B. Douglas

The relative enthalpy of two samples of $BeO \cdot Al_2O_3$ was measured at
the National Bureau of Standards in 1962 and 1963. The results of these
measurements have been presented in a previous report [3]. The results
of low-temperature heat-capacity measurements on this compound were
combined with the then existing high temperature measurements to yield
a smooth table of thermodynamic functions extending from 0 to 2150°K [3].

Since then, repairs and modifications to the ice calorimeter as
well as improved thermometry has made it possible to attain a better
precision than that of the above measurements. An additional determina-
tion of the relative enthalpy of $BeO \cdot Al_2O_3$ from 273 to 1173°K was
therefore undertaken. The samples were chosen from the same material which
had been used in measurements of the low temperature heat capacity [4].
A sample of pure $BeO \cdot 3Al_2O_3$ also became available. Again, portions of
the same material used in the low-temperature heat-capacity measurements
(reported in Chapter 4 of the present report) were used in the high
temperature enthalpy measurements on this compound.

SAMPLES

Two separate samples of $BeO \cdot Al_2O_3$ were used, hereafter referred to
as samples 3 and 4. In details of preparation and composition, they
correspond to "Sample 2" described in the previous report [3]. The two
samples of $BeO \cdot 3Al_2O_3$ are referred to as samples 5 and 6. Details of
their preparation, analysis and composition are given in Chapter 4 of
the present report.

EXPERIMENTAL

The high-temperature enthalpy measurements were made by the "dropping"
method using a Bunsen ice calorimeter. The method, which has been de-
scribed in detail in previous publications [5,6,7,8], is as follows:
The sample, enclosed in a suitable container - in the present case, of
pure silver - is suspended inside a thick walled silver pipe in a re-
sistance furnace until it attains the constant furnace temperature. It
is then dropped, with nearly free fall, into the ice calorimeter, which
measures the heat evolved by the samples plus container in cooling to 0°C.
In order to account for the enthalpy of the container and the small but
appreciable heat lost during the drop, similar measurements are made with
an identical empty container over the same range of furnace temperatures.
In the present case, the enthalpy data for the empty silver container was
fit to an equation by the method of least squares. The empirical equation
was then used to determine the container enthalpy minus heat lost during
the drop at appropriate furnace temperatures. See Table 1.

Table 1

Enthalpy Measurements on Empty Silver Capsule

Furnace Temperature (°C)	Measured Heat (cal.)[a]	Mean Meas. Heat (cal.)	Calculated Heat (cal.)[b]
50.0	36.88 36.62 37.19	36.90	36.75
100.0	74.08 74.02 73.84	73.98	74.02
200.0	149.87 149.33 149.80	149.67	149.79
300.0	227.09 226.79 227.14	227.01	227.02
400.0	306.43 305.62 306.12	306.06	305.75
500.0	385.99 385.60 386.25 386.08	385.99	386.14
600.0	468.25 468.40 468.20	468.28	468.37
700.0	552.73 552.87 552.70	552.77	552.67
800.0	639.43 638.95 639.50	639.30	639.28
900.0	728.31 728.28 728.62	728.40	728.42

[a] 1 defined cal. = 4.1840 abs. joules.

[b] $H_T - H_{0°C} = (0.76152)T + (2.3649)10^{-5} T^2 + (0.42246)10^{-7} T^3 - (8.9987) [T/(273.15 + T)]$ H, (cal)   T, (°C)

Sample containers used in the present investigation were loaded and their tops capped, in an atmosphere of air in a dry-box. They were weighed directly upon removal and sealed by flame welding immediately thereafter. Samples 3 (BeO•Al$_2$O$_3$) and 5 (BeO•3Al$_2$O$_3$) were removed from their containers after completion of some measurements at each temperature. Small amounts were removed for petrographic examination and the remaining samples resealed in new silver containers as above. Measurements on the resealed samples were then carried out at selected temperatures. At 500°C and below, furnace temperatures were measured with a platinum resistance thermometer and a Pt--Pt 10% Rh thermocouple. Above 500°C, temperatures were measured with the above thermocouple and another independently calibrated Pt --Pt 10% Rh thermocouple. The thermocouples and resistance thermometer were intercompared over the range 50 - 500°C in place in the furnace; the observed differences were then extrapolated to correct the thermocouple calibrations above 500°C.

As a check on the accuracy of the calorimeter before the present series of runs, the relative enthalpy of a sample of α-aluminum oxide sealed in a silver capsule was measured at 100, 500 and 900°C. The values so obtained agreed with previously published measurements on aluminum oxide [8] to within 0.2%.

RESULTS

Tables 2 and 3 present the combined results of the measurements. Columns 2, 3, 10 and 11 are observed, unsmoothed heat values for the appropriate samples with containers. Values in parentheses correspond to measurements on samples opened and resealed as described above. The entries in column 10 for sample 5 of BeO•3Al$_2$O$_3$ marked with asterisks yielded relative enthalpy values (column 12) which were an average of 0.15% below any plausible extrapolation of the data at lower temperatures. Also, they disagreed by the same amount with measurements on sample 6 as well as measurements on sample 5 resealed. For these reasons, they were given no weight in the least squares fit of the data. The cause of the systematic deviation of this one set of measurements on sample 5 above 500°C is unknown.

Columns 4, 5, 12 and 13 give net enthalpy values for the samples corresponding to the gross measured heat values of columns 2, 3, 10 and 11, respectively. These values were derived by subtracting the appropriate empty container value (Table 1) from the gross sample and container value and expressing the result in terms of one mole of sample. The actual sample masses used are entered in the footnotes to the tables. Columns 6 and 14 give the mean of all observations on all samples of the appropriate compound with exceptions as described above.

Table 2

Enthalpy Measurements on $BeO \cdot A\ell_2O_3$

1	2	3	4	5	6	7	8
Furnace Temperature $t^\circ C$ [a]	Gross Measured Heat (cal) [b]		$H_t - H_{0^\circ C}$ net for Sample (cal/mole) [b,c]				
	Sample 3 [d] and Container	Sample 4 [e] and Container	Sample 3	Sample 4	Mean Obs.	Calc. from eq. (1)	Mean obs.− Calc. (%)
50.0	95.23 95.18 95.25 [95.36 95.47 95.51 95.23 95.41 95.32]	97.96 97.87 97.76 97.86 97.88 97.80	1250. 1249. 1251. [1259. 1262. 1263. 1257. 1261. 1259.]	1262. 1260. 1258. 1260. 1260. 1259.	1258.	1257.0	+0.08
100.0	199.39 199.26 198.79 198.59 198.72 198.80 [199.52 199.45 199.37]	204.35 204.53 204.14 203.69 203.79	2680.5 2677.7 2667.8 2663.4 2666.3 2667.9 [2696.7 2695.1 2693.5]	2687.1 2690.8 2682.8 2673.5 2675.5	2679.9	2681.2	−0.05
200.0	424.79 424.11 425.27 424.50 423.96 424.04 425.28 423.09 424.73 424.82 422.88 424.04 423.27 424.75 424.16 424.16		5879.8 5865.4 5890.1 5869.5 5862.1 5863.7 5890.4 5843.4 5878.5 5880.5 5839.0 5863.7 5847.4 5878.9 5866.2 5866.4		5867.8	5881.0	−0.22
300.0	665.49 666.24 665.73 665.77 665.75 665.87 666.06 665.86		9374.8 9390.9 9380.1 9380.9 9380.5 9383.1 9387.1 9382.9		9382.5	9404.8	−0.24
400.0	921.62 921.47 921.53		13168. 13165. 13166.		13166.	13150.	+0.12
500.0	1184.62 1184.42 1184.44 1184.30		17072. 17068. 17068. 17065.		17068.	17053.	+0.09
600.0	1454.46 1454.47 1455.20		21084. 21084. 21099.		21089.	21074.	+0.07
700.0	1729.56 1729.25 1729.05		25163. 25156. 25152.		25157.	25182.	−0.10
800.0	2011.98 2011.68 2011.79		29350. 29343. 29346.		29346.	29353.	−0.02
900.0	2299.10 2298.83 2299.01		33583. 33577. 33581.		33580.	33571.	+0.03

[a] International Temperature Scale of 1948, as modified in 1954.
[b] 1 Defined cal.= 4.1840 abs. joules.
[c] Molecular weight = 126.9728
[d] Values in this column are derived from two independent sets of measurements on sample 3. All values from the second set are enclosed in brackets. The sample mass corresponding to the first set was 5.9385 g. Some of this sample was removed for analysis. The sample mass corresponding to the second set was 5.9090 g.
[e] Mass of sample 4 = 6.1583 g.

Table 3

Enthalpy Measurements on $BeO \cdot 3Al_2O_3$

9	10	11	12	13	14	15	16
	Gross Measured Heat (cal)		$H_t-H_{0°C}$ net for Sample (cal/mole)[f]				
Furnace Temperature t°C	Sample 5[g] and Container	Sample 6[h] and Container	Sample 5	Sample 6	Mean Obs.	Calc. from eq. (2)	Mean obs. - Calc. (%)
50.0	101.96 102.13 101.89	134.64 134.61 134.63 134.37 134.91 134.64 134.57 134.75 134.62 134.49	3170.1 3177.9 3166.6	3170.5 3169.4 3170.1 3161.5 3179.1 3170.3 3168.2 3174.0 3169.6 3165.7	3170.2	3163.6	+0.21
100.0	212.33 211.99 212.43	281.75 281.73 281.48	6723.2 6706.9 6728.3	6727.9 6727.3 6719.1	6722.1	6726.9	−0.07
200.0	451.73 451.85 451.75		14678. 14683. 14679.		14680.	14687.	−0.05
300.0	708.35 708.33 708.17		23398. 23397. 23390.		23395.	23387.	+0.03
400.0	976.14 976.06 975.92		32588. 32584. 32577.		32583.	32574.	+0.03
500.0	1252.48 1252.30 1252.59 [1219.43 1219.67 1219.23]	1685.23 1685.08 1684.98 1684.34 1685.55 1685.46 1685.55 1685.40	42114. 42105. 42119. [42134. 42144. 42124.]	42075. 42070. 42066. 42046. 42085. 42082. 42085. 42080.	42095.	42109.	−0.03
600.0	*1534.45*[k] *1534.23* *1534.50* [1495.67 1494.97 1495.10]	2071.08 2070.99 2070.80 2070.43 2070.48	*51824.* *51813.* *51826.* [51944. 51908. 51915.]	51908. 51905. 51899. 51887. 51889.	51907.	51910.	−0.01
700.0	*1824.64* *1824.82* *1824.69* [1777.53 1777.18 1777.20]	2464.92 2465.26 2465.13	*61832.* *61841.* *61834.* [61932. 61915. 61916.]	61933. 61944. 61940.	61930.	61928.	0.00
800.0	*2121.84* *2121.74* [2065.63 2065.99 2065.58]	2866.84 2866.79 2866.96	*72069.* *72064.* [72120. 72139. 72118.]	72145. 72144. 72149.	72136.	72128.	+0.01
900.0	*2422.96* *2423.15* *2422.78* [2360.07 2359.83 2360.06 2359.10 2359.89 2359.69]	3275.92 3274.90 3274.96 3275.03	*82374.* *82383.* *82365.* [82501. 82489. 82501. 82452. 82492. 82482.]	82474. 82476. 82479.	82483.	82490.	−0.01

[f] Molecular weight = 330.8952

[g] Values in this column are derived from two independent sets of measurements on sample 5. All values from the second set are enclosed in brackets. The sample mass corresponding to the first set was 6.8068 g. Some of this sample was removed for analysis. The sample mass corresponding to the second set was 6.5441 g.

[h] Mass of sample 6 = 10.2170 g.

[k] Starred values not included in least squares fit of data. (See text.)

84

These two sets of mean observed values were then fit by the method of least squares to empirical equations, weighting all means equally. In the case of $BeO \cdot Al_2O_3$, some of the data obtained by low temperature adiabatic calorimetry in the range 0–100°C [4] were also included in order to obtain thermodynamic functions merging more smoothly with those derived from low-temperature data above. These equations, where H_T is the relative high-temperature enthalpy in cal/mole and T the temperature in deg. K are as follows (σ is the standard deviation of the mean observed values from the equation values):

$$BeO \cdot Al_2O_3 : \quad H_T - H_{273.15°K} = (-1.00242)10^{-6} \, T^3 + (2.65426)10^{-3} \, T^2$$

$$+ (45.8430)T - (6.54908)10^3 \, lnT + 24040.8 \tag{1}$$

$$\sigma_1 = \pm 13.41 \text{ cal/mole}$$

$$BeO \cdot 3Al_2O_3 : \quad H_T - H_{273.15°K} = (4.51018)10^{-3} \, T^2 + (97.1407)T$$

$$+ (5.09824)10^6 \, T^{-1} - (2.76996)10^8 \, T^{-2} - 41822.6 \tag{2}$$

$$\sigma_3 = \pm 10.54 \text{ cal/mole}$$

The percentage deviations of calculated from observed values are given in columns 8 and 16. While the equations do not yield values consistently within the current precision of measurement, the deviation of the calculated from the mean observed values is usually less than 0.1%.

THERMODYNAMIC FUNCTIONS, DISCUSSION OF RESULTS

In order to obtain continuous and smooth tables of thermodynamic functions extending over the solid range of these compounds, some compromise of both the low- [4,9] and high-temperature data was necessary. Also, the appropriate form of extrapolation above the measuring range had to be considered. The results are presented as tables B-83 (second revision) and B-151 of this report (Appendix I). Details of the derivation of these tables are as follows. All mathematical work was performed on an IBM 7090 computer. Smooth tables of heat capacity from 0°K to 1173°K were first obtained by numerically smoothing the Debye characteristic temperatures (θ_D) derived from the smoothed low-temperature heat capacity data and those calculated from equations (1) and (2). These tables were then examined in light of the possible errors entering into the low- and high-temperature measurements. This initial smoothing adequately represented both the low- and high-temperature results for $BeO \cdot 3Al_2O_3$. In the case of $BeO \cdot Al_2O_3$, a preliminary graphical smoothing of the high temperature heat capacity values in the range 0–450°C had to be performed before the machine smoothing. The deviations of the low- and high-temperature heat capacities relative to the compromise smooth values are shown in figures 1 and 2. In table 4, values of $H_{373.15°K} - H_{273.15°K}$ are given as derived from the low- and high-temperature measurements, along with the compromise value.

Table 4. Comparison of the enthalpy increment $H_{100°C} - H_{0°C}$ determined by two methods and compromise value.

Method	$H_{100°C} - H_{0°C} = \int_{273.15°K}^{373.15°K} C_p dT$, cal./mole	
	$BeO \cdot Al_2O_3$	$BeO \cdot 3Al_2O_3$
adiabatic calorimeter	2685.4	6719.
"dropping" calorimeter	2681.2	6727.
tabulated value	2685.6	6722.

86
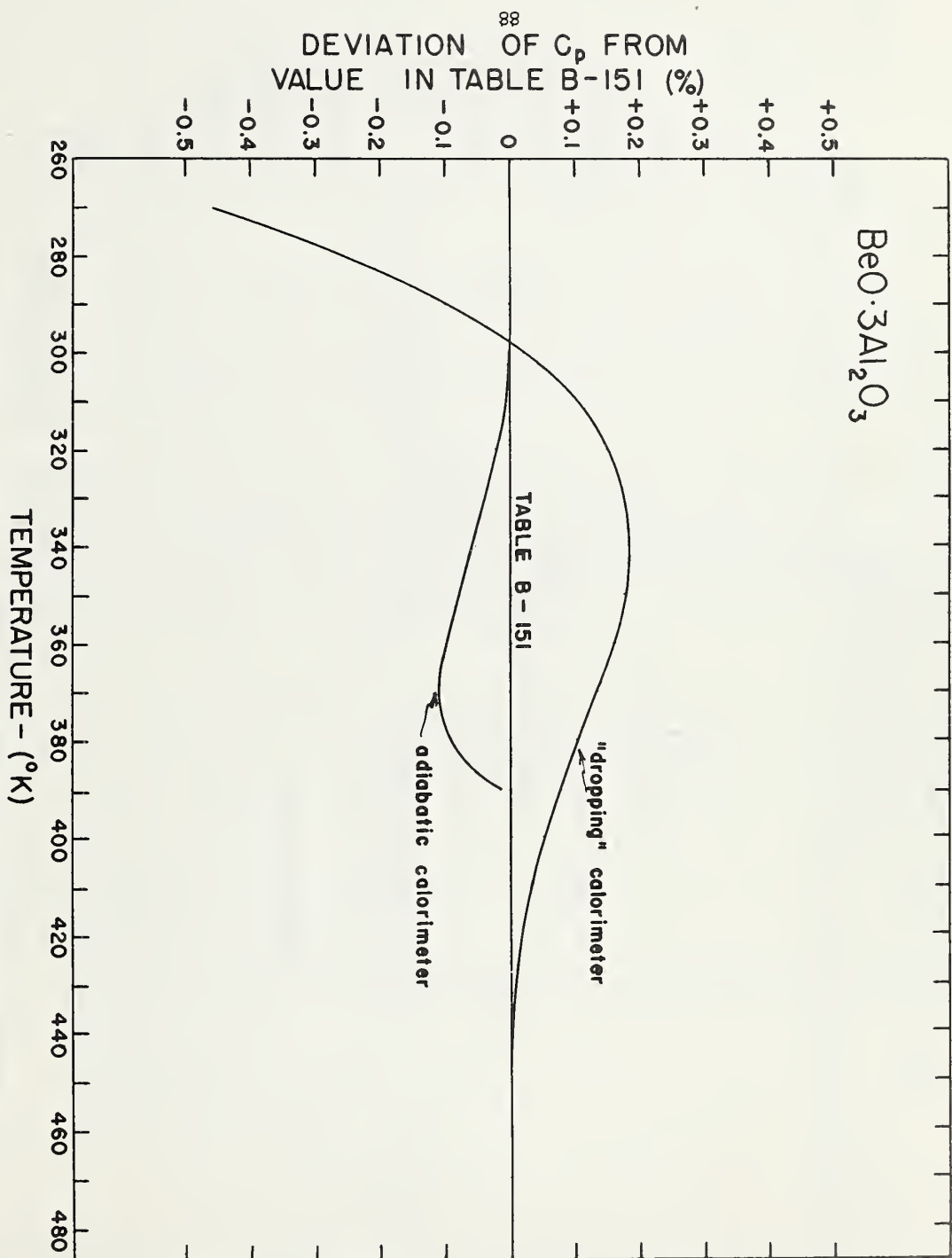
Figure 2. BeO·3Al₂O₃: Comparison of smoothed heat capacity determined by two methods with values of Table B-151.
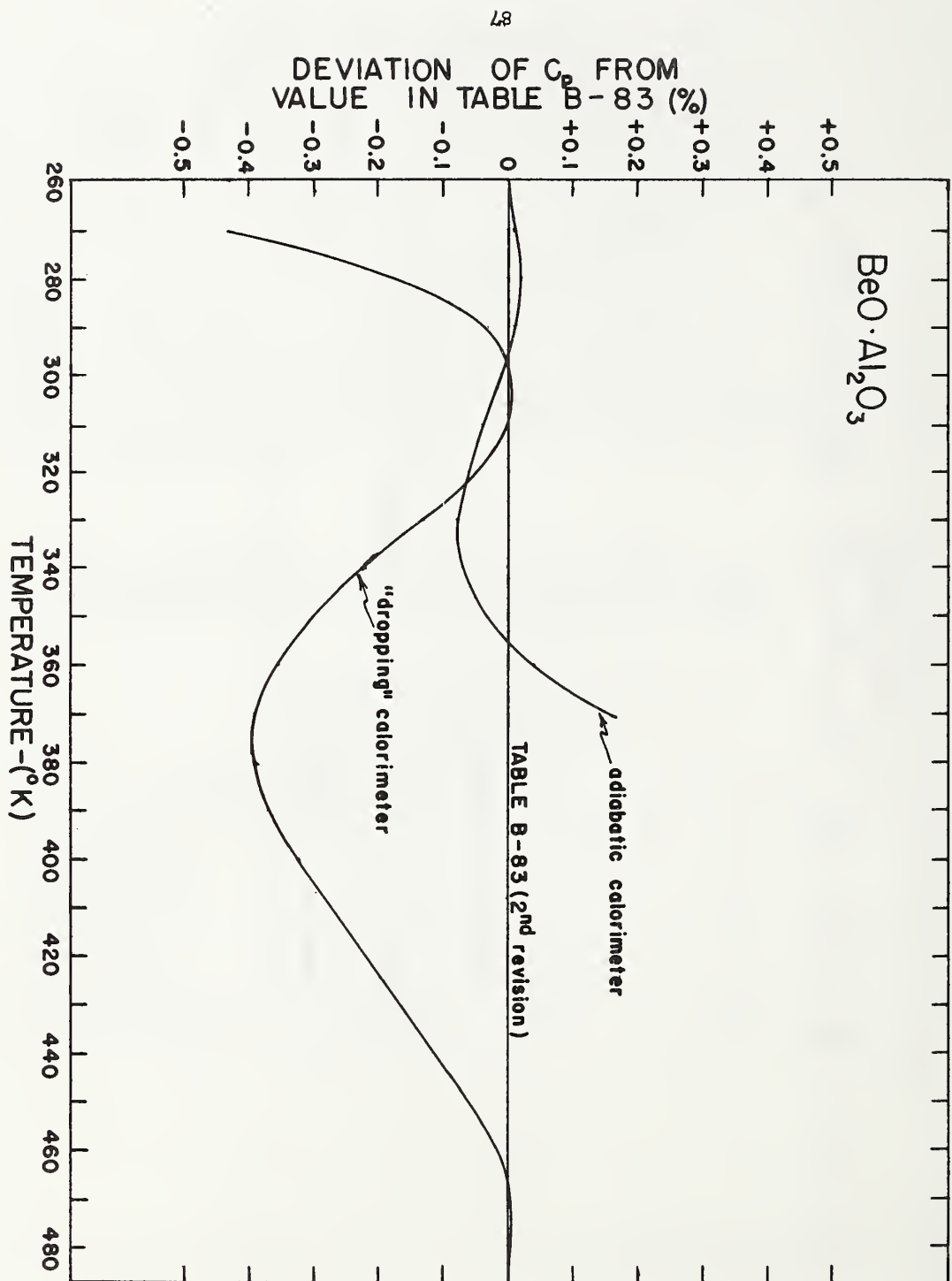
Figure 1. BeO·Al$_2$O$_3$: Comparison of smoothed heat capacity determined by two methods with values of Table B-83 (2nd revision).

The high temperature heat capacity functions were then extrapolated to 2150°K, near the reported melting point of each compound [10]. In the case of BeO·3Al$_2$O$_3$, this was done by continuing equation (2) to 2150°K. This seemed justified by the good fit of the equation to the data and the fact that its form at higher temperatures met the requirements of theory. The equation chosen to represent the BeO·Al$_2$O$_3$ data did not allow this type of extrapolation. Therefore, the heat capacity function derived from equation (1) was extrapolated by a straight line whose slope was chosen with reference to bounds determined for the heat capacity at 2150°K. An upper bound was determined by a linear extrapolation of the heat capacity function from 1100°K, using the slope at that temperature. The heat capacity at constant volume (C$_v$) was calculated next from the values of θ_D determined during the smoothing process, assuming a Debye shape for the heat capacity function. To get the lower bound, the heat capacity function as determined from equation (1) was extrapolated linearly from the point at which its slope equalled that of the C$_v$ function near the upper end of the range of extrapolation. The mean of the upper and lower bounds was chosen as the heat capacity at 2150°K, and the linear extrapolation of the heat capacity function chosen to give nearly this mean value at 2150°K. The linear extrapolation starts at 1200°K. The two smooth heat capacity functions were then numerically differentiated, integrated and combined, using well-known thermodynamic relationships to yield tables B-83 and B-151 of Appendix I.

Functional representation of the tables and interpolation in the upper portion of the temperature range has been facilitated by the method of generation employed. The following equations were derived using constants supplied partly by the low temperature heat capacity measurements and represent the tabulated values in the indicated temperature ranges with an error not exceeding 0.01%.

BeO·Al$_2$O$_3$
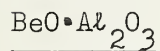
$$H_T - H_0 = (-1.00242)10^{-6}T^3 + (2.65426)10^{-3}T^2 + (45.8430)T$$
$$- (6.54908)10^3 \ln T + 26575.2 \qquad (3)$$
$$1200 \geq T°K \geq 450$$

$$H_T - H_0 = (1.3195)10^{-3}T^2 + (39.258)T - 11767. \qquad (4)$$
$$2150 \geq T°K \geq 1200$$

$$C_p = (-3.00726)10^{-6}T^2 + (5.30852)10^{-3}T - (6.54908)10^3 T^{-1} + 45.843 \qquad (5)$$
$$1200 \geq T°K \geq 475$$

$$C_p = (2.6389)10^{-3}T + 39.258 \qquad (6)$$
$$2150 \geq T°K \geq 1200$$

89

$\underline{BeO \cdot 3Al_2O_3}$
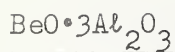
$$H_T - H_0 = (4.51018)10^{-3}T^2 + (97.1407)T + (5.09824)10^6T^{-1}$$
$$- (2.76996)10^8T^{-2} - 35203.5 \qquad (7)$$
$$2150 \geq T°K \geq 450$$

$$C_p = (9.02036)10^{-3}T - (5.09824)10^6T^{-2} + (5.53992)10^8T^{-3} + 97.1407 \qquad (8)$$
$$2150 \geq T°K \geq 450$$

Lacking complete heat capacity data, the heat capacity of mixed-metal oxide compounds, such as those investigated in the present report, is often approximated by summing the individual values for the component oxides. The present measurements provide a valuable check on the validity of this approach. Accurate values of heat capacity have already been determined by the "dropping" method for BeO and Al_2O_3. A comparison of the measured heat capacity with the heat capacity calculated by summing previously tabulated values for the component oxides of $BeO \cdot Al_2O_3$ and $BeO \cdot 3Al_2O_3$ is presented in table 5. Here, it is shown that the "additive" values represent the total heat capacity to about a percent over the range 300°K-1200°K. There is some indication that the approximation agrees the best between 600°K and 700°K but grows worse above and below this interval. The deviations, however, must be considered in light of possible errors in the values of heat capacity derived from the high temperature enthalpy data.

Table 5. Deviation of the high-temperature heat capacity of BeO·Aℓ$_2$O$_3$ and BeO·3Aℓ$_2$O$_3$ from additivity based on mixtures of the two component oxides

Temperature °K	"Additive" heat capacity C$_p^o$, cal./mole [a]		Measured heat capacity C$_p^o$, cal./mole			
	BeO·Aℓ$_2$O$_3$	BeO·3Aℓ$_2$O$_3$	BeO·Aℓ$_2$O$_3$ [b]	ΔC$_p^o$ (Compound minus mixture) %	BeO·3Aℓ$_2$O$_3$	ΔC$_p^o$ (Compound minus mixture) %
300	25.15	63.16	25.33	+0.7	63.71	+0.9
400	31.07	77.06	31.21	+0.5	77.50	+0.6
500	34.65	85.34	34.64	-0.0	85.69	+0.4
600	37.00	90.75	37.03	+0.1	90.96	+0.2
700	38.64	94.53	38.73	+0.2	94.67	+0.1
800	39.86	97.30	39.98	+0.3	97.47	+0.2
900	40.80	99.40	40.91	+0.3	99.73	+0.3
1000	41.54	101.03	41.60	+0.1	101.62	+0.6
1100	42.15	102.33	42.11	-0.1	103.27	+0.9
1200	42.66	103.38	42.44	-0.5	104.74	+1.3

a Smoothed BeO values from reference [1].
  Smoothed Aℓ$_2$O$_3$ values from reference [2].
b From Table B-83 (Second revision), (Appendix I).
c From Table B-151, (Appendix I).

ACCURACY OF THE DATA

The overall accuracy of the tabulated enthalpy values between 100°C and 900°C (tables B-83 and B-151, Appendix I) has been estimated by considering contributions due to random measuring errors and curve-smoothing procedures, likely systematic errors and the measurements on α-Al_2O_3 referred to above. The mean unsmoothed net enthalpy for the two compounds (columns 4 and 5, 12 and 13 of tables 2 and 3 respectively) can be shown to have an average probable error of ±0.23 cal. Considering the sample masses involved, this corresponds to about ±5. cal./mole for $BeO \cdot Al_2O_3$ and ±10. cal./mole for $BeO \cdot 3Al_2O_3$. The smoothing procedure leading to equations (1) and (2) introduces an additional uncertainty leading to an average probable error of the smoothed values for both materials of ±14. cal./mole. This represents from 0.5% to 0.04% of the measured enthalpy values for $BeO \cdot Al_2O_3$ and from 0.2% to 0.02% of the values for $BeO \cdot 3Al_2O_3$.

It is felt that the most significant systematic error would be introduced in temperature measurement. Lesser ones might be errors in sample mass or calorimeter calibration factor, sample impurity or differences between heat losses during the drops of the filled and empty containers. The platinum resistance thermometer used at 500°C and below and the Pt—Pt 10 Rh thermocouples used above 500°C were calibrated by the Temperature Physics Section of the National Bureau of Standards immediately prior to the present measurements. The ice point resistance of the resistance thermometer was checked frequently during the measurements and did not change. The resistance thermometer and thermocouples were compared in the furnace up to 500°C. Any small differences between the NBS certified calibrations and the calibration determined "in place" were then linearly extrapolated to obtain corrections to thermocouple readings applicable above 500°C. The temperature error at temperatures measured with the platinum resistance thermometer is felt to be insignificant. Above 500°C, the maximum error in the enthalpy measurements due to uncertainty in the thermocouple calibrations should not exceed 0.05% and is probably a good deal less than this as a result of the comparison in place with the resistance thermometer.

Heat loss during the drop (time duration approximately 0.1 sec) is a significant though small fraction of the total measured heat only at the highest temperatures. It is felt that the care used in materials and design of the silver containers and the steps taken to ensure constancy of the drop time were adequate to eliminate the possibility of significant differences between the heat loss during the drop for the full and empty containers. The silver tubes used in container fabrication were all chosen from a single length of highly polished pure silver tubing. They were of the same dimensions. During the course of the experiments, no

indications of oxidation on the exterior surfaces were noted. The sample container is attached by a fine nichrome wire to a brass plunger which is part of the sample air braking system. Together, they make up the effective dropping mass. Small riders are added to or removed from the plunger when sample containers are changed in order that the dropping mass be the same in all experiments.

Analyses of the samples are described in detail in [4] and [9]. Within the precision of analysis, they showed the samples to contain the stoichiometrically correct ratios of constituent elements and negligible impurities. It is believed that the assumption of 100% purity for both samples would introduce negligible error into the heat measurements. Possible errors due to uncertainties in sample mass or in the accepted value of the calorimeter calibration factor probably do not introduce error in the enthalpy measurements exceeding 0.02%.

Considering these sources of error and the measurements on aluminum oxide referred to above, it is felt that the smoothed high temperature enthalpy values derived from equation (1) (BeO·Al$_2$O$_3$) can be considered to have a probable error decreasing from 0.5% at 100°C to 0.2% at 900°C. On the same basis, the probable error corresponding to enthalpy values derived from equation (2) (BeO·3Al$_2$O$_3$) would be from 0.3% at 100°C to 0.2% at 900°C. The probable error in the values of heat capacity calculated from these equations should be from 0.5% to 0.7% for BeO·Al$_2$O$_3$ and from 0.3% to 0.5% for BeO·3Al$_2$O$_3$ over the same temperature ranges.

It is possible to estimate the maximum error in the extrapolated value of the heat capacity at 2150°K for BeO·Al$_2$O$_3$. The upper and lower limits referred to in the discussion of the extrapolation above are 46.4 cal./mole and 43.4 cal./mole. Therefore, the error in the mean value at 2150°K should not exceed ±3.3%.

REFERENCES

1. A. C. Victor and T. B. Douglas, J. Research Natl. Bur. Standards 67A, 325-329 (1963).

2. D. C. Ginnings, J. Phys. Chem. 67, 1917-1918 (1963).

3. NBS Report 8186, National Bureau of Standards, Washington, D.C., 1 January 1964, pp. 62-67, 160, 161.

4. Ibid, pp. 50-61.

5. D. C. Ginnings and R. J. Corruccini, J. Research NBS 38, 593 (1947).

6. D. C. Ginnings and R. J. Corruccini, J. Research NBS 38, 583 (1947).

7. D. C. Ginnings, T. B. Douglas, and A. F. Ball, J. Research NBS 45, 23 (1950).

8. G. T. Furukawa, T. B. Douglas, R. E. McCoskey, and D. C. Ginnings, J. Research NBS 57, 67-82 (1956).

9. G. T. Furukawa, W. G. Saba, Chapter 4, this report.

10. S. M. Lang, C. L. Fillmore, and L. H. Maxwell, J. Research NBS 48, 298 (1952).

Chapter 9

FLAME CALORIMETRY OF FLUORINE COMPOUNDS:

A NEW BURNER DESIGN FOR GAS-PHASE REACTIONS

by R. C. King and G. T. Armstrong

I. INTRODUCTION

In recent years a considerable number of thermochemical studies
have been conducted on the direct reactions of fluorine with solids
[1,2,3]. These investigations have led to reliable heat-of-formation
data for such fluorides as AlF_3, BeF_2, MoF_6, SiF_4, and BF_3. However,
comparatively few single phase gaseous reactions have been studied for
the purpose of deriving heats of formation data of fluorine compounds.
There exists a large body of inorganic and organic gaseous fluorides
for which very little, if any, thermochemical data are available. This
is particularly true of such important compounds as the oxygen fluorides
and the interhalogen fluorides. Also, there is indication that some of
the earlier work on gaseous fluorides should be repeated [5,8].

The possibility of obtaining accurate thermochemical data from gas
phase reactions by means of fluorine flame calorimetry [4,5] has been
discussed. This technique is particularly applicable for studying
reactions involving only gaseous reactants. It can also be applied to
measuring heats of reactions in which a solid ignites spontaneously in
fluorine and to reactions of very volatile substances with fluorine.
Most notable among recent studies employing this technique are those
pertaining to the reactions of fluorine with methane [6] and ammonia [4].
Some time ago, von Wartenberg and Fitzner [7] made a thermochemical
study of the hydrogen-fluorine reaction using a flow system, and
several other similar studies were also carried out.

For the purpose of providing reliable heat-of-formation data for
gaseous fluorides, a new flame calorimetric apparatus has been set up
in this laboratory. It is planned that this apparatus will be used for
thermochemical studies on the reactions involving oxygen difluoride and
interhalogen compounds, as well as the reactions of fluorine with other
gases. At the present time the compound being studied is oxygen di-
fluoride.

The reaction undertaken for study is that of oxygen difluoride with
hydrogen at 25°C. To obtain the heat of formation of oxygen difluoride,
the measured heat of this reaction may be combined with the heats of
reaction of hydrogen directly with oxygen and fluorine. A suitable
series of reactions is given in equations (1)-(5).

$$OF_2(g) + 2H_2(g) \xrightarrow{\quad b \quad} [2HF \cdot H_2O](g+\ell) \tag{1}$$
$$OF_2(g) + 2H_2(g) \xrightarrow{\quad a \quad} 2HF(g) + H_2O(\ell)$$

$$\tfrac{1}{2} O_2(g) + H_2(g) \longrightarrow H_2O(\ell) \tag{2}$$

$$F_2(g) + H_2(g) \longrightarrow 2HF(g) \tag{3}$$

$$2HF(g) + H_2O(\ell) \longrightarrow [2HF \cdot H_2O](g+\ell) \tag{4}$$

$$F_2(g) + \tfrac{1}{2} O_2(g) \longrightarrow OF_2(g) \tag{5}$$
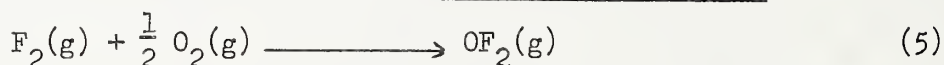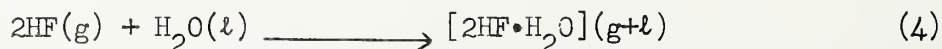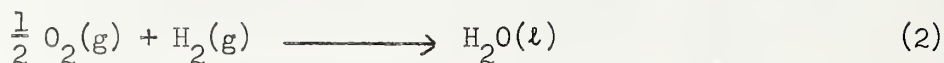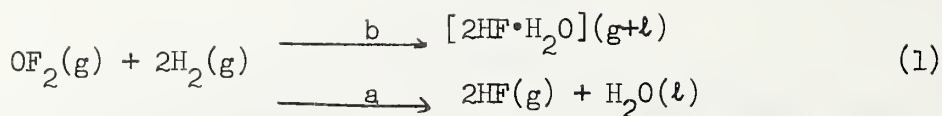
Path b in reaction (1) is included as a reminder that the extreme solu-
bility of hydrogen fluoride in water makes it very misleading to assume
the two can be formed separately in such a reaction at room temperature.
In the usual manner, the heat data for reactions (2), (3), and (4) may
be obtained from the literature, or preferably, can be measured in the
same apparatus and applied to reaction (1) to obtain the heat of reaction
in equation (5).

In the initial phase of the study, oxygen difluoride was reacted in
a hydrogen atmosphere in a Monel reaction vessel similar to the design
previously used at the National Bureau of Standards for fluorine flame
calorimetry [5]. A diagram of this burner is shown in Figure 1. In
a burner of this design the fuel (F_2O) enters opening A and the
atmosphere (H_2) is introduced through annular opening B. The reaction
product(s) along with the excess hydrogen exit the reaction chamber at D.
In the early experiments of the current study it was found that after
burning the desired amount of OF_2 in H_2 most of the product H_2O remained
condensed in the burner chamber, saturated with HF, while the remainder
of the HF was either in the vapor phase above the solution, or had been
carried from the burner in the effluent atmosphere.

Such a state of the reaction products at the end of the experiment
introduces many uncertainties in the heat of formation for oxygen di-
fluoride derived on the basis of equations (1)-(5). Foremost among these
problems is the difficulty in analyzing for the reaction products.
Secondly, the uncertainty in the concentration of the HF-H_2O solution
remaining in the burner chamber makes it impossible to apply a reliable
correction to the heat data for the heat of formation of this solution.
Also, the existing uncertainty in the heat of formation of gaseous hydrogen
fluoride [equation (3)] poses a disadvantage. Because of these problems a
new burner was designed for studying the heat of reaction of oxygen
difluoride with hydrogen.

96
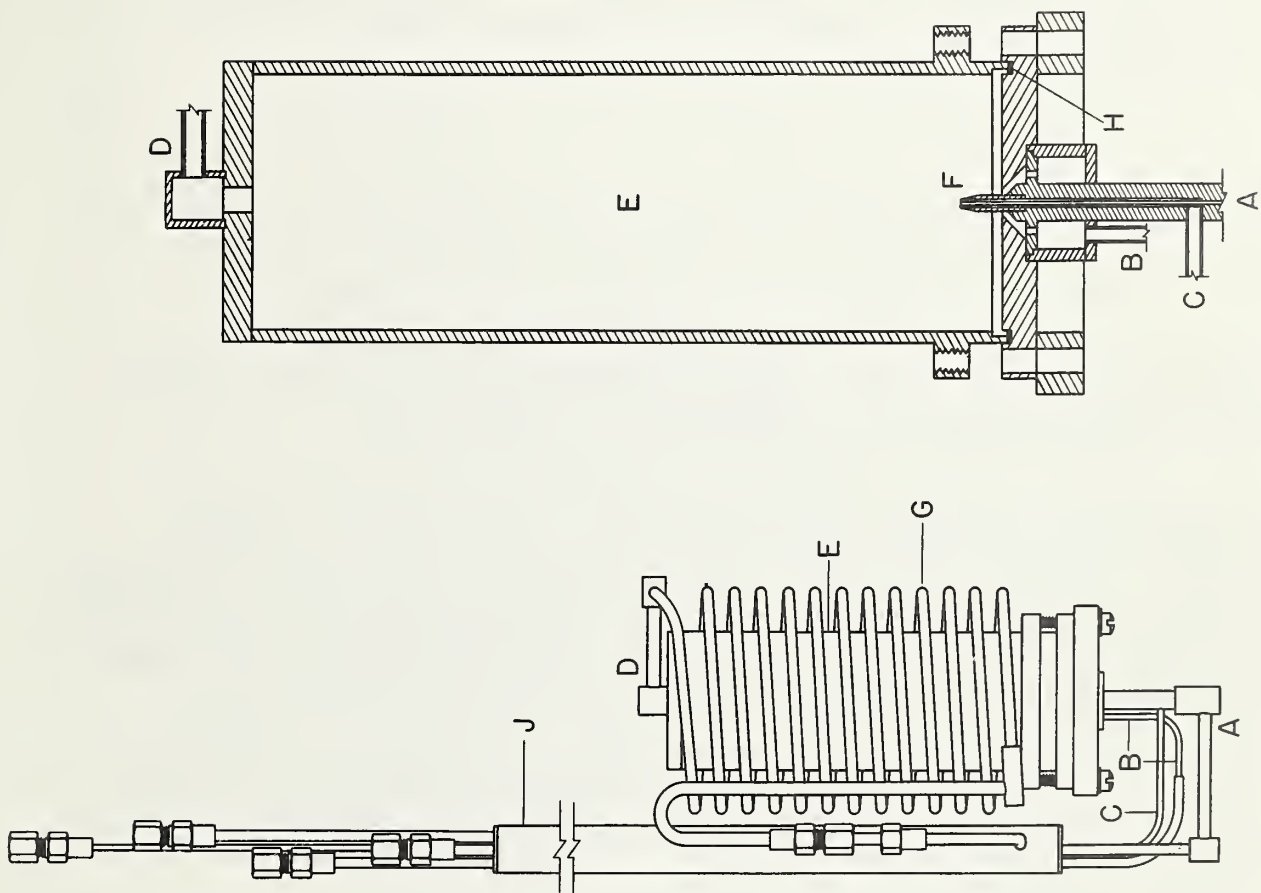
Figure 1. -- Burner for Fluorine Flame Calorimetry

II. BURNER DESIGN

In a general way the new burner design may be described as a two-chambered reaction vessel. In the upper chamber (A) the oxygen difluoride and hydrogen (excess) are mixed and ignited, producing a flame. In the lower chamber (B) the products are dissolved in a known volume of water, producing a solution of determinable concentration. The excess hydrogen removes the product HF and H_2O from the upper chamber into the lower chamber. A gas dispersion system forces the gas mixture as fine bubbles through the aqueous solution and causes complete removal of the HF from the flowing hydrogen. The reaction in equation (6) takes place in the upper chamber and equation (7) shows the reaction occurring in the solution chamber. The overall reaction for which the heat effect is measured is given by equation (8). Quantities shown are actual amounts used in the experiments.

$$0.06 \ OF_2(g) + 0.12 \ H_2(g) \longrightarrow [0.12 \ HF \ 0.06 \ H_2O](g+\ell) \qquad (6)$$

$$[0.12 \ HF(g) \ 0.06 \ H_2O](g+\ell) + 5.55 \ H_2O(\ell) \rightarrow [0.12 \ HF \ 5.61 \ H_2O](\ell) \qquad (7)$$

$$0.06 \ OF_2(g) + 0.12 \ H_2(g) + 5.55 \ H_2O(\ell) \rightarrow [0.12 \ HF \ 5.61 \ H_2O](\ell) \qquad (8)$$
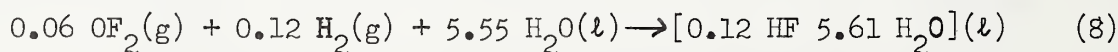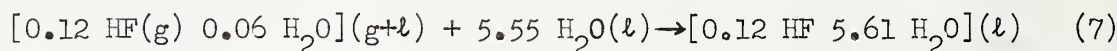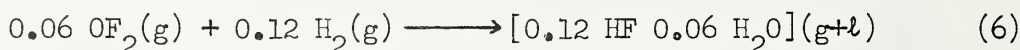
Dissolving the HF in water in the calorimeter causes the heat of formation of oxygen difluoride obtained to depend on the heat of formation of the aqueous solution of HF, rather than on gaseous HF.

An over-all view of the burner is shown in Figure 2. With the exception of the primary solution chamber, B, the burner is composed almost entirely of Monel and soldered with silver at all of the permanent joints. In a manner similar to that in the earlier burner, the gases are brought to the burner from the exterior of the calorimeter by Monel tubes passing through interchanger C, through which also pass the exit gases. The exit and entrance gases are thus at the same temperature and no correction needs to be applied to the data for the rise in temperature of the gases passing through the burner. The outlet, E, on the primary solution vessel connects to a smaller solution vessel similarly lettered (shown in Figure 3). The effluent gases leaving the secondary solution chamber at F pass through a helix of thin-wall Monel tubing, D, before passing through the interchanger, C.

Details of the combustion chamber A, are shown in Figure 4. The body which is cup shaped is made of Monel, 1.25 in. O.D., and 2 in. high, with 0.0625 in. wall. The inlet tubes for reacting gases, the igniter, and the flame tip are all attached to the lid of the combustion chamber. On the outer side of the lid, the tubing is 0.125 in. O.D., 0.010 wall Monel. On the inside, the tubing leading to the flame tip, L, is 0.0625 in. O.D., 0.010 in. wall. The fuel is introduced through inlet H,
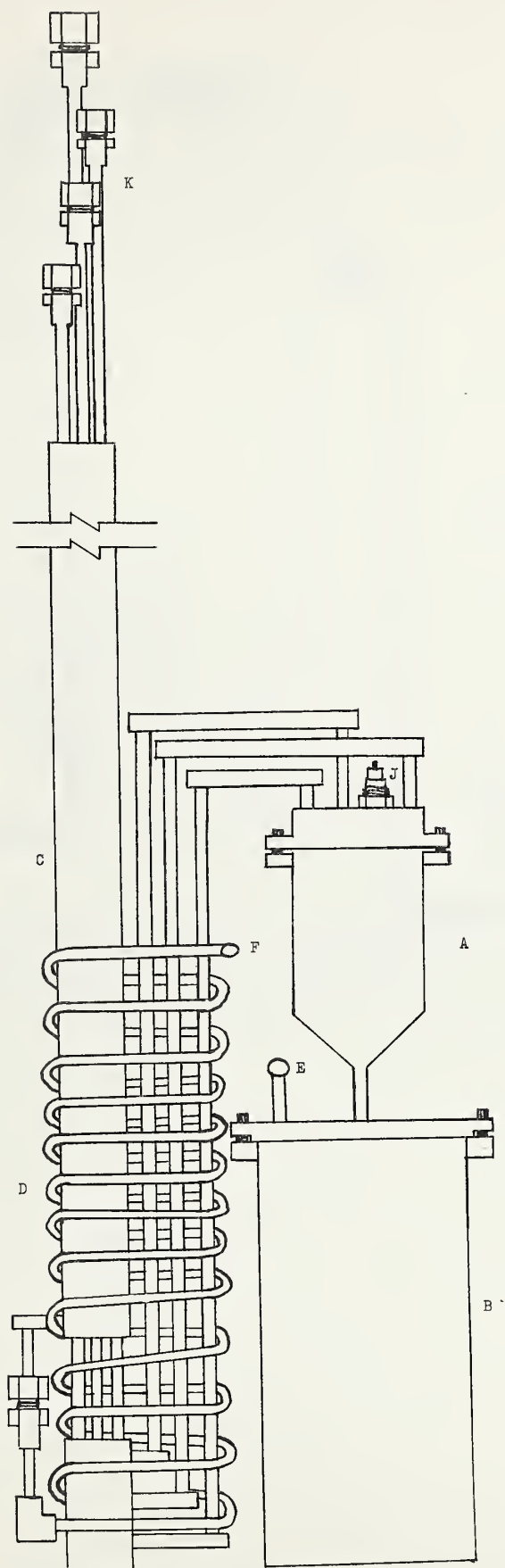
Figure 2. - - Burner for Fluorine Flame Calorimetry (New Design)

Copper

Teflon
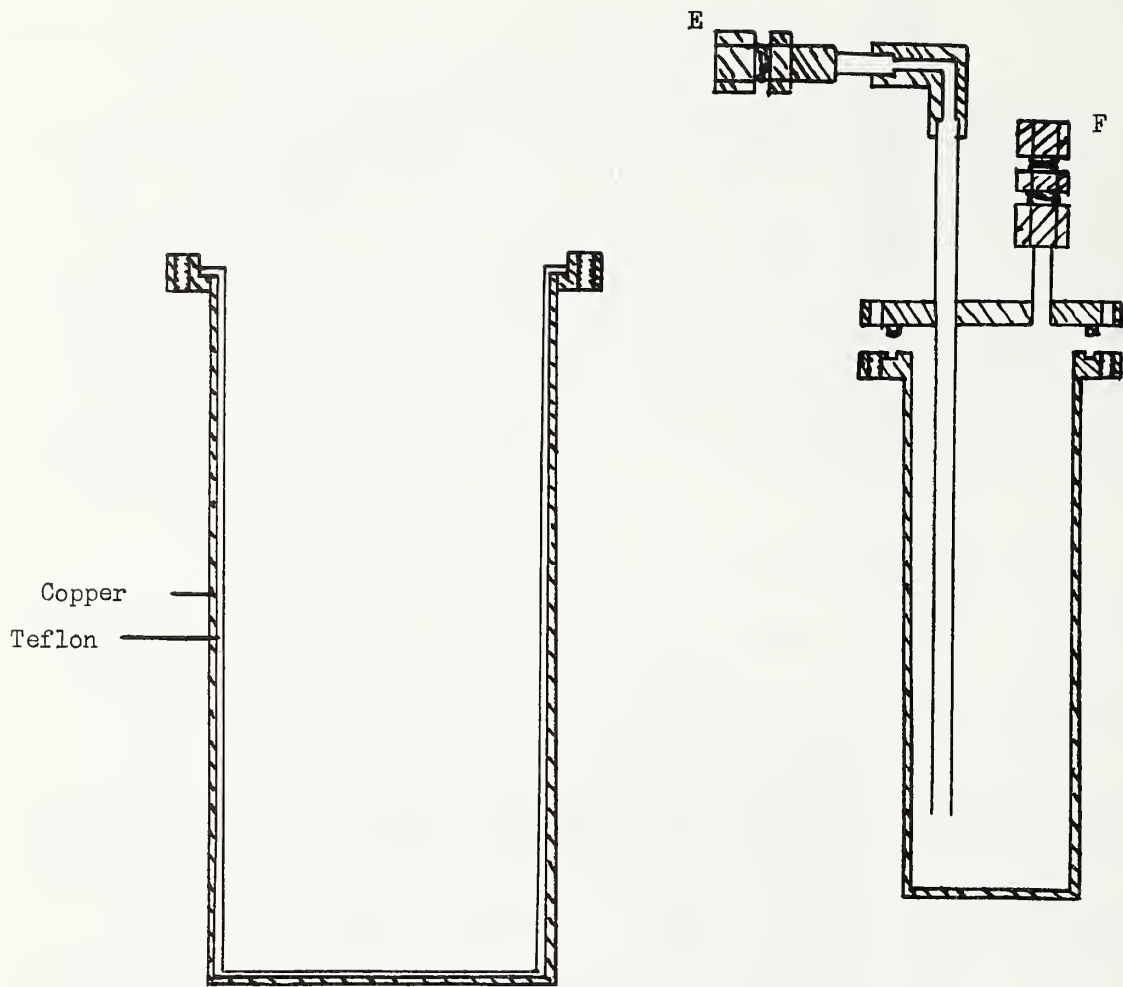
Figure 3. - - Solution Vessels

100
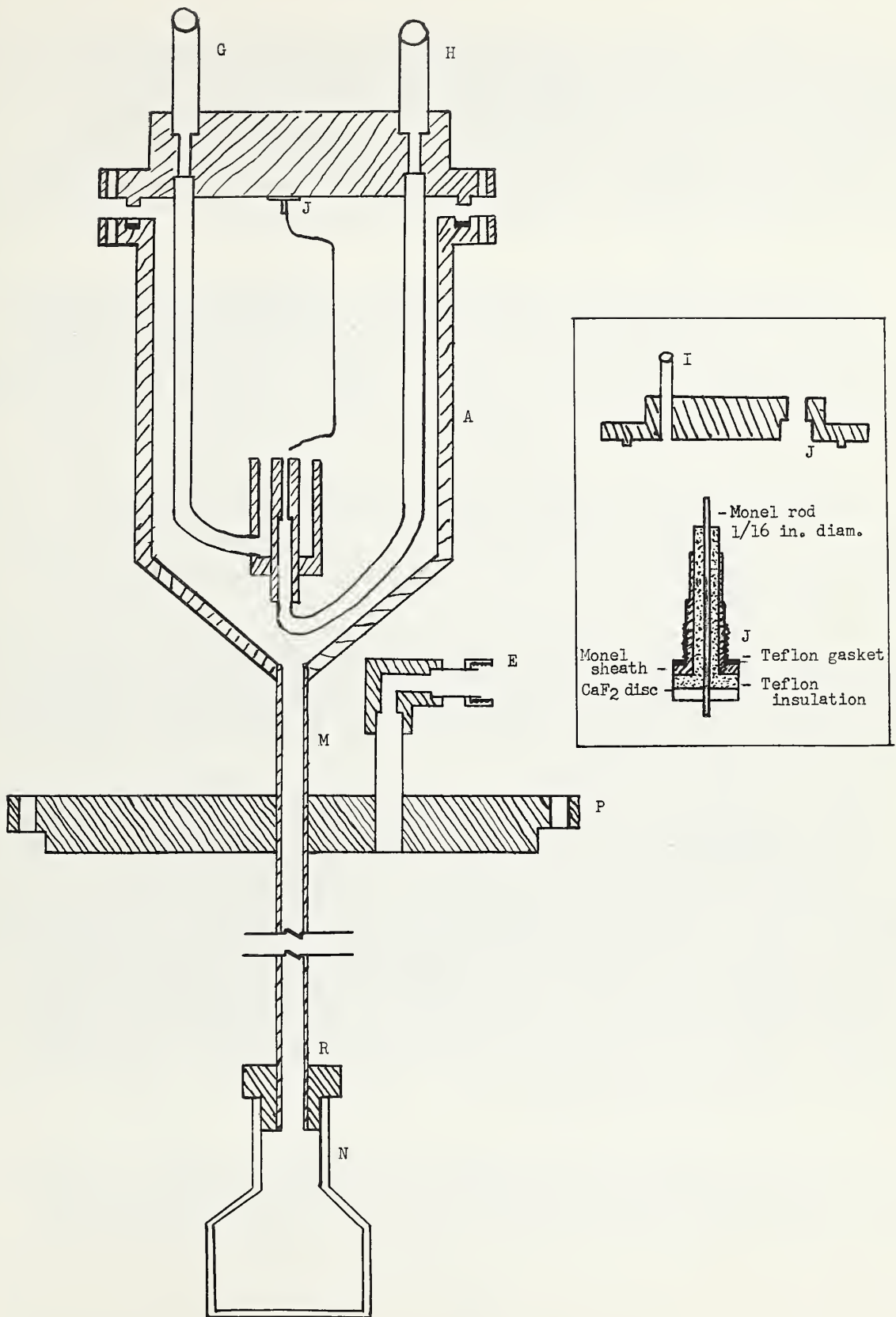
Figure 4. - - Combustion Chamber and Gas Dispersion System

101

and what may be called the primary atmosphere enters through inlet G.
Additional atmosphere is introduced through inlet I. The orifice at L
through which the fuel enters is 0.050 in. The secondary atmosphere
entering through inlet I serves two-fold: (1) it provides additional
atmosphere for the reaction and (2) it helps to flush the products down
into the solution chamber. The joint between the cover and the combustion
chamber is made by a 0.030 in. thick Teflon gasket placed in the groove on
the flange of the cup.

At N is the opening for the high voltage electrode used for initiating
the reaction. The electrode is a Monel-Teflon unit as shown in the insert
in Figure 4. A calcium fluoride disc (0.095 in. thick) placed over the
electrode serves as a heat sink. The Monel sheath surrounding the Teflon
insulation also helps to cool the Teflon. A three in. piece of 0.010 in. diam.
nickel wire is attached to the electrode at J, and positioned over the
flame tip, L.

The tube, M, leading into the solution chamber is platinum with
0.125 in. O.D. and 0.013 in. wall thickness. The end of the tube is
fitted with a polyethylene cap having a porous lower surface and connected
with a small Teflon adapter, R. The cover to the solution chamber is of
nickel-plated steel.

The details of the solution vessels are shown in Figure 3. The
primary solution vessel is two in. O.D., four in. high, with a 0.032 in.
wall thickness. The cylinder is made of nickel-plated copper. The flange
with threaded holes is nickel plated steel. The container has a Teflon
liner which also has a 0.032 in. wall. The flange on the liner makes the
seal when the vessel is closed.

For an experiment, the primary solution vessel contains 100 cc. de-
mineralized water. The volume of the secondary vessel is 30 cc. During
an experiment it contains 20 cc of water. This secondary solution re-
moves any HF from the effluent gas that may be carried over from the
primary solution. Since the secondary solution is so dilute it also assures
that upon leaving the burner the effluent gas flows through a solution
whose vapor pressure is essentially unchanged during the experiment. In
the main solution vessel, the liquid is pure water during the fore drift,
and contains about two weight percent HF in the final drift. The vapor
pressure of water over this solution is 23.46 mm Hg at 25°C [9], whereas
it is 23.77 mm. Hg over the pure water. The vapor pressure of HF over the
solution is 0.048 mm. Hg at 25°C.

The gas flow system for this combustion reaction is similar to that
which has been described for other flame calorimetric work [5]. However,
several changes have been introduced, making use of new materials, and
also adapting the system to the properties of the gases being handled.

In preliminary experiments carried out with the burner, to lessen the effect of the removal of water vapor from the burner on the temperature drift rate, the hydrogen is passed through a gas washer immediately prior to entering the burner. The amount of water vapor removed from the burner is measured in each experiment. This amounts to approximately 0.8 gram for each experiment. Similar measurements are planned to determine the amount of water vapor carried into the burner.

III. EXPERIMENTAL PROCEDURE

Preparation of burner. -- To prepare the burner for an experiment, the solution chambers are charged with water. The vessels are covered immediately. Note that the cover for the primary solution vessel is attached to the gas inlet tube. The two solution vessels are connected at E. Next the lid to the combustion chamber is put in place. Note that this lid is attached to the interchanger, C. The positions F on the secondary solution vessel and on the cooling helix are connected. At this point the burner is ready to be situated in the calorimeter. The burner is supported in the calorimeter by a stand, approximately 0.250 in. high, that has only point contacts with the bottom of the can.

Calorimeter and gas flow system. -- The calorimetric equipment, gas flow system and the procedure for the conduct of an experiment will be described in detail in a later report. Consequently, only brief mention will be made here. The combustion chamber and most of the interchanger, C, are immersed in the stirred water of the calorimeter, which is a modification of the Dickinson design [10]. The modifications were introduced by Prosen, et al. [11]. The calorimeter is calibrated electrically.

Reaction experiments and results. -- The flow lines are first purged with helium and then the flowing hydrogen atmosphere is introduced into the burner. The reaction is initiated by simultaneously beginning the sparking and releasing the fuel from a weighable sample bulb. Ignition occurs in ten to fifteen seconds. When the desired amount of reaction has taken place, the fuel is flushed from the fuel flow line with helium. The sample bulb is weighed to 0.1 mg. before and after the experiment. This gives the amount of fuel introduced into the burner and allows one to check the mass balance in the experiment, by comparing the reacted OF_2 with the acid in the solution chamber. The acid can be determined by titration with standard sodium hydroxide solution.

103

Preliminary results from five experiments give promising evidence that the products of reaction can be collected and analyzed. The results are tabulated below. The theoretical acid was calculated from the known composition of the OF_2 sample used. Many additional experiments are planned from which the heat of formation of OF_2 will be derived.

Experiment No.	Wt. of OF_2 Sample Reacted	Acid Formed	
	g.	meq.	
		theoretical	observed
I	3.5450	130.12	129.1940
II	2.9080	106.9034	106.5930
III	3.4370	126.3504	125.8862
IV	3.5261	129.6259	129.4133
V	3.0869	113.4802	113.5854

References

[1] W. N. Hubbard, "Fluorine Bomb Calorimetry", Chapter 6, Experimental Thermochemistry, Vol. II, H. A. Skinner, Editor, (Interscience Publishers Inc., New York, N.Y., 1962).

[2] E. S. Domalski and G. T. Armstrong, J. Res. Natl. Bur. Standards 69A, 137 (1965).

[3] K. L. Churney and G. T. Armstrong, NBS Report 8919, July 1, 1965.

[4] G. T. Armstrong and R. S. Jessup, J. Res. Natl. Bur. Standards 64A, 49 (1960).

[5] G. T. Armstrong, "Fluorine Flame Calorimetry", Chapter 7, Experimental Thermochemistry, Vol. II, H. A. Skinner, Editor, (interscience Publishers, Inc., New York, N. Y., 1962).

[6] R. S. Jessup, R. E. McCoskey and R. A. Nelson, J. Am. Chem. Soc. 77, 244 (1955).

[7] H. von Wartenberg and O. Fitzner, Z. anorg. u. allgem. Chem. 151, 313 (1926).

[8] H. M. Feder, W. N. Hubbard, S. S. Wise, and J. L. Margrave, J. Phys. Chem. 67, 1148 (1963).

[9] J. C. Brosheer, F. A. Lenfesty, and K. L. Ellmore, Ind. and Ind. Eng. Chem. 39, 423 (1947).

[10] H. C. Dickinson, Bull. Bur. Standards 11, 189 (1914).

[11] E. J. Prosen, W. H. Johnson, and F. Y. Pergiel, J. Res. Natl. Bur. Standards 62, 43 (1959).

APPENDIX I

THERMODYNAMIC FUNCTIONS OF SOME SELECTED
SUBSTANCES IN THE SOLID AND LIQUID STATES

(See Chapters 4 and 8 for background and discussion.)

106

TABLE B-83(2ND REVISION)

THERMODYNAMIC FUNCTIONS FOR BERYLLIUM 1:1-ALUMINATE (BEO·AL$_2$O$_3$)
SOLID PHASE

GRAM MOLECULAR WT.=126.9728 GRAMS   1 CAL=4.1840 ABS J
T DEG K = 273.15 + T DEG C

T	$-(G_T^0-H_0^C)/T$	$(H_T^0-H_0^C)/T$	$(S_T-S_0^C)$	$(H_T^0-H_0^C)$	C_P^0	$-(G_T^0-H_0^C)$
DEG K	CAL / DEG MOLE	CAL / DEG MOLE	CAL / DEG MOLE	CAL / MOLE	CAL / DEG MOLE	CAL / MOLE
0.00	0.000	0.000	0.000	0.000	0.000	0.000
5.00	0.000	0.000	0.000	0.000	0.000	0.000
10.00	0.000	0.001	0.001	0.008	0.003	0.003
15.00	0.001	0.003	0.004	0.040	0.011	0.013
20.00	0.002	0.006	0.009	0.128	0.026	0.042
25.00	0.004	0.012	0.017	0.311	0.050	0.104
30.00	0.007	0.022	0.029	0.649	0.088	0.215
35.00	0.011	0.035	0.046	1.219	0.143	0.400
40.00	0.017	0.053	0.070	2.119	0.221	0.689
45.00	0.025	0.077	0.102	3.474	0.327	1.115
50.00	0.034	0.109	0.143	5.441	0.466	1.724
55.00	0.047	0.149	0.196	8.198	0.644	2.567
60.00	0.062	0.199	0.261	11.942	0.860	3.703
65.00	0.080	0.259	0.339	16.863	1.115	5.197
70.00	0.102	0.331	0.432	23.151	1.407	7.121
75.00	0.127	0.413	0.541	30.994	1.737	9.547
80.00	0.157	0.507	0.664	40.588	2.108	12.552
85.00	0.191	0.613	0.804	52.143	2.519	16.216
90.00	0.229	0.731	0.960	65.822	2.956	20.621
95.00	0.272	0.861	1.133	81.748	3.419	25.848
100.00	0.320	1.001	1.320	100.06	3.911	31.973
105.00	0.372	1.151	1.524	120.90	4.430	39.077
110.00	0.429	1.313	1.742	144.40	4.972	47.235
115.00	0.492	1.484	1.975	170.65	5.533	56.523
120.00	0.558	1.665	2.223	199.76	6.112	67.013
125.00	0.630	1.854	2.485	231.80	6.706	78.777
130.00	0.707	2.053	2.759	266.84	7.311	91.882
135.00	0.788	2.259	3.047	304.93	7.925	106.39
140.00	0.874	2.472	3.346	346.10	8.546	122.37
145.00	0.965	2.692	3.657	390.39	9.171	139.87
150.00	1.060	2.919	3.978	437.81	9.799	158.96
155.00	1.159	3.151	4.310	488.38	10.427	179.67
160.00	1.263	3.388	4.651	542.08	11.053	202.07
165.00	1.371	3.630	5.001	598.91	11.678	226.20
170.00	1.483	3.876	5.358	658.85	12.298	252.09
175.00	1.599	4.125	5.724	721.87	12.912	279.80
180.00	1.719	4.378	6.096	787.96	13.521	309.34
185.00	1.842	4.633	6.475	857.07	14.123	340.77
190.00	1.969	4.890	6.859	929.17	14.716	374.10
195.00	2.099	5.150	7.249	1004.2	15.301	409.37
200.00	2.233	5.411	7.644	1082.2	15.877	446.60
205.00	2.370	5.673	8.043	1163.0	16.444	485.82
210.00	2.510	5.936	8.446	1246.6	17.000	527.04
215.00	2.652	6.200	8.852	1333.0	17.547	570.28
220.00	2.798	6.464	9.262	1422.0	18.084	615.56
225.00	2.946	6.728	9.674	1513.8	18.610	662.90
230.00	3.097	6.992	10.089	1608.1	19.127	712.31
235.00	3.250	7.255	10.506	1705.0	19.633	763.80
240.00	3.406	7.519	10.924	1804.4	20.130	817.37
245.00	3.563	7.781	11.344	1906.3	20.617	873.04
250.00	3.723	8.042	11.766	2010.6	21.094	930.81
255.00	3.885	8.303	12.188	2117.2	21.561	990.70
260.00	4.049	8.562	12.611	2226.2	22.018	1052.7
265.00	4.214	8.820	13.035	2337.4	22.466	1116.8
270.00	4.382	9.077	13.459	2450.8	22.904	1183.0
273.15	4.488	9.238	13.726	2523.4	23.172	1225.9
275.00	4.551	9.332	13.883	2566.4	23.327	1251.4
280.00	4.721	9.586	14.307	2684.1	23.745	1321.9
285.00	4.893	9.838	14.731	2803.8	24.154	1394.5
290.00	5.066	10.088	15.154	2925.6	24.554	1469.2
295.00	5.241	10.337	15.578	3049.4	24.945	1546.0
298.15	5.351	10.492	15.844	3128.3	25.188	1595.5
300.00	5.417	10.584	16.000	3175.1	25.329	1625.0

H_0^C AND S_0^C APPLY TO THE REFERENCE STATE OF THE SOLID AT ZERO DEG K

THIS TABLE SUPERSEDES TABLE B-83 OF NBS REPORT 7587 AND TABLE B-83
REVISED OF NBS REPORT 8186.

TABLE B-83(CONT. 2ND REVISION)

THERMODYNAMIC FUNCTIONS FOR BERYLLIUM 1:1-ALUMINATE (BEO·AL$_2$O$_3$)
SOLID PHASE

GRAM MOLECULAR WT.=126.9728 GRAMS   1 CAL=4.1840 ABS J

T DEG K = 273.15 + T DEG C

T	$-(G_T^0-H_0^C)/T$	$(H_T^0-H_0^C)/T$	$(S_T-S_0^C)$	$(H_T^0-H_0^C)$	C_P^0	$-(G_T^0-H_0^C)$
DEG K	CAL / DEG MOLE	CAL / DEG MOLE	CAL / DEG MOLE	CAL / MOLE	CAL / DEG MOLE	CAL / MOLE
300.00	5.417	10.584	16.000	3175.1	25.329	1625.0
310.00	5.772	11.071	16.843	3432.1	26.071	1789.2
320.00	6.131	11.551	17.682	3696.4	26.781	1961.8
330.00	6.493	12.023	18.516	3967.6	27.457	2142.8
340.00	6.859	12.486	19.346	4245.4	28.100	2332.1
350.00	7.228	12.941	20.169	4529.5	28.706	2529.7
360.00	7.599	13.387	20.986	4819.4	29.276	2735.5
370.00	7.971	13.824	21.795	5114.9	29.810	2949.4
373.15	8.089	13.960	22.049	5209.0	29.971	3018.4
380.00	8.346	14.251	22.597	5415.5	30.309	3171.3
390.00	8.721	14.669	23.390	5720.9	30.776	3401.3
400.00	9.098	15.077	24.175	6030.9	31.214	3639.1
425.00	10.042	16.056	26.098	6823.9	32.207	4267.6
450.00	10.986	16.979	27.964	7640.4	33.093	4943.5
475.00	11.927	17.848	29.775	8477.9	33.901	5665.4
500.00	12.864	18.670	31.533	9334.8	34.643	6431.9
550.00	14.715	20.183	34.898	11101.	35.946	8093.5
600.00	16.531	21.543	38.074	12926.	37.030	9918.5
650.00	18.305	22.771	41.075	14801.	37.948	11898.
700.00	20.033	23.883	43.917	16718.	38.730	14023.
750.00	21.716	24.896	46.612	18672.	39.401	16287.
800.00	23.353	25.821	49.174	20657.	39.979	18682.
850.00	24.944	26.669	51.613	22669.	40.478	21203.
900.00	26.491	27.448	53.939	24703.	40.908	23842.
950.00	27.994	28.167	56.161	26758.	41.278	26595.
1000.00	29.456	28.830	58.287	28830.	41.595	29456.
1050.00	30.878	29.445	60.323	30917.	41.864	32422.
1100.00	32.261	30.015	62.276	33016.	42.090	35487.
1150.00	33.607	30.544	64.151	35125.	42.276	38648.
1200.00	34.918	31.036	65.953	37243.	42.425	41901.
1250.00	36.194	31.494	67.688	39368.	42.557	45242.
1300.00	37.438	31.922	69.360	41499.	42.689	48669.
1350.00	38.650	32.323	70.973	43637.	42.821	52177.
1400.00	39.832	32.701	72.533	45781.	42.953	55765.
1450.00	40.986	33.056	74.043	47932.	43.085	59430.
1500.00	42.112	33.393	75.505	50089.	43.217	63169.
1550.00	43.213	33.712	76.925	52254.	43.349	66980.
1600.00	44.288	34.015	78.303	54424.	43.481	70860.
1650.00	45.339	34.304	79.643	56602.	43.613	74809.
1700.00	46.367	34.580	80.947	58786.	43.745	78824.
1750.00	47.373	34.844	82.217	60976.	43.877	82903.
1800.00	48.359	35.096	83.455	63173.	44.009	87045.
1850.00	49.323	35.339	84.662	65377.	44.141	91248.
1900.00	50.269	35.572	85.841	67587.	44.273	95511.
1950.00	51.196	35.797	86.993	69804.	44.405	99832.
2000.00	52.105	36.014	88.119	72028.	44.537	104210.
2050.00	52.997	36.223	89.220	74258.	44.668	108644.
2100.00	53.872	36.426	90.298	76495.	44.800	113132.
2150.00	54.732	36.622	91.354	78738.	44.932	117673.

H_0^C AND S_0^C APPLY TO THE REFERENCE STATE OF THE SOLID AT ZERO DEG K

THIS TABLE SUPERSEDES TABLE B-83 OF NBS REPORT 7587 AND TABLE B-83
REVISED OF NBS REPORT 8186.

TABLE B-151

THERMODYNAMIC FUNCTIONS FOR BERYLLIUM 1:3-ALUMINATE (BEO·3AL$_2$O$_3$)
SOLID PHASE

GRAM MOLECULAR WT.=330.8952 GRAMS   1 CAL=4.1840 ABS J
T DEG K = 273.15 + T DEG C

T	$-(G_T^0-H_0^C)/T$	$(H_T^0-H_0^C)/T$	$(S_T-S_0^C)$	$(H_T^0-H_0^C)$	C_P^0	$-(G_T^0-H_0^C)$
DEG K	CAL DEG MOLE	CAL DEG MOLE	CAL DEG MOLE	CAL MOLE	CAL DEG MOLE	CAL MOLE
0.00	0.000	0.000	0.000	0.000	0.000	0.000
5.00	0.000	0.000	0.000	0.002	0.001	0.001
10.00	0.001	0.002	0.003	0.024	0.010	0.008
15.00	0.003	0.008	0.011	0.122	0.032	0.041
20.00	0.006	0.019	0.026	0.385	0.078	0.128
25.00	0.013	0.038	0.051	0.957	0.157	0.314
30.00	0.022	0.067	0.089	2.024	0.279	0.659
35.00	0.035	0.110	0.145	3.841	0.459	1.237
40.00	0.054	0.168	0.222	6.731	0.711	2.145
45.00	0.078	0.246	0.324	11.091	1.049	3.499
50.00	0.109	0.348	0.456	17.380	1.484	5.437
55.00	0.148	0.475	0.622	26.104	2.024	8.119
60.00	0.195	0.630	0.825	37.807	2.676	11.722
65.00	0.253	0.816	1.069	53.037	3.432	16.440
70.00	0.321	1.033	1.354	72.278	4.281	22.479
75.00	0.401	1.280	1.681	96.013	5.231	30.048
80.00	0.492	1.559	2.051	124.76	6.284	39.360
85.00	0.596	1.871	2.467	159.02	7.436	50.636
90.00	0.712	2.214	2.926	199.22	8.651	64.099
95.00	0.842	2.585	3.427	245.61	9.915	79.965
100.00	0.984	2.985	3.969	298.49	11.245	98.439
105.00	1.140	3.411	4.551	358.16	12.633	119.72
110.00	1.309	3.863	5.172	424.90	14.068	144.02
115.00	1.491	4.338	5.830	498.90	15.540	171.50
120.00	1.686	4.836	6.523	580.36	17.047	202.37
125.00	1.894	5.355	7.250	669.42	18.580	236.79
130.00	2.115	5.894	8.009	766.19	20.133	274.92
135.00	2.348	6.450	8.798	870.77	21.699	316.92
140.00	2.592	7.023	9.615	983.20	23.273	362.95
145.00	2.849	7.610	10.459	1103.5	24.849	413.12
150.00	3.117	8.211	11.328	1231.7	26.423	467.58
155.00	3.396	8.824	12.220	1367.7	27.989	526.44
160.00	3.686	9.447	13.134	1511.6	29.545	589.82
165.00	3.987	10.080	14.066	1663.2	31.088	657.81
170.00	4.297	10.720	15.017	1822.4	32.614	730.52
175.00	4.617	11.367	15.984	1989.3	34.122	808.01
180.00	4.947	12.020	16.967	2163.6	35.610	890.38
185.00	5.285	12.677	17.962	2345.3	37.076	977.70
190.00	5.632	13.339	18.970	2534.3	38.519	1070.0
195.00	5.987	14.002	19.989	2730.5	39.937	1167.4
200.00	6.350	14.668	21.018	2933.7	41.330	1269.9
205.00	6.720	15.335	22.055	3143.7	42.697	1377.6
210.00	7.098	16.003	23.100	3360.6	44.038	1490.5
215.00	7.482	16.670	24.152	3584.1	45.352	1608.6
220.00	7.873	17.337	25.210	3814.1	46.639	1732.0
225.00	8.270	18.002	26.272	4050.4	47.899	1860.7
230.00	8.673	18.665	27.338	4293.0	49.133	1994.8
235.00	9.081	19.326	28.408	4541.7	50.339	2134.1
240.00	9.495	19.985	29.480	4796.4	51.519	2278.8
245.00	9.914	20.640	30.554	5056.8	52.673	2428.9
250.00	10.338	21.292	31.630	5323.0	53.800	2584.4
255.00	10.766	21.940	32.706	5594.8	54.902	2745.2
260.00	11.198	22.585	33.783	5872.0	55.977	2911.4
265.00	11.634	23.225	34.859	6154.5	57.028	3083.0
270.00	12.074	23.860	35.934	6442.3	58.054	3260.0
273.15	12.353	24.258	36.611	6626.1	58.687	3374.3
275.00	12.518	24.491	37.009	6735.0	59.055	3442.4
280.00	12.965	25.117	38.082	7032.8	60.032	3630.1
285.00	13.415	25.738	39.153	7335.3	60.985	3823.2
290.00	13.868	26.354	40.221	7642.6	61.914	4021.6
295.00	14.323	26.964	41.288	7954.4	62.821	4225.4
298.15	14.612	27.346	41.958	8153.2	63.381	4356.5
300.00	14.782	27.569	42.351	8270.7	63.706	4434.5

H$_0^C$ AND S$_0^C$ APPLY TO THE REFERENCE STATE OF THE SOLID AT ZERO DEG K

THERMODYNAMIC FUNCTIONS FOR BERYLLIUM 1:3-ALUMINATE (BEO·3AL$_2$O$_3$)
SOLID PHASE

GRAM MOLECULAR WT.=330.8952 GRAMS   1 CAL=4.1840 ABS J

$$T\ DEG\ K = 273.15 + T\ DEG\ C$$

T	$-(G_T^0-H_0^C)/T$	$(H_T^0-H_0^C)/T$	$(S_T-S_0^C)$	$(H_T^0-H_0^C)$	C_P^0	$-(G_T^0-H_0^C)$
DEG K	$\dfrac{CAL}{DEG\ MOLE}$	$\dfrac{CAL}{DEG\ MOLE}$	$\dfrac{CAL}{DEG\ MOLE}$	$\dfrac{CAL}{MOLE}$	$\dfrac{CAL}{DEG\ MOLE}$	$\dfrac{CAL}{MOLE}$
300.00	14.782	27.569	42.351	8270.7	63.706	4434.5
310.00	15.705	28.763	44.468	8916.4	65.410	4868.6
320.00	16.637	29.934	46.571	9578.8	67.048	5323.8
330.00	17.576	31.082	48.658	10257.	68.598	5800.0
340.00	18.520	32.207	50.728	10950.	70.072	6296.9
350.00	19.470	33.309	52.779	11658.	71.474	6814.5
360.00	20.423	34.388	54.812	12380.	72.808	7352.4
370.00	21.380	35.444	56.824	13114.	74.075	7910.6
373.15	21.682	35.771	57.453	13348.	74.461	8090.6
380.00	22.339	36.476	58.815	13861.	75.279	8488.8
390.00	23.300	37.486	60.786	14620.	76.420	9086.9
400.00	24.261	38.473	62.734	15389.	77.502	9704.5
425.00	26.665	40.843	67.508	17358.	79.960	11333.
450.00	29.064	43.077	72.140	19384.	82.109	13079.
475.00	31.450	45.182	76.632	21462.	84.003	14939.
500.00	33.818	47.166	80.984	23583.	85.690	16909.
550.00	38.488	50.804	89.291	27942.	88.578	21168.
600.00	43.050	54.054	97.104	32432.	90.956	25830.
650.00	47.494	56.972	104.47	37032.	92.954	30871.
700.00	51.814	59.604	111.42	41723.	94.666	36270.
750.00	56.009	61.993	118.00	46494.	96.156	42007.
800.00	60.080	64.170	124.25	51336.	97.473	48064.
850.00	64.031	66.164	130.20	56240.	98.654	54427.
900.00	67.866	67.999	135.87	61199.	99.725	61079.
950.00	71.588	69.695	141.28	66211.	100.71	68009.
1000.00	75.204	71.269	146.47	71269.	101.62	75204.
1050.00	78.717	72.735	151.45	76371.	102.47	82653.
1100.00	82.132	74.104	156.24	81515.	103.27	90346.
1150.00	85.455	75.389	160.84	86697.	104.02	98273.
1200.00	88.689	76.597	165.29	91916.	104.74	106427.
1250.00	91.840	77.737	169.58	97171.	105.44	114800.
1300.00	94.910	78.815	173.72	102460.	106.10	123383.
1350.00	97.904	79.838	177.74	107781.	106.75	132170.
1400.00	100.82	80.810	181.63	113134.	107.37	141155.
1450.00	103.68	81.736	185.41	118518.	107.98	150331.
1500.00	106.46	82.621	189.08	123932.	108.57	159694.
1550.00	109.19	83.467	192.65	129375.	109.15	169238.
1600.00	111.85	84.279	196.13	134846.	109.72	178958.
1650.00	114.45	85.058	199.51	140346.	110.27	188849.
1700.00	117.00	85.808	202.81	145874.	110.82	198908.
1750.00	119.50	86.530	206.03	151428.	111.36	209129.
1800.00	121.95	87.228	209.18	157010.	111.90	219510.
1850.00	124.35	87.902	212.25	162618.	112.43	230046.
1900.00	126.70	88.554	215.26	168252.	112.95	240734.
1950.00	129.01	89.186	218.20	173913.	113.46	251570.
2000.00	131.28	89.799	221.08	179599.	113.98	262552.
2050.00	133.50	90.395	223.90	185310.	114.48	273677.
2100.00	135.69	90.975	226.66	191047.	114.99	284941.
2150.00	137.83	91.539	229.37	196809.	115.49	296342.

H_0^C AND S_0^C APPLY TO THE REFERENCE STATE OF THE SOLID AT ZERO DEG K

110